Division of Hydrologic Sciences
Annual Technical Report
FY 2010

Introduction

Research Program Introduction

None.

Quagga Mussel Invasion in Lake Mead: Ecological Impact and Containment

Basic Information

Title:	Quagga Mussel Invasion in Lake Mead: Ecological Impact and Containment
Project Number:	2008NV137B
Start Date:	3/1/2008
End Date:	2/28/2011
Funding Source:	104B
Congressional District:	Nevada 01
Research Category:	Biological Sciences
Focus Category:	Acid Deposition, Ecology, Water Quality
Descriptors:	
Principal Investigators:	Kumud Acharya, Charalambos Papelis, Mark Stone

Publications

1. Link, C., K. Acharya, L. Papelis, 2009. “Will Quagga Mussels Potentially Impact the Native Species’ Food Web in Lake Mead by Affecting Plankton and Nutrient Availability?” Lake Mead Science Symposium, Las Vegas, Nevada, January 13-14.
2. Link, C. 2010. Filtration and growth rate of Lake Mead Quagga mussels (Dreissena bugensis) in laboratory studies and analyses of bioconcentration. Univ. Nevada – Las Vegas Masters thesis.

Annual Report

Title: **Quagga Mussel Invasion in Lake Mead: Ecological Impact and Containment**
PI: Acharya, Kumud (Desert Research Institute) and Papelis, Charalambos
Graduate Students: Link, Carolyn, Lynn Schwaebe (UNLV, Water Resource Management)

Problem and Research Objectives

In January of 2007, Quagga mussels (*Dreissena bugensis*) were discovered in Lake Mead, for the first time west of the 100th meridian. This invasive species and the related Zebra mussel (*Dreissena polymorpha*) have disrupted ecosystems in a number of waterways elsewhere in the US and have cost billions of dollars in control efforts. Given the seriousness of the recent Quagga mussel invasion for the ecology and economy of the broader region, and for the overall management of the important water resources of the region, the primary goal of the proposed research was to study the ecology and biology of Quagga mussels and their impact on aquatic biodiversity and water quality in Lake Mead.
The experience and data collected from the proposed study would then support competitive proposals to national funding agencies to further contribute to our understanding of the problem and viable management strategies. Additional goal of this project was to establish Quagga mussel research infrastructure in Las Vegas, and involve students in the project.

Methodology

The study focused on the ecological impact and physiological ecology of the species. These studies include development of models for quantifying algae clearance, ammonia production, and measurement of growth rates of the species in controlled laboratory settings using spectrophotometry based regressions. Prefacing laboratory based studies, development of field sampling protocols for collecting mussels via SCUBA and shore collection were undertaken, as well as water collection for laboratory aquaria. Permitting applications for scientific collection were obtained through the Nevada Department of Wildlife. Establishment and maintenance of in-lab aquaria capable of maintaining cultures of the species involved extensive background research along with trial experiments to arrive at appropriate water temperature, flow rate, light cycle, water chemistry, and maintenance schedule parameters. Clearance rate, ammonia production and growth rate studies required development of lengthy experimental designs to ensure proper quantification and minimum variability between samples. Experiments required incubators to ensure proper light allowance or exclusion, and trials were completed during off-peak hours to minimize interference from other experiments and to ensure machine availability at exact required testing times.

Principle Findings and Significance

The data indicates Lake Mead quagga mussels are aggressive feeders of algae. The clearance rate experiments completed in this study indicated the quagga mussels in Lake Mead filter at higher rates per mass when still in an early growth stage, and that they filter smaller

algae particles faster than larger ones. The highest filtration rates were observed in the waters with high sediment and low nutrient concentration, an important indication mussel impact. Waters in lakes and rivers that experience high turbidity, or times or high turbidity, may potentially see a larger impact in water clarity and clearance by the mussels.

Our growth study results suggest that quagga mussel growth in Lake Mead may be food limited at this time, and it would be reasonable to predict significant increases in their growth at times during the year when algae concentration is greater, inclusive of summertime increases in lake productivity. Based on our preliminary data, quagga mussels' increasing population could have dramatic implications in the clarity and overall foodweb of the Lake Mead.

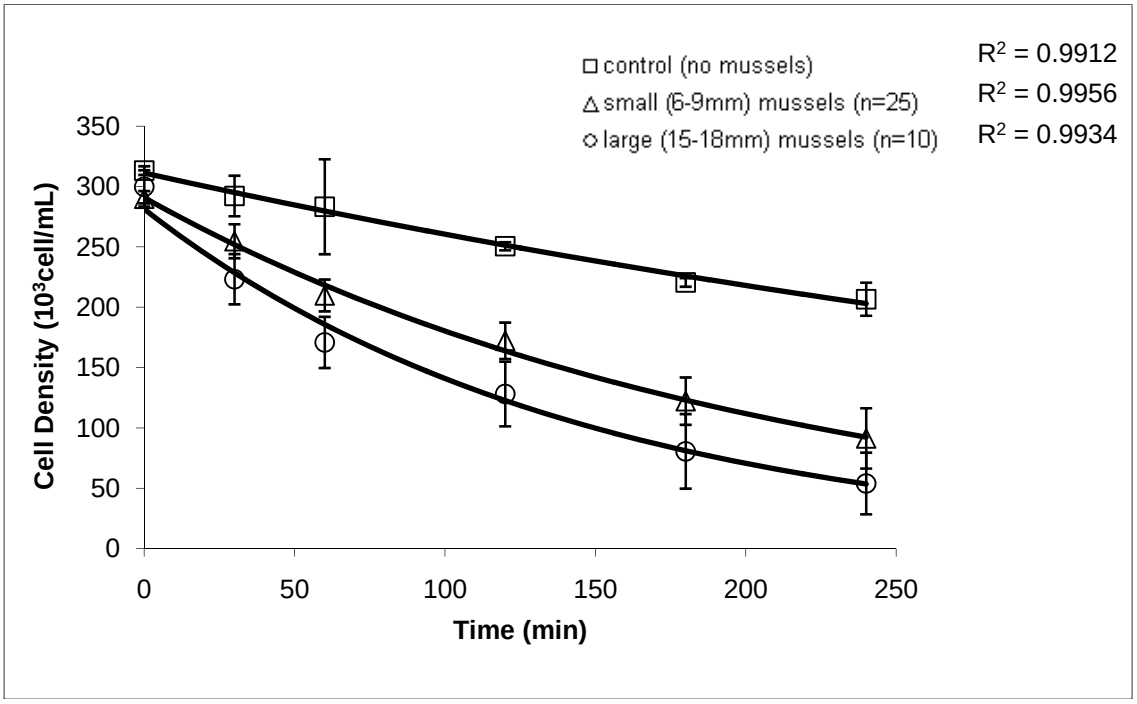

Figure 1.1 Graph of small algae Density over Time in 1L Vessels with Large and Small Quagga Mussels

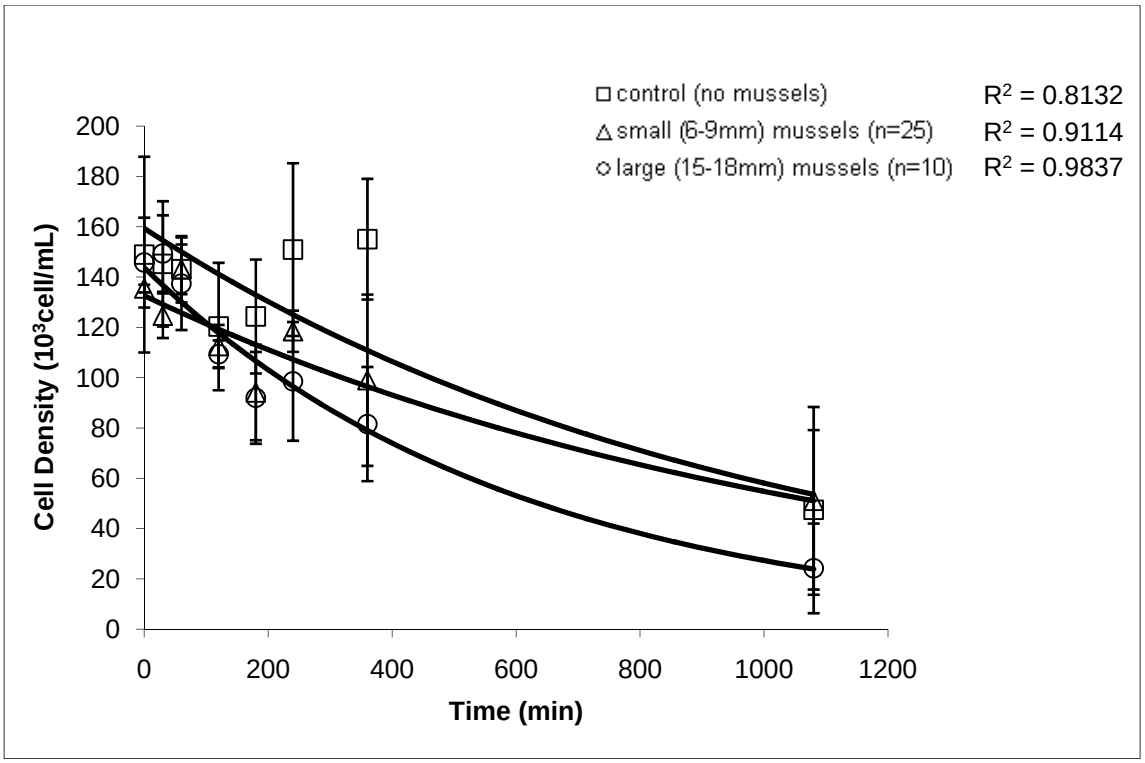

Figure 1.2 Graph of large algae Density over Time in 1L Vessels with Large and Small Quagga Mussels

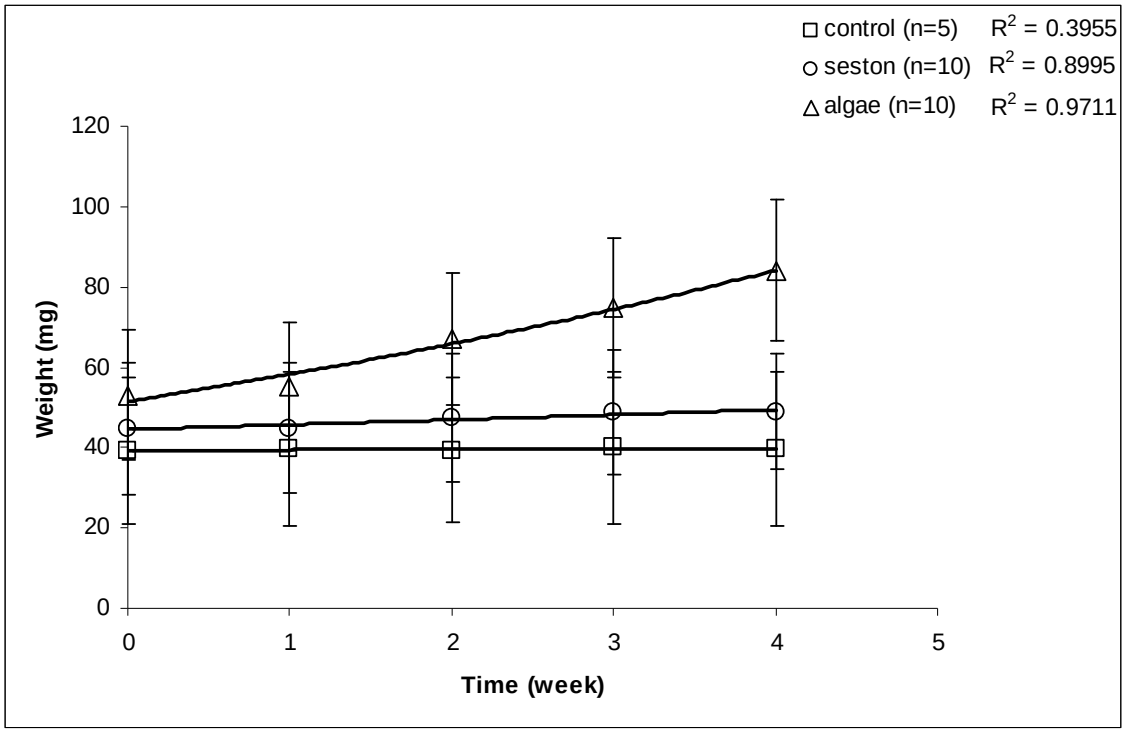

Figure 2.1 Growth in Milligrams of Quagga Mussels in Media over Time

Information Transfer Activities

Results obtained were presented at the Lake Mead Science Symposium, in Las Vegas, NV, in January 2009 before stake holders and research communities. The PI and the graduate student (Carolyn Link) regularly attended the quarterly meeting of Quagga mussels held at Southern Nevada Water Authority (SNWA) for information exchange.

Student Support

The project funded two M.S. students, one full time (Carolyn Link) and one half time (Lynn Schwaebe) both from the Water Resources Management Program of University of Nevada, Las Vegas. Carolyn has already graduated and Lynn will graduate in summer, 2011.

Other Accomplishments

The project allowed the PI (Acharya) to collect preliminary data. The preliminary data led to additional funding through two new projects by National Park Service and NSF-SBIR through the Marrone Bio-innovations, a California based bio-control company. The project has allowed the PI to establish Quagga mussel research infrastructure in DRI. This has increased institute's competitiveness in the field of Quagga mussel research and provided additional local research capability for Southern Nevada and Lake Mead.

Uncertainty and Sensitivity of Ground-Water Discharge Estimates for the Shrublands in the Great Basin Area

Basic Information

Title:	Uncertainty and Sensitivity of Ground-Water Discharge Estimates for the Shrublands in the Great Basin Area
Project Number:	2008NV139B
Start Date:	3/1/2009
End Date:	2/28/2011
Funding Source:	104B
Congressional District:	Nevada 01
Research Category:	Climate and Hydrologic Processes
Focus Category:	Hydrology, Water Supply, Groundwater
Descriptors:	None
Principal Investigators:	Jianting Julian Zhu

Publications

1. Zhu, J., and Young, M. H., Sensitivity and Uncertainty of Ground-Water Discharge Estimates for Semi-Arid Shrublands, Journal of the American Water Resources Association, in press, 2009.
2. Zhu J., and Young, M. H., Uncertainty and Sensitivity of Evapotranspiration Estimates for Semi-Arid Shrublands, Nevada Water Resources Association Annual Conference, Mesquite, Nevada, March 5 – 6, 2008.
3. Pan, F., J. Zhu, M. Ye, Y. A. Pachepsky, and Y.-S. Wu. 2010. Sensitivity analysis of unsaturated flow and contaminant transport with correlated parameters. Journal of Hydrology. doi:10.1016/j.jhydrol.2010.11.045.
4. Zhu, J., K. Pohlmann, J. B. Chapman, C. E. Russell, R. W. H. Carroll, and D. S. Shafer. 2010. Sensitivity to Formation Porosity of Contaminant Transport from Nevada Test Site to Yucca Mountain, Practice Periodical of Hazardous, Toxic, and Radioactive Waste Management, ASCE, 2010. doi:10.1061/(ASCE)HZ.1944-8376.0000047.
5. Zhu, J., and M. Young. 2009. Sensitivity of evapotranspiration estimates for semi-arid shrublands, 94th ESA Annual Meeting, Albuquerque, New Mexico, U. S. A., August 2–7, 2009.

Uncertainty and Sensitivity of Ground-Water Discharge Estimates for the Shrublands in the Great Basin Area

Final Report

Problem and Research Objectives

The current limited water supply to Las Vegas area mainly from Colorado River is not likely enough to support its potential future growth. With future needs of water resources in mind, local water authorities are looking northeast to the Great Basin. One plan – among many others – proposes to pump water from the Great Basin aquifers. Before such action can be taken, it is necessary to investigate the way in which the aquifers are influenced and the potential for long-term pumping to affect water availability to phreatophytic vegetation. Federal legislation (Section 131 of the Lincoln County Conservation, Recreation, and Development Act of 2004) was enacted to conduct a water resources study of the alluvial and carbonate aquifers in Nevada and Utah. The study was known as the Basin and Range Carbonate Aquifer System Study, or BARCAS study. The study area includes 30 sub-basins in 12 valleys. Of particular focus in the BARCAS study was the amount of ground water lost through evapotranspiration (ET). While groundwater ET as an overall water budget component has been estimated in other studies, including BARCAS, the sensitivity and uncertainty of groundwater ET estimates have not been systematically analyzed.

Given the large size of the study area and the dearth of previous studies of the valleys, groundwater discharge through ET was estimated using a rather sparse dataset. As a result, the ET rate and area uncertainty have significant influence on the groundwater discharge estimates. It is therefore beneficial to quantify the uncertainty associated with these estimates in order to help maximize future data collection efforts. This project seeks to develop an integral approach to quantify the uncertainty and sensitivity of groundwater discharge estimates.

Methodology

We first present the general steps for quantifying fractional contributions of uncertainties in individual variables to the estimation uncertainty of groundwater discharge by ET, when large numbers of independent variables are involved:

1. Establish model(s) to estimate groundwater discharge that relate independent variables to the calculations of groundwater discharge.

2. Estimate uncertainty ranges and probability density functions for the independent variables based on field characterization, professional judgment, etc.

3. Randomly select realizations from the prescribed probability distributions of the independent variables, and calculate groundwater discharge values based on the selected model(s) in Step 1 for all realizations.

4. Select influential independent variables, based on the physical characteristics and model structure of the considered problems. The main goal of this step is to reduce the number of independent variables included in the subsequent sensitivity analysis.

5. Conduct sensitivity analysis to quantify the uncertainty contributions from individual independent variables.

To quantify how parameter-level uncertainty affects groundwater discharge estimates, we conduct Monte Carlo simulations that represent independent variables as statistical distributions rather than as single values. Each independent variable is assumed to be characterized by a probability density function, with the mean ET rate estimated either through remote sensing analyses, values taken from the literature, or from existing data. To examine the sensitivity of the total groundwater discharge estimate to the three independent variable categories in general (i.e., ET rate, acreage, and precipitation rate), we also systematically vary the standard deviations for the independent variables. The Monte Carlo simulations based on the estimated standard deviations are considered as the Base Case. By comparing the results relative to the Base Case, we can assess how uncertainty from each independent variable category contributes to the uncertainty of the total groundwater discharge estimate. For this purpose, we investigate two main themes: (1) varying the standard deviations of one individual independent variable category, while holding constant the standard deviations of the other two categories at the Base Case levels; and (2) varying the standard deviations of one individual independent variable category while using the mean of the other two independent variable categories (i.e., standard deviations equal zero). By investigating theme (2), we can explore how uncertainties in individual variable categories propagate to the uncertainty in the total groundwater discharge. After the Monte Carlo simulations, we develop regression models that relate total groundwater discharge to individual independent variables, and we use these models to assess overall sensitivity of the total groundwater discharge estimate to the individual independent variables. The squared values of standardized regression coefficients simply represent the fractional contributions from the individual independent variables to the total variance of the groundwater discharge.

Principal Findings and Significance

The principal findings are:

- Although the independent variables in this study typically have small CVs, the CV of groundwater discharge estimates in some sub-basins can be quite large.
- The uncertainty of ET rates is the most significant contributor to the uncertainty of groundwater discharge estimates. We find that a total of 630 variables affect the estimates of total groundwater discharge, but that only seven variables account for almost all of the variability in the discharge estimates. We demonstrate that groundwater discharge estimates using the simplified regression relationship and the full relationship correlate very closely (correlation coefficient is 0.982).
- Quantitatively, the variability in ET rates for the moderately dense desert shrubland contributes to 75% of the variance in the total groundwater discharge estimates. The results indicate that field data collection to reduce overall uncertainty should focus primarily on this ET unit, and less on other units.

Information Transfer Activities

Journal Papers:

Zhu, J., and M. H. Young. 2009. Sensitivity and uncertainty of ground-water discharge estimates for semi-arid shrublands. Journal of the American Water Resources Association (JAWRA). 45(3):641-653, doi:10.1111/j.1752-1688.2009.00312.x.

Pan, F., J. Zhu, M. Ye, Y. A. Pachepsky, and Y.-S. Wu. 2010. Sensitivity analysis of unsaturated flow and contaminant transport with correlated parameters. Journal of Hydrology. doi:10.1016/j.jhydrol.2010.11.045.

Zhu, J., K. Pohlmann, J. B. Chapman, C. E. Russell, R. W. H. Carroll, and D. S. Shafer. 2010. Sensitivity to Formation Porosity of Contaminant Transport from Nevada Test Site to Yucca Mountain, Practice Periodical of Hazardous, Toxic, and Radioactive Waste Management, ASCE, 2010. doi:10.1061/(ASCE)HZ.1944-8376.0000047.

Abstracts and Presentations:

Zhu J., and Young, M. H. 2008. Uncertainty and sensitivity of evapotranspiration estimates for semi-arid shrublands, Nevada Water Resources Association Annual Conference, Mesquite, Nevada, March 5 – 6, 2008.

Zhu, J., and M. Young. 2009. Sensitivity of evapotranspiration estimates for semi-arid shrublands, 94th ESA Annual Meeting, Albuquerque, New Mexico, U. S. A., August 2–7, 2009.

Student Support

This grant was partly used to fund student training. Feng Pan (a Ph.D. student at University of Nevada Las Vegas, Department of Geoscience) was partially funded from this grant to do sensitivity analysis. Siqi Tan (a MS student at University of Nevada Las Vegas, Department of Mathematics) was partially funded to help with data analysis.

Black Carbon in Sierra Nevada Snow: Impacts on Snowmelt and Water Supply

Basic Information

Title:	Black Carbon in Sierra Nevada Snow: Impacts on Snowmelt and Water Supply
Project Number:	2009NV150B
Start Date:	3/1/2009
End Date:	2/28/2011
Funding Source:	104B
Congressional District:	02
Research Category:	Climate and Hydrologic Processes
Focus Category:	Surface Water, Climatological Processes, Non Point Pollution
Descriptors:	
Principal Investigators:	Joe McConnell

Publications

1. Sterle, K.M., J.R. McConnell, J. Dozier, R. Edwards, and M. Flanner, Retention and radiative forcing of black carbon in eastern Sierra Nevada snow, Geophysical Research Letters, Submitted.
2. Sterle, K., and J. R. McConnell (2010) Black carbon science at DRI (Invited), Presented at the Impurities in Snow and Ice (ISI) Workshop, Silverton, USA.

Synopsis

The vast majority of Nevada's water supplies originate as mountain snow so quantitative understanding of processes that influence snow melt and spring runoff is critical to Nevada's economic growth and ecological sustainability. Black carbon (BC or soot) aerosols emitted during combustion and deposited on snow decrease reflectance, leading to enhanced snow pack warming, sublimation and melt, but sources of BC and impacts are poorly understood. Measurements of black carbon (BC) in a sequence of snow pits and surface snow samples in the eastern Sierra Nevada during the snow accumulation and melt seasons of 2009/10 showed that surface concentrations of BC were enhanced seven fold in surface snow (~25 ng/g) compared to bulk values in the snowpack (~3 ng/g). Unlike major ions which are preferentially released during initial melt, BC and continental dust were retained in the snow, enhancing concentrations late into spring, until a final flush well into the melt period. We estimate a combined BC and continental dust surface radiative forcing of 20 to 40 W/m^2 during April and May, with dust likely contributing a greater share of the forcing than BC.

Final Report

Problem and research objectives

Because >85% of Nevada's water supplies originate as mountain snow, quantitative understanding of processes that influence snow melt and spring runoff is critical to Nevada's economic growth and ecological sustainability. Although the sources and impacts are poorly understood, black carbon aerosols emitted during combustion and deposited on snow decrease reflectance, leading to enhanced snow pack warming, sublimation and melt. Because local emissions are significant, abatement efforts in Nevada and California could help preserve Sierra Nevada snow resources.

Primary objectives of this research were to (1) characterize concentrations of BC in fresh Sierra Nevada snow using samples from a series of snow pits excavated throughout the snow accumulation and snow melt seasons, (2) measure changes in concentration and movement of BC in snow during melt by comparing mean and layer snow pack concentrations during the snow accumulation and snow melt seasons , and (3) simulate surface radiative forcing from BC on snow throughout winter snow accumulation and spring melt periods using the Snow, Ice, and Aerosol Radiative (SNICAR) model. Field research primarily was conducted in 2009 and 2010 at two Sierra Nevada locations: the Cooperative Snow Study Site on Mammoth Mountain and the Sagehen Creek Field Station, both of which are administered by the U. of California.

Principal findings and significance

BC and continental dust concentrations measured in eastern Sierra Nevada snow in 2009 were significant enough to reduce snow albedo changes and alter water resources in the region. Temporal variability investigated at Mammoth suggests that BC accrued during the accumulation period because there was little melt or transport through the snowpack. During the melt season, BC was conserved in snowpack well after the initial elution of solutes, and remained stable well into the ablation season (with some relocation in the snowpack), until a final flush was observed at the end of the 2009 sampling period. BC concentrations at the surface continued to increase until the final flush near the end of May.

Comparisons of BC, continental dust, and major ions concentrations indicate that, unlike major ions which are preferentially released during initial melt, BC and continental dust are retained in the snowpack and then flushed well into the melt season. The retained BC and dust enhance radiative forcing in the eastern Sierra Nevada's spring snowpack, with dust contributing greater forcing than BC.

Although speculative, we hypothesize that melt scavenging ratios could provide better tracking of the ionic pulse and final release of BC and dust through the snowpack, particularly in the top 30 cm. Expanded sampling networks would improve quantification of BC in Sierra Nevada snow and future investigations of ice layers, source trajectories and duration of exposed surfaces would contribute to the understanding of high concentration layers that exist within the snowpack and vary inter-annually.

Papers:

This research formed the basis of K. Sterle's M.S. thesis "Black Carbon in Eastern Sierra Nevada Snow Pack" at the University of Nevada, Reno.

Sterle, K.M., J.R. McConnell, J. Dozier, R. Edwards, and M. Flanner, Retention and radiative forcing of black carbon in eastern Sierra Nevada snow, *Geophysical Research Letters, Submitted*.

Presentations:

Sterle, K., and J. R. McConnell (2010) Black carbon science at DRI (Invited), Presented at the *Impurities in Snow and Ice (ISI) Workshop*, Silverton, USA.

Partition of Evapotranspiration and Scale Issues in Arid Landscape

Basic Information

Title:	Partition of Evapotranspiration and Scale Issues in Arid Landscape
Project Number:	2010NV160B
Start Date:	3/1/2010
End Date:	2/28/2011
Funding Source:	104B
Congressional District:	NV01
Research Category:	Climate and Hydrologic Processes
Focus Category:	Hydrology, Water Use, Ecology
Descriptors:	None
Principal Investigators:	Jianting Julian Zhu

Publications

1. Sun, D., and J. Zhu. 2010. Interactions of evaportranspiration between two parallel columns, AGU Fall Meeting, December 13–17, 2010, San Francisco, California, U.S.A.
2. Sun, D., and J. Zhu. 2010. Modeling transpiration and evaporation in parallel columns, ASA-CSSA-SSSA 2010 International Annual Meetings, October 31 – November 4, 2010, Long Beach, California, U. S. A.

Partition of Evapotranspiration and Scale Issues in Arid Landscape

Final Report

Problem and Research Objectives

In arid regions of the southwestern United States, water is a major determinant affecting vegetation cover and desert landscape. In turn, vegetation cover and biomass affect various hydrologic phenomena, including infiltration, runoff, interception, and erosion. Thus, any controls on water movement can exert a major influence on plant community composition, function, and structure. Ecohydrology of arid environments is strongly coupled to available water. Surface soil structure and texture affect the depth of water penetration, and hence root distributions of perennial plants, and the diversity and vigor of native vegetation. The physical (i.e., particle size distribution and bulk density), hydraulic (i.e., saturated hydraulic conductivity and water retention characteristics), and structural properties (i.e., ped size and shapes) of near-surface soil can affect the amount of water that enters the soil through infiltration as well as the water-holding capacity of the soil after infiltration. Therefore, the amount of water that becomes available for root water uptake also is affected. Along with greater soil structure and deeper horizonation, surface soil properties largely determine the depth of wetting for particular classes of precipitation events, and, therefore, also will affect water availability for different growth forms, depending on their phenology and rooting characteristics. Recent investigations have identified linkages among ecohydrological processes that may operate at different scales. Uncertainty and spatial heterogeneity of these linkages, however, affect our ability to upscale or downscale observed processes to other scales of interest.

This project is designed to investigate scale effects of numerical predictions on water budget, specifically on evapotranspiration (ET) partitioning into evaporation and transpiration, in arid environments. The objectives are to investigate: (1) the effects of plant cover spatial patterns on the field scale water budget of desert landscape, and (2) the scale effects of numerical models on the water budget predictions in the desert environments at various scales.

Methodology

The study is built on previous field campaign conducted at the Mojave Global Change Facility (MGCF), located approximately 90 km northwest of Las Vegas, Nevada on the Nevada Test Site. Vegetation at the site is representative of both Mojave and Great Basin Deserts consisting primarily of *Larrea tridentata* (creosotebush), *Lycium pallidum* (desert thorn), *Ambrosia dumosa* (white bursage), and *Ephedra nevadensis* (Mormon tea). The measurements are focused on the dominant vegetation by percent cover: *L. tridentata* (LATR) and *L. pallidum* (LYPA). A total of six shrubs (three LATR and three LYPA) are chosen along the east-central boundary of the MGFC. Vegetation size is varied to cover a range of canopy diameters for LATR (45, 100, and 190 cm) and LYPA (40, 80, 120 cm). The hydraulic properties are obtained using discrete measurements of unsaturated hydraulic conductivity along four transects radiating outward from each shrub to the interspace. For the spatial distribution of plant covers, sequential Gaussian simulation (SGSIM) of

GSLIB (Geostatistical Software Library) is used to generate the conditional heterogeneous parameter realizations to characterize local-scale heterogeneity and associated uncertainty. Spatial distributions of desert shrubs are generated for a field of 450m x 450m synthetically based on different ranges of spatial correlations. The mean fraction is assumed to be about 10% of shrub coverage for a typical desert setting. For the 450m x 450m field, we use three correlation ranges of 45m, 90m, 135m. Given the generated distributions of the shrub coverage, we then generate two separate fields for the hydraulic parameters, based on the statistics obtained from the previous field characterizations. The first field is the under-canopy hydraulic parameters, and the second one is the interspace hydraulic parameters. Then we combine these two fields to produce one complete spatial distribution of the hydraulic parameters.

HYDRUS-1D is then used to examine the effect of hydraulic property and plant cover heterogeneity and the associated scale effects on soil water balance and partitioning of ET into evaporation and plant transpiration.The upper boundary is controlled by the prescribed atmospheric conditions. The upper boundary is kept identical for all simulations and generated using locally measured climate data at 0.5 hour time steps (e.g., precipitation and potential ET), collected using an eddy covariance station at the site. The effect of grid cell size on the scale water budget at large scale heterogeneous landscape is investigated. We also examine how the spatial structure of shrub cover influences the large scale water partition in arid environments.

Principal Findings and Significance

The principal findings are:

- In middle range of simulation grid cell aggregation, significant differences exist in terms of transpiration and evaporation partitioning among the different correlation ranges due to the highly non-linear relationship between potential transpiration and percentage shrub cover as.
- At both end of aggregation regimes, the simulated results of transpiration and evaporation partition converge regardless of the plant cover pattern (expressed in terms of correlation range of shrub cover distribution).
- The ratio of transpiration over total evapotranspiration increases as the aggregated simulation grid cell sizes increase, which shown significant implications that the size of grid cell size would significantly affect the simulation results.

Information Transfer Activities

Journal Paper:

Zhu, J., Sun, D., M. Young, and T. Caldwell. 2011. Shrub cover patterns and large scale evapotranspiration in arid environments, Journal of Arid Environments, manuscript in preparation, to be submitted.

Abstracts and Presentations:

Sun, D., and J. Zhu. 2010. Interactions of evaportranspiration between two parallel columns, AGU Fall Meeting, December 13–17, 2010, San Francisco, California, U.S.A.

Sun, D., and J. Zhu. 2010. Modeling transpiration and evaporation in parallel columns, ASA-CSSA-SSSA 2010 International Annual Meetings, October 31 – November 4, 2010, Long Beach, California, U. S. A.

Student Support

This grant was partly used to fund student training. Rongrong Zhang (a Ph.D. student from Hohai University, Nanjing, China) was partially funded from this grant to help in data analysis.

Predicting Solar Still Water Production by Using Artificial Intelligence Techniques

Basic Information

Title:	Predicting Solar Still Water Production by Using Artificial Intelligence Techniques
Project Number:	2010NV161B
Start Date:	3/1/2010
End Date:	2/28/2011
Funding Source:	104B
Congressional District:	NV01
Research Category:	Water Quality
Focus Category:	Water Supply, Water Quantity, Water Quality
Descriptors:	
Principal Investigators:	Aly Said, David Earl James

Publication

1. Santos, N., Said, A.M, James, D.E., and Venkatesh, N.H. 2011. Comparing multivariate regression and artificial neural networks to model solar still production. 40th American Solar Energy Society National Conference, Raleigh, NC, May 17-21, 2011.

PREDICTING SOLAR STILL PRODUCTION USING ARTIFICIAL INTELLIGENCE TECHNIQUES

FINAL REPORT

PROBLEM AND RESEARCH OBJECTIVES

With the rising cost and limited supply of traditional fossil fuels, both water transportation costs and distillation processes such as multistage flash, multiple effect, vapor compression, reverse osmosis, electrolysis, phase change, and solvent extraction will see their price per unit of water increase drastically. Solar distillation is a simple and clean technology which can be used to distill brackish or polluted water into drinkable water and can be used to reduce fossil fuel dependence that presently exists at distillation plants. Being able to predict solar still performance from long-term solar irradiance, air temperature, wind speed, wind direction, and cloud cover data, while taking into account meteorological variations, will prove to be a novel scientific investment to better the quality of life for Nevada and many people in need of potable water worldwide.

The objectives of this study included the following:

1) Acquire long term hourly and daily weather data for global incident solar radiation (insolation), average ambient temperature, average wind speed, average wind direction, and average cloud cover.

2) Purchase/install data-logging equipment on two solar stills to measure and record distilland temperature, headspace (gap between distilland and glass cover surface) temperature, and inner/outer glass cover temperature.

3) Develop new artificial neural network (ANN) and genetic algorithm (GA) models to predict daily solar still production.

4) Publish results in peer reviewed journals that associate with renewable energy technologies and water resource applications.

METHODOLOGY

This study used daily solar still production data acquired by a previous graduate student which contained 300 to 615 records of still production. This study paired each daily production record with the corresponding weather conditions with respect to insolation, ambient temperature, wind speed, wind direction, and cloud cover.

The newly developed database of still production and weather data was split up into training and testing data sets to be used by the artificial neural networks. The artificial neural network's training process allows it to determine weights between the connections for the input variables (weather data) and the target variable (daily production). The training process was carried out

with 80% of the total data set being used for training and the remaining 20% being used to test the predictive capabilities of the developed network.
The same data set is being used to develop new genetic algorithm models based on evolution and crossover mutation to develop equations with a minimized error. The genetic algorithms are still currently under development. However, once solid results are found, the findings will be published in peer review journals.

The ANN and GA model development was carried out along side real time solar still production testing. New data-logging equipment was purchased and installed on two solar stills. 5 minute readings were recorded to measure the distilland, headspace, and the inner/outer glass temperature. These readings were then averaged out to develop hourly readings. These hourly readings will further be processed to create new ANN and GA models to predict hourly solar still production and to compare with existing numerical methods that estimate hourly production.

PRINCIPAL FINDINGS AND SIGNIFICANCE

As a result of this study, an artificial neural network was developed that could predict daily distillate production by using local weather data. The results of the developed ANN are as follows:

1) The ANN was able to produce results whereby 89% of the predictions were within 20% of the actual value. The ANN exceeded the performance of a typical multivariate regression technique which could only achieve 84% of the predictions being within 20%.

2) The ANN showed increasing performance levels with the addition and combination of different weather variables. The best performing ANN was found to be the one utilizing insolation, temperature, distilland volume, and wind speed for a particular solar still.

3) Using the developed ANN model, the 95% confidence interval for solar still production was developed to provide accurate average monthly daily predictions. It was found that ANN predictions were within 10% of the actual average monthly daily production.

4) By using the acquired data-logging equipment, it was found that solar stills produce 20-25% of their daily distillate after sun set.

5) The data-logging data acquisition also showed that there is 1-2 hour delay between peak sunlight and peak still production. A result that has not yet been reported in past studies.

6) Using a parametric study, the ANN predicted that maximum production occurs for periods of high insolation and high wind speeds.

7) A second parametric study also predicted higher distillate production for solar stills running with deeper distilland basins during periods of low insolation compared to basins with low depth during periods of low insolation. This parametric study also predicted higher production for basins with low depth during periods of high insolation compared to basins with high depth during periods of high insolation.

8) The prediction capabilities of the ANN model will help to accurately determine the total amount of solar still basin area required to economically meet the daily clean water demand of any location or community.

INFORMATION TRANSFER ACTIVITIIES

Papers:

1) Santos, N.I., Said, A.M., James, D.E., and Venkatesh, N.H. Modeling solar still production using local weather data and artificial neural networks. *Renewable Energy*. (2011 Accepted).

2) Santos, N.I., Venkatesh, N.H., James, D.E., and Said, A.M. Performance evaluation of single basin solar stills in Las Vegas, Nevada. *Advances in Water Resources*. (2011 In Progress).

3) Santos, N.I., Said, A.M., James, D.E., and Venkatesh, N.H. Modeling solar still production using local weather data and genetic algorithms. *Renewable Energy.* (2011 In Progress).

Presentations:

1) Santos, N., Said, A.M, James, D.E., and Venkatesh, N.H. 2011. Comparing multivariate regression and artificial neural networks to model solar still production. 40th American Solar Energy Society National Conference, Raleigh, NC, May 17-21, 2011.

STUDENT SUPPORT

This grant funded the research endeavors (time, instruments, and conference travel) for the completion of Noe Santos's master's degree in civil and environmental engineering. Noe Santos was able to recently present the findings of this study at the American Solar Energy Society National Conference which was held in Raleigh, NC from May 17th – 21st.

Water Quality and Eutrophication Modeling of Lake Mead under Changing Water Levels

Basic Information

Title:	Water Quality and Eutrophication Modeling of Lake Mead under Changing Water Levels
Project Number:	2010NV165B
Start Date:	3/1/2010
End Date:	2/28/2011
Funding Source:	104B
Congressional District:	NV01
Research Category:	Water Quality
Focus Category:	Models, Surface Water, Water Supply
Descriptors:	None
Principal Investigators:	Dong Chen

Publication

1. Li Y, Acharya K., Chen D., and Stone M. (2010) Modeling water ages and thermal structure of Lake Mead under changing water levels. Lake and Reservoir Management 26(4), 258-272

Hydrodynamic and Water Quality Modeling of Lake Mead under Changing Water Levels

Technical Report

Desert Research Institute
Department of Hydrologic Sciences
Las Vegas, Nevada

May, 2011

Hydrodynamic and Water Quality Modeling of Lake Mead under Changing Water Levels

Report Prepared by

Dong Chen, Ph.D., Professional Engineer

Department of Hydrologic Sciences, Desert Research Institute

Prepared for

Nevada Water Resources Research Institute

Desert Research Institute

Department of Hydrologic Sciences

Las Vegas, Nevada

May, 2011

THIS PAGE INTENTIONALLY LEFT BLANK

Executive Summary

Lake Mead is one of the most important water bodies in the United States; providing recreational opportunities, fish and wildlife habitat, and drinking, irrigation, and industrial water for approximately 25 million people. Consequently, it is crucial that the quality of this water be maintained to provide a reliable and safe source of water for its many uses. Rapid urban development in southern Nevada, combined with modified upstream land use and the emergence of invasive species has gradually degraded Lake Mead water quality. Concurrently, sustained drought since 2000 has led to a significant drop (about 100-feet) of the lake's water level, further stressing the water quality and ecological processes. *A three-dimensional hydrodynamic and water quality model of Lake Mead was developed to investigate eutrophication processes and predict their trends in future.* The model integrates previous water monitoring efforts by the Southern Nevada Water Authority, U.S. Geological Survey, and the U.S. Bureau of Reclamation. The numerical model applied to Lake Mead will be the three-dimensional Environmental Fluid Dynamics Code (EFDC). DRI scientists have been applying EFDC to investigate changes in the flow circulation patterns of Lake Mead (Chen et al., 2009). In this study, we continue to model the water age and thermal structure of Lake Mead under changing water levels. Changes in temperature and water age due to continuous drought were proved to have a strong influence on the water quality and ecosystem of Lake Mead. Besides, lake water quality and eutrophication processes under various scenarios (e.g., winter and summer, high and low water stages) was predicted by using CE-QUAL-ICM. This study provides a numerical tool to support adaptive management of regional water resources by lake managers.

Publication

Li Y, Acharya *K.*, ***Chen D.,*** *and Stone M.* (2010) Modeling water ages and thermal structure of Lake Mead under changing water levels. ***Lake and Reservoir Management*** 26(4), 258-272

Student Support

This project has financially supported Naveen Kumar Veeramisti who is a graduate student from University of Nevada, Las Vegas.

Table of Contents

Index of Figures

Index of Tables

1 Project Background

Lake Mead is the largest man-made reservoir in the United States by volume, formed by the construction of Hoover Dam in the Black Canyon of the Colorado River in the 1930s (Greene and Miller, 1986). It is located on the Colorado River about 30 miles (48 km) southeast of Las Vegas, Nevada, in the states of Nevada and Arizona. Formed by water impounded by Hoover Dam, it extends 110 mi (180 km) behind the dam (Figure 1). It provides power generation, recreational opportunities, fish and wildlife habitat, and drinking, irrigation, and industrial water for approximately 25 million people. Consequently, it is crucial that the quality of this water be maintained to provide a reliable and safe source of water for its many uses. Rapid urban development in southern Nevada, combined with modified upstream land use and the emergence of invasive species has gradually degraded Lake Mead water quality. Concurrently, sustained drought since 2000 has led to a significant drop (about 100-feet) of the lake's water level, further stressing the water quality and ecological processes (See Figure 2) (www.msnbc.msn.com). This problem was demonstrated by a widespread bloom of the green algal (Pyramichlamys) throughout bays and coves at Lake Mead in the spring of 2001 (See Figure 1 insert) (www.nps.gov).

Concerns over water quality were the impetus for intensive monitoring efforts by at least eight agencies including the U.S. Bureau of Reclamation (USBR), the Southern Nevada Water Authority (SNWA), and the U.S. Geological Survey (USGS) in Lake Mead, the Colorado River and its tributaries over the past 10-15 years. Although the monitoring efforts have provided an outstanding record of spatial and temporal circulation and water quality trends, modeling efforts are sparse. Besides, the agencies do not have a robust adaptive tool to integrate data and support their management needs, especially under the sustained drought situation. The complexity of the circulation processes in the lake suggests the application of numerical modeling approaches to obtain a detailed description of thermal stratification, nutrient gradients and their temporal and spatial variation. Moreover, numerical models are economical tools to experiment all possible scenarios in future.

Large lakes and reservoirs in arid and semi-arid regions are prone to substantial fluctuations in water surface elevations due to cyclic climate patterns and increasing water demands. The intensity of both climate patterns (wet and drought periods) and water demand are expected to increase under climate change (IPCC 2008). Nowhere is this phenomenon more apparent than in Lake Mead, Nevada, U.S., where water surface elevations have dropped about 35 m since its modern peak of 370 m in 2000 (LMWD 2009). Understanding how lake processes and characteristics are likely to change under receding water elevations is critical to support adaptive management of these systems under unprecedented conditions.

Changes in the water level of lakes — especially the extent, frequency and duration of the changes — play an important role in lakes' physical and hydrological processes, and afterward affect the aquatic habitat, water quality and algal growth (Brauns et al. 2008). Recently, much attention has been paid to the impact of water level fluctuations (WLF)

on socioeconomic and ecological processes in rivers (Junk and Wantzen 2004) and lakes including the Aral Sea (Usmanova 2003), Lake Chad (Coe and Foley 2001) and the Salton Sea (Bourne et al. 2005), among others. The literature describes how WLF affect the ambient environment (e.g., physical environment, biota, geomorphologic processes, landscape) and how WLF are projected to be impacted by climate change (Wantzen et al. 2008) as well as how to manage and address WLF. In general, WLF will change the lake morphometry and affect communities of littoral macrophytes, macroinvertebrates, fish (Sutela and Vehanen 2008), and water circulation and temperature regime of lakes, which can be reflected by water residence time and thermal stratification.

The reasons for and causes of WLF can be anthropogenic disturbances and natural hydrologically induced fluctuation (Hofmann et al. 2008). Anthropogenic disturbances are connected to the construction of dams and reservoirs for hydropower production and flood control, water abstraction for irrigation, and other water uses (Dynesius and Nilsson 1994). Hydrologically induced WLF are associated with climatic changes, depending on the amounts of snowmelt, precipitation and evaporation (Brennwald et al. 2004). The WLF in some lakes are caused either by anthropogenic disturbances or hydrologically induced fluctuation, while some lakes' WLF are caused by both, such as in Lake Mead (Barnett and Pierce 2008). However, much of the previous research has concentrated on the impacts of WLF on the hydrological and ecological processes in rivers, large shallow lakes, or small reservoirs (Wantzen et al. 2008). The impacts of WLF on large deep lakes with intense water level decline caused by both anthropogenic disturbances and hydrologically induced fluctuation, such as Lake Mead, until recently have not been well understood (Nash and Gleick 1991, Hoerling and Eischeid 2000).

Lake Mead is the world's largest man-made reservoir, with an area of 635 km2 and a total volume of 35.5 km3. It was formed by the construction of Hoover Dam in the Black Canyon of the Colorado River in the 1930s (Fig. 1). Lake Mead provides recreational opportunities, fish and wildlife habitat, and drinking, irrigation and industrial water for approximately 25 million people (NASA 2003). Approximately 96 percent of the inflow water of Lake Mead comes from the Colorado River, and the outflow from Lake Mead is similar from year to year (NASA 2003). Due to the sustained decrease in runoff from the Colorado River because of global warming, the outflow has exceeded the inflow in Lake Mead for a long time, resulting in a sharp decrease (about 35 m) in the water level since the year 2000. The IPCC Working Group II concludes with very high confidence that there will be a 10–30% run off reduction over some dry regions at mid-latitudes, including the Colorado River Basin, during the next 50 years. This decrease will be caused by increasing temperature and evapotranspiration and decreasing precipitation (IPCC 2008).Therefore, the decline of water level in Lake Mead will be continuing to exist and even get worse. Barnett and Pierce (2008) argued that there is 50% chance that Lake Mead will reach minimum power pool levels by 2017 and become functionally dry by 2021 if the climate changes continue as expected and future water use is not limited.

To manage this valuable water resource in the face of high uncertainty, it is necessary to develop both an improved conceptual understanding and numerical models to support management decisions. Models can be used to investigate projected changes in spatial

and temporal patterns of circulation, mixing, density stratification and ecological processes. Moreover, numerical models can provide a useful method to analyze the impact of different water availability and management scenarios. However, recent research on Lake Mead has primarily focused on field measurements and lab experiments to understand the past and present limnological conditions (Labounty and Burns 2007, Steinberg et al. 2009). Few attempts have been made to predict future hydrodynamic processes should water levels continue to drop.

This study aims at providing a numerical tool to support adaptive management by regional water resources and lake managers. In this study, water age and thermal structure of Lake Mead were simulated using the three-dimensional hydrodynamic model Environmental Fluid Dynamics Code (EFDC) under both high- and low-water surface elevation conditions. Water age is defined as "the time that has elapsed since the particle under consideration left the region in which its age is prescribed as being zero" (Delhez et al. 1999, Gong et al. 2009). Besides, lake water quality and eutrophication processes under various scenarios (e.g., winter and summer, high and low water stages) was predicted by using CE-QUAL-ICM.

The following agencies have provided support for the development of a water quality model:

United States Geological Survey: The USGS has monitored water quantity and quality in Lake Mead since the lake's existence. Ronald J. Veley (USGS personnel) has lent essential support to us by offering meteorological and water quality data at Sentinel Island from Oct 1, 2004 to present.

U.S. Bureau of Reclamation: The USBR is responsible for reservoir operations at Hoover Dam. The products of the study will be beneficial to USBR to evaluate alternative lake operating plans in future. We obtained the data of water stages from USBR.

Southern Nevada Water Authority: The SNWA depends on the Lake Mead as a source of 90 percent of the municipal water to the Las Vegas Valley. We obtained the water quality data of Las Vegas Wash from SNWA.

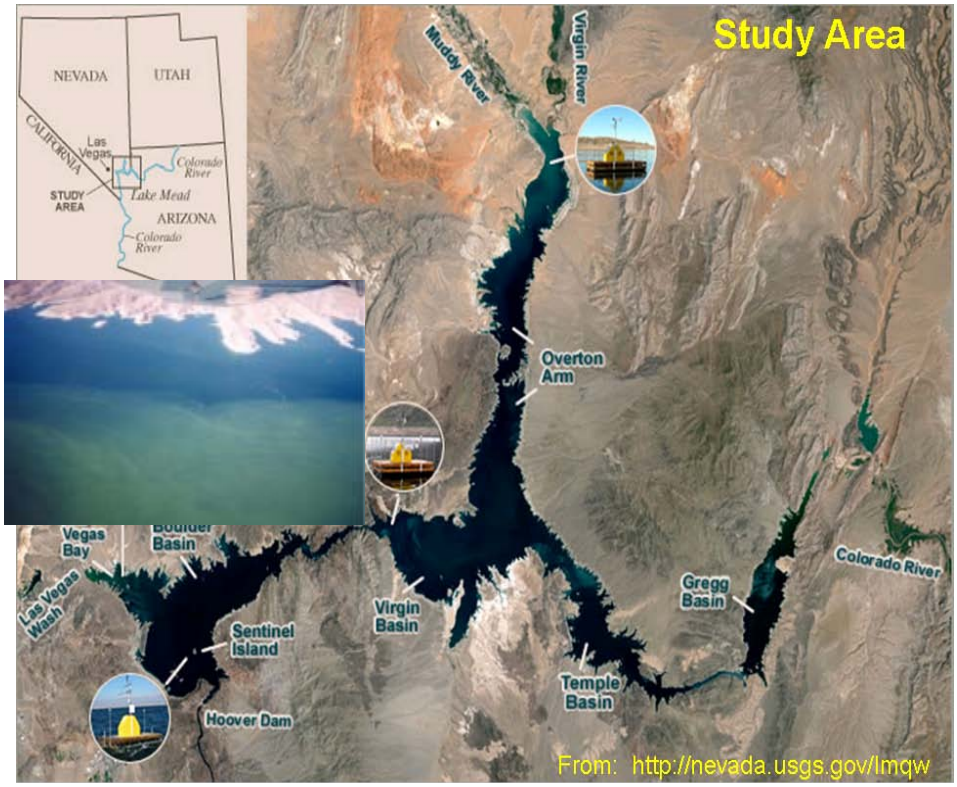

Figure 1. Lake Mead boundary (www.USGS.gov) and insert of an aerial photo of the 2001 algal bloom at Boulder Basin (www.nps.gov)

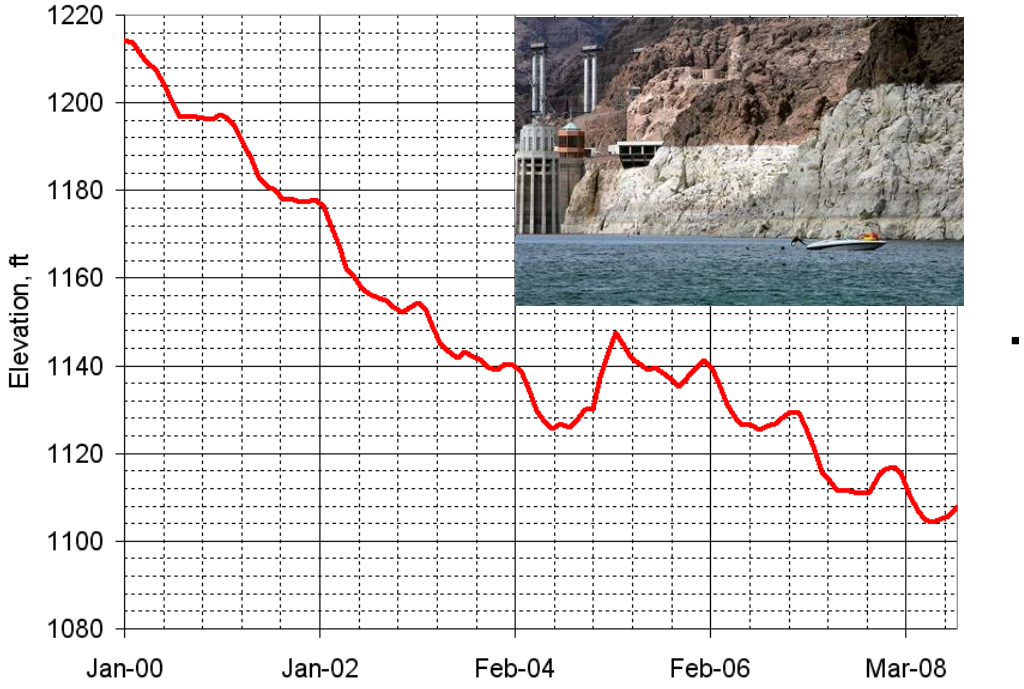

Figure 2. Lake Mead water surface elevation since 2000 (with insert of a photo from www.msnbc.msn.com)

2 Study Objective

The goal of this research was to develop a hydrodynamic and water quality model of Lake Mead to investigate changes in the water age, thermal structure, water quality and eutrophication processes in the lake under various scenarios (e.g., winter and summer, high and low water stages). The model integrates previous water monitoring efforts by the U.S. Geological Survey (USGS), the Sothern Nevada Water Authority (SNWA), and the U.S. Bureau of Reclamation (USBR). The hydrodynamic model applied to Lake Mead was the three-dimensional Environmental Fluid Dynamics Code (EFDC), while the water quality and eutrophication processes were predicted by using CE-QUAL-ICM. Stratified (up to 16 layers) Cartesian computational meshes including both sigma and generalized vertical coordinate (*GVC*) coordinates were employed to simulate the water body in Las Vegas Bay and Boulder Basin. Besides the inflow of Las Vegas Wash and the Colorado River, the model considered atmospheric changes as well as the boundary conditions restricted by the operation of Hoover Dam. The water withdrawn from SNWA intake was also considered.

3 Data

Due to the great regional and national significance of Lake Mead, a large number of federal, state, and local stakeholders are involved in the management and protection of its resources. Concerns over water quality were the impetus for intensive sampling efforts by the U.S. Bureau of Reclamation (USBR), the Southern Nevada Water Authority (SNWA), the U.S. Geological Survey (USGS), and others in Lake Mead over the past 15 years. A partial list of available data is contained in Table 1.

Table 1. Partial list of existing Lake Mead data

Agency	Parameters	Frequency	Stations
USGS	Flow rate	Hourly	LV Wash, Colorado River, Virgin River
	Velocity Field	Continuous	4 stations, starting 2006
	Topography	NA	Bottom bathymetry and land surface
	Water temp., pH, specific conductance, dissolved oxygen, turbidity, fluorescence, air temp., wind velocity, relative humidity. Solar radiation, bar. pressure	4 times daily	4 vertical profiles: LV Bay, near Sentinel Island, Virgin Basin, Overton Basin
USBR	Flow rate and Water Surface Elevations	Hourly	Hoover Dam
	Velocity Field	Monthly	Throughout Lake Mead, 2001-2002
	Water temp., pH, specific conductance, dissolved oxygen, turbidity, ammonia, nitrate, secchi depth, chlorophyll-*a*, phytoplankton, zooplankton	Monthly	12 stations in Boulder Basin, several stations in Virgin, Temple, and Greg Basins
SNWA	Flow rate	Hourly	SNWA intake structures
	Water temp., dissolved oxygen, pH, specific conductance, total	In-situ Daily, Grabs	LA Wash (with the City of Henderson) and Boulder Basin

	dissolved solids, total organic carbon, fecal coliform, phosphate, nitrate, ammonia, chlorophyll-a	bi-weekly	

Although the monitoring efforts have provided an outstanding record of spatial and temporal circulation and water quality trends, this data has not been incorporated into a unifying tool to support management and research efforts. Input data for the 3D model were collected from various investigators/agencies which set their raw data with diverse time scales, formats, and units. The data sets include information of flow discharges (Colorado River and the tributaries), wind speeds and directions, Hoover Dam operations, water temperature, and atmospheric data (rainfall, evaporation, dry/wet bulb ATM temperature, cloud cover, and solar radiation, etc.).

3.1 Bathymetric and Topographic data

The Environmental Fluid Dynamics Code (EFDC) used for the current study is a three-dimensional (3D) hydrodynamic model. A 3D model requires detailed bottom bathymetric data and land topographic data (from above the lake water surface). Lake morphology was obtained using recently conducted sidescan sonar imagery and high-resolution seismic-reflection profiles collected by the USGS and UNLV (Twichell et al. 2003). Figure 3 shows the locations of the survey tracklines. The topographic data from above the lake water surface were obtained from a USGS Data Digital Elevation Model (DEM). Figure 4 shows the discretized bottom elevations of the study domain by using the computational mesh.

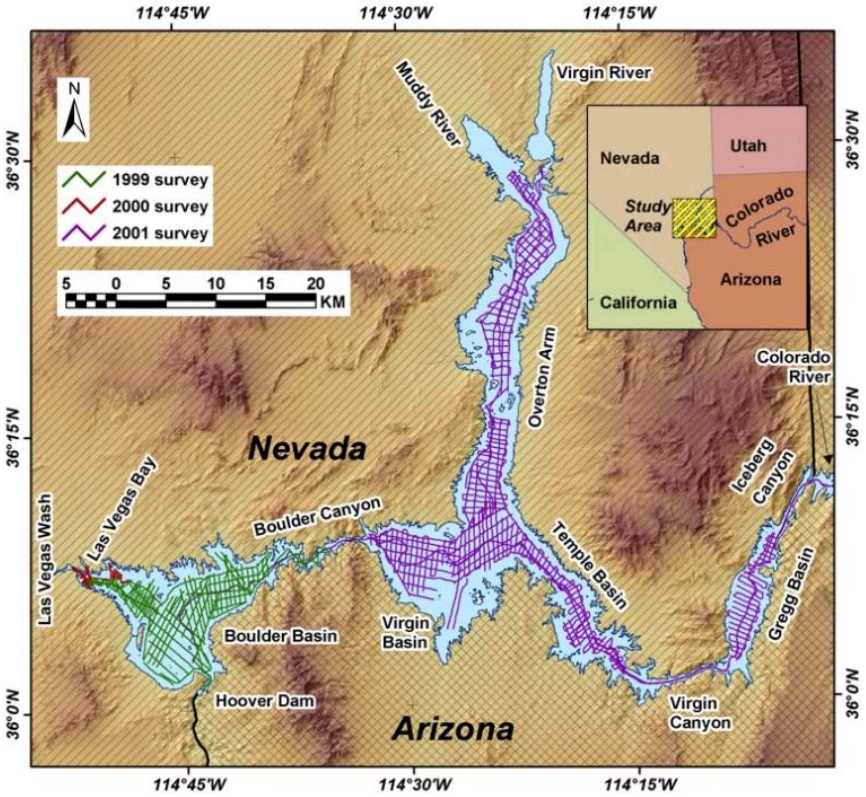

Figure 1. Map showing the location of the survey tracklines (Twichell et al. 2003)

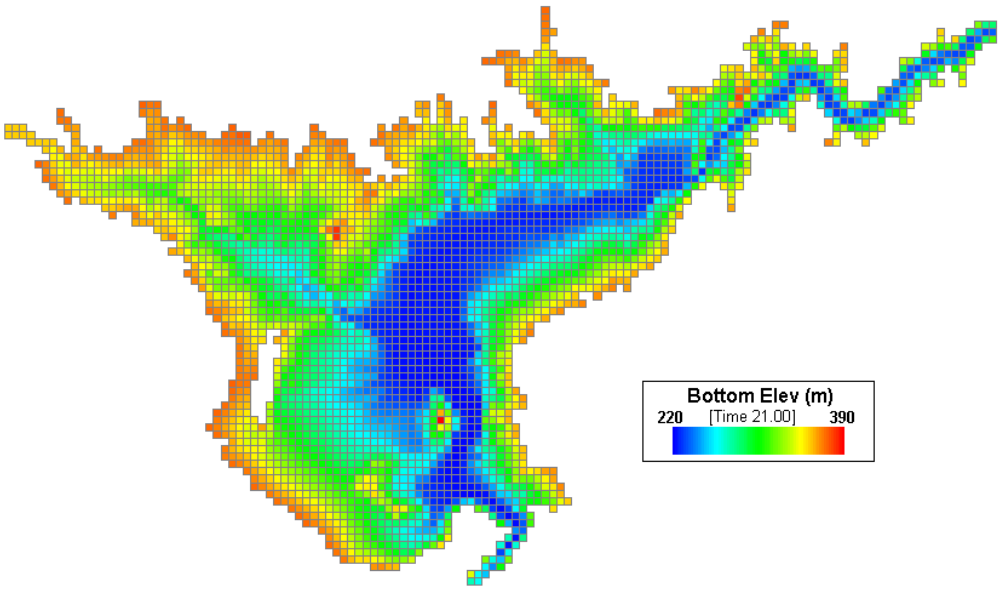

Figure 2. Bottom Elevations discretized with the computational mesh

3.2 Flow data

Flow data include Las Vegas Wash inflow, Colorado River inflow, Hoover Dam outflow, and SNWA Pumping rate. The USGS flow gage (#09419700) located at Pabco RD near Henderson, NV and flow gage (#09421500) located on the Colorado River below Hoover Dam take a good record of flow discharges of the Las Vegas Wash and Hoover Dam outflow, respectively. The SNWA pumping rates in summers and winters were obtained by personal communication with SNWA personnel. There is no USGS gage in the Boulder Canyon. However, the Colorado River inflow data could be calculated by mass balance method since we were simulating steady flow cases. Table 2 summarizes all the flow data we used in the four model scenarios.

Table 2. Flow boundary conditions

	August 1998	January 1999	August 2007	January 2008
Colorado River	623.15	438.91	449.48	623.15
Las Vegas Wash	5.95	7.36	9.83	5.95
SNWA Pumping	-20.22	-8.27	-20.22	-20.22
Hoover Outflow	-608.88	-438.01	-439.09	-608.88

Note: The unit of discharges is m^3/s. Negative values mean outflows.

3.3 Lake Mead Water-quality and Atmospheric Data

The U.S. Geological Survey, in cooperation with the Southern Nevada Water Authority and the national Park Service (NPS) is monitoring water quality on a "real-time" basis at five floating platforms on Lake Mead (http://nevada.usgs.gov/lmqw/). Two of the platforms are located in the Boulder Basin of Lake Mead, in Las Vegas Bay and near Sentinel Island. In addition to monitoring water quality, meteorological data are collected at the Sentinel Island platform, in cooperation with the Clark County Water Reclamation District. Table 3 listed the water quality and meteorological parameters measured at the Sentinel Island platform. Among other atmospheric parameters, evaporation impacts have not been considered in this project which may result in some uncertainty.

Table 3. Lists the water-quality and meteorological parameters measured at the Sentinel Island platform.

1. Water Temperature	7. Air Temperature
2. pH	8. Wind Speed and Direction
3. Specific Conductance	9. Relative Humidity
4. Dissolved Oxygen	10. Solar Radiation
5. Turbidity	11. Barometric Pressure
6. Percent Fluorescence	

3.4 Lake Mead Water Surface Elevation

Lake Mead water surface elevations (WSE) at Hoover Dam are recorded hourly by USBR (http://www.usbr.gov/lc/region/g4000/hourly/mead-elv.html). Figure 5 illustrates the WSE change from January 1998 to present (May 2009). The WSE has been dropped more than 35 meters in the past 10 years. As of May 2009, the lake is currently at 43 percent of its capacity, threatening to make the Las Vegas valley's primary raw water intake inoperable. Table 4 shows the WSE values used in the model as initial conditions.

Table 4. Lake Mead Water Surface Elevations (WSE) used in the model

	August 1998	January 1999	August 2007	January 2008
WSE (m)	370.12	369.69	338.89	340.30

Figure 3. Lake Mead Water Surface Elevation at Hoover Dam (data from USBR)

4 Methods of Analysis

4.1 Introduction to EFDC

The three-dimensional (3D) Environmental Fluid Dynamics Code (EFDC) is one of the most widely used hydrodynamics modeling codes. EFDC has a state-of-art 3-D hydrodynamics code that is designed to simulate complex, hydrodynamic processes in rivers, lakes, and estuaries. Its capabilities include, among others, stratified flow modeling, wetting and drying processes, atmospheric forcing, wind- and boating-driven waves and their resulting shear forces on the sediment bed, Coriolis forces, and full water quality modeling (Hamrick 1992). Figure 6 shows the Boundary Condition (BC) interface of EFDC-Explorer3.

Thermal structure and water age of Lake Mead were simulated using hydrodynamics and water quality modules of the EFDC in this study. The water age is ”zero” at inflow inlets of connecting rivers and the age at a given location in the horizontal or vertical domain represents the ‘time elapsed’ for a dissolved substance to be transported from its source to that location. In this study, temperatures were simulated by using the surface heat exchange algorithm from CE-QUAL-W2 (version 3.1, Cole and Wells 2005), while water age was computed based on tracer and age concentrations as (Ji et al. 2007):

$$\frac{\partial c(t,\vec{x})}{\partial t} + \nabla(uc(t,\vec{x})) - K\nabla c(t,\vec{x}) = 0 \qquad (1)$$

$$\frac{\partial \alpha(t,\vec{x})}{\partial t} + \nabla(u\alpha(t,\vec{x})) - K\nabla\alpha(t,\vec{x}) = c(t,\vec{x}) \tag{2}$$

where c is the tracer concentration, α is the age concentration, u is the velocity field in space and time domains, K is the diffusivity tensor, t is time and $\vec{x}$ is coordinate. The average "α" can be calculated as:

$$\alpha(t,\vec{x}) = \alpha(t,\vec{x}) / c(t,\vec{x}) \tag{3}$$

The above equations were solved with specified initial and boundary conditions.

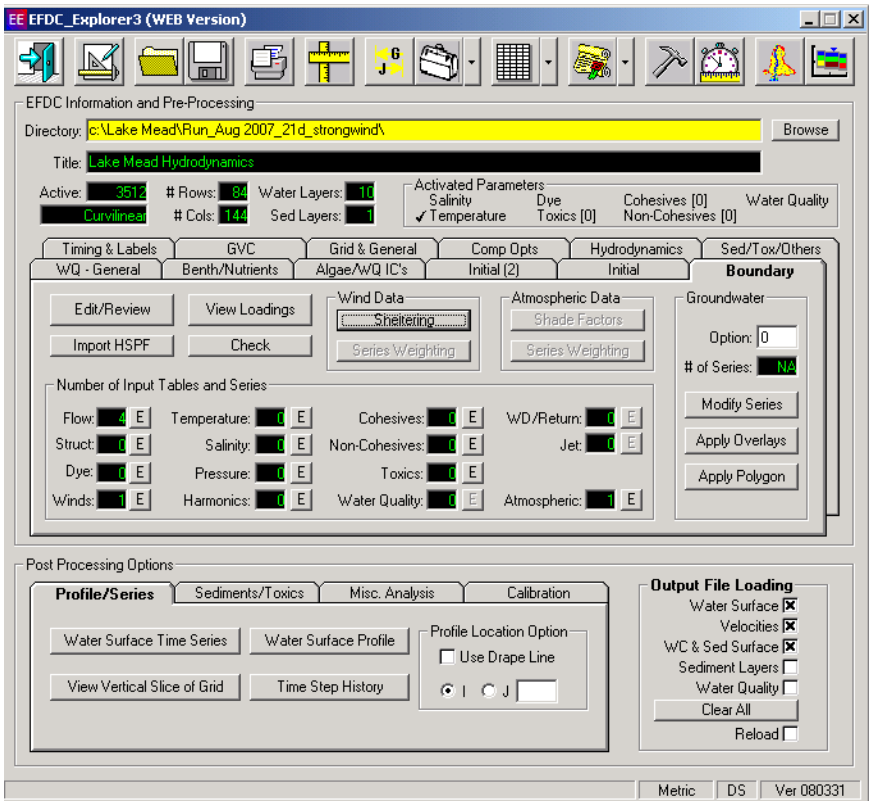

Figure 4. Boundary Interface of EFDC-Explorer3

4.2 Modeling Scenarios

Water age and thermal structure of Lake Mead were modeled using the three-dimensional hydrodynamic model Environmental Fluid Dynamics Code (EFDC). The model was calibrated using observed data from 2005 and then applied to simulate two scenarios: the year 2000 with an initial water level of 370.0 m and the year 2017 with a projected initial water level of 320.0 m. The high-stage simulation of 2000 described pre-drought lake hydrodynamics while the low-stage simulation of 2017 projected how lake circulation could respond under significant lake drawdown, should drought conditions persist.

There are four simulated cases for water quality modeling: (1) high-stage simulation (August 1998) with a lake stage of 370.12 m; (2) high-stage simulation (January 1999) with a lake stage of 369.69 m; (3) drawdown simulation (August 2007) with a lake stage of 338.39 m; and (4) drawdown simulation (January 2008) with a lake stage of 340.30 m. The high-stage simulations described the pre-drought lake mixing processes while the drawdown simulations shed light on the drawdown impact on such processes.

4.3 Mesh Generation

The study area was restricted to Las Vegas Bay and Boulder Basin due to data availability and the significance of this region to water management (outflow through Hoover Dam and outtakes for southern Nevada are located in this region). Water quality and eutrophication processes were predicted by using generalized vertical coordinate (*GVC*) coordinates, while Sigma coordinates were employed to simulate the water edge and thermal structures.

The uniformly stratified (30 layers) Cartesian computational mesh (sigma coordinates) was generated using the EFDC-Explorer3 pre-processor and constructed in a rectangular and vertical sigma-stretched coordinate system. It contained 3512 cells in the horizontal plane with a uniform grid size of 216 m, while the vertical cell thickness was determined by the local water depth.The 3D mesh is generated by using the EFDC-Explorer3 pre-processor. To generate the mesh, XYZ (topography) and DS (domain boundary) files are needed. Both XYZ and DS file are created in ArcMap 12.0 based on bottom bathymetric data and land topographic data described in Section 3.1. Figure 7 and 8 show the computational meshes for high-stage and drawdown simulation cases, respectively. The colors in Figure 7 and 8 demonstrate the water depth and it can be seen that the main channel thalweg (the lowest points along the length of the valley) is close to east shore of Boulder Basin; the Las Vegas Bay is relatively shallow area. Comparing Figure 7 with Figure 8, the drop of lake level in drawdown simulation cases is more than 30 meters. In addition, the lake surface area has been dramatically reduced. The dry nodes due to lake level drop are illustrated with grey color in Figure 8.

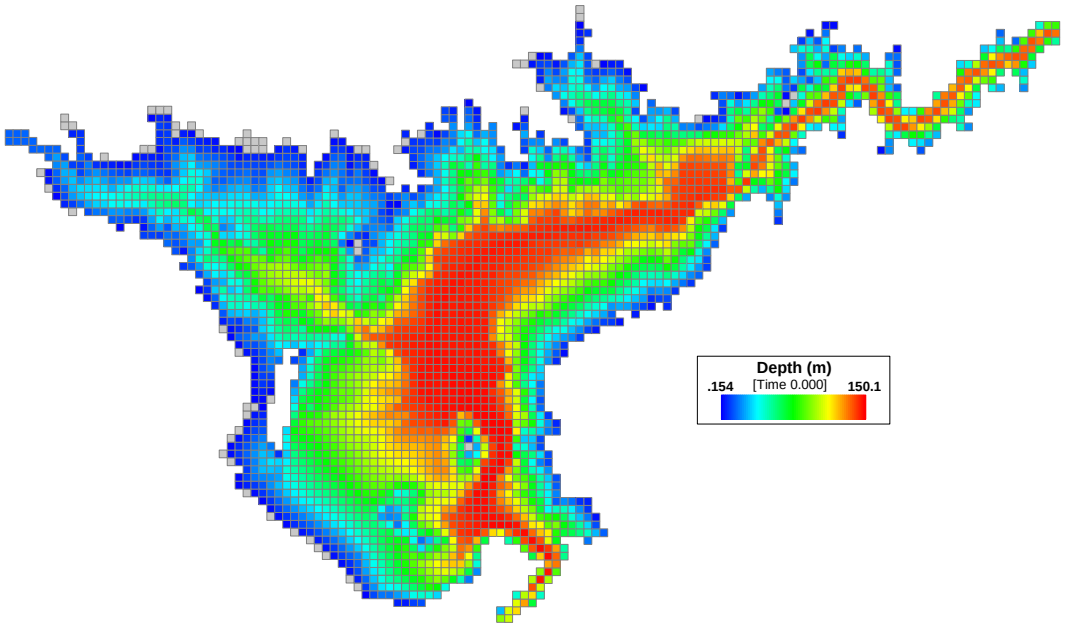

Figure 5. Computational mesh of high-stage simulation cases

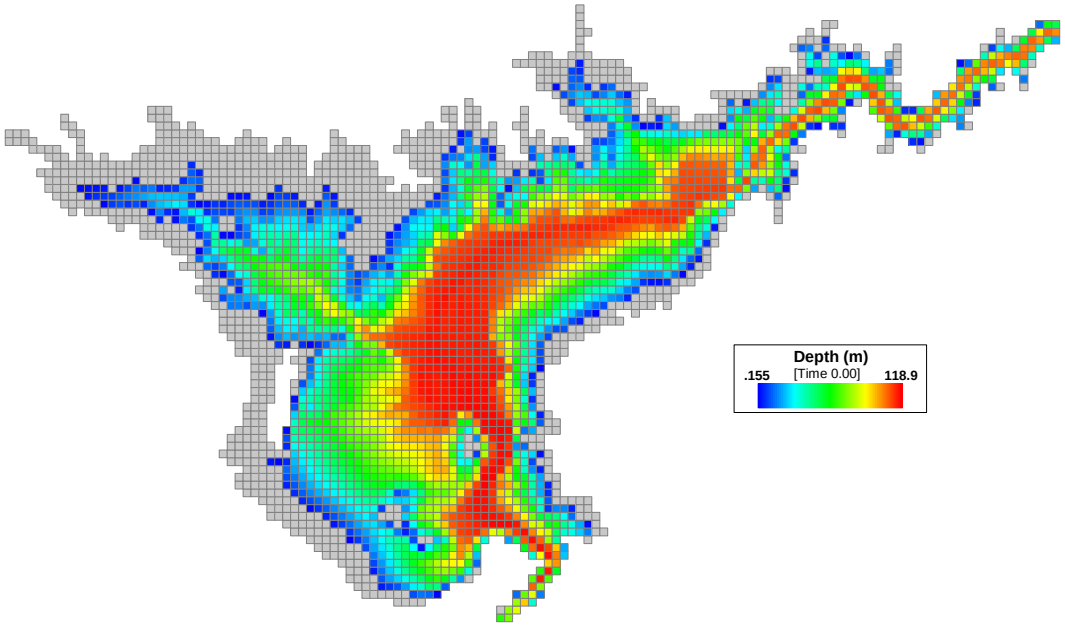

Figure 6. Computational mesh of drawdown simulation cases

4.4 Initial and Boundary Conditions

Initial conditions included water surface evaluations, water column and bed temperatures, while boundary conditions consisted of atmospheric forcing, surface wind stress, lake inflows and outflows. Temperatures of the water column and lake bottom were initialized as the observed values at Las Vegas Bay and Sentinel Island when computational time equals zero. Temperature data was obtained from the USGS Water Quality Monitoring program, which operates five monitoring platforms in Lake Mead that record water temperature profiles every six hours. Water surface elevations, including initial values and the following time series, were obtained from the U.S. Bureau of Reclamation.

Lake inflow and outflow data were derived from USGS gauges on the Las Vegas Wash (gauge #09419700) and Hoover Dam (gauge #09421500), and the U.S. Department of the Interior provided pumping rates of the intake structure located near Saddle Island (Vermeyen 2003). Figure 9 shows the geographic locations of the four flow boundaries. To access better water quality and prepare for the inevitable future drought, a new SNWA intake (No. 3), which is located close to the north shore, has been under construction. In the present study, we considered the currently-used intake (No.2) which is located south-east of the Saddle Island (See Figure 9). The flows at the boundary locations have been distributed vertically within 10 layers assuming the horizontal resultant velocities follow the traditional logarithmic law along the vertical.

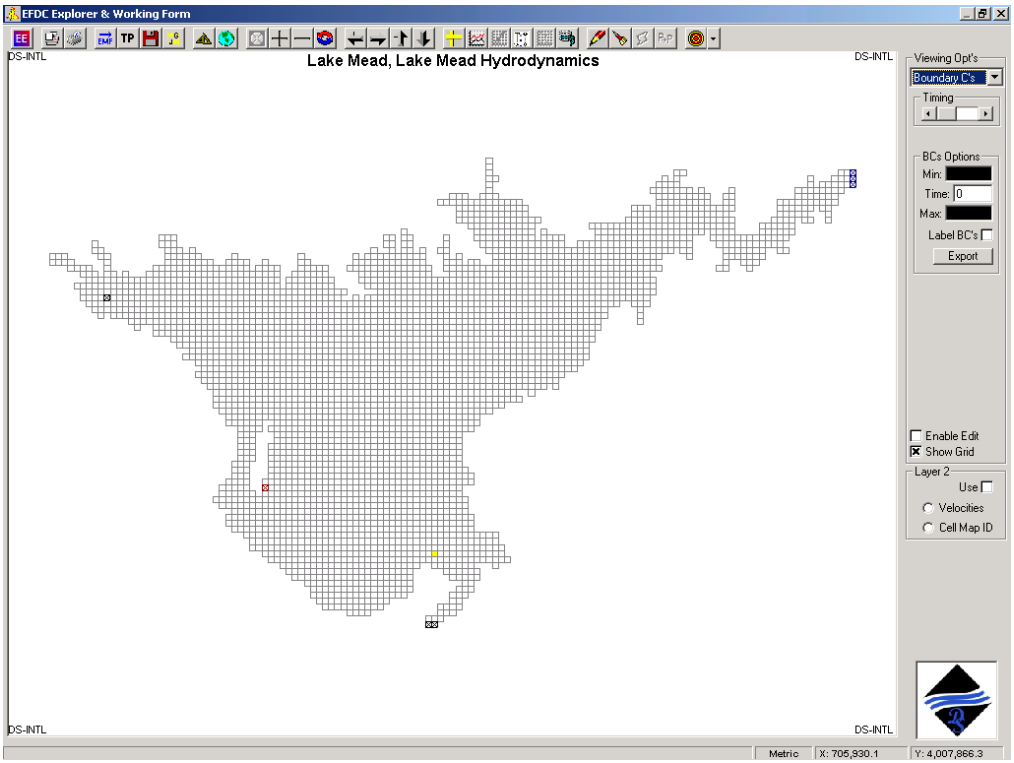

Figure 7. Geographic Locations of the four flow boundaries

Meteorological data were also obtained for the USGS monitoring platforms and included solar radiation, wind speed and direction, relative humidity, air temperature and barometric pressure. Figure 10 and 11 show the time series of wind speed (m/s) and wind direction (Degree) in August 2007 and January 2008, respectively. Based on Figure 8 and 9, summer winds mainly blow toward south-east (90-180 degree) with a daily periodicity and an averaged value 3.67 m/s, however, almost all the winter winds blow northward with less periodic characteristic and the speed magnitude ranges from 2.5 to 10 m/s. Wind speeds and directions in the cases of August 1998 and January 1999 are assumed to be the same as ones in August 2007 and January 2008, respectively.

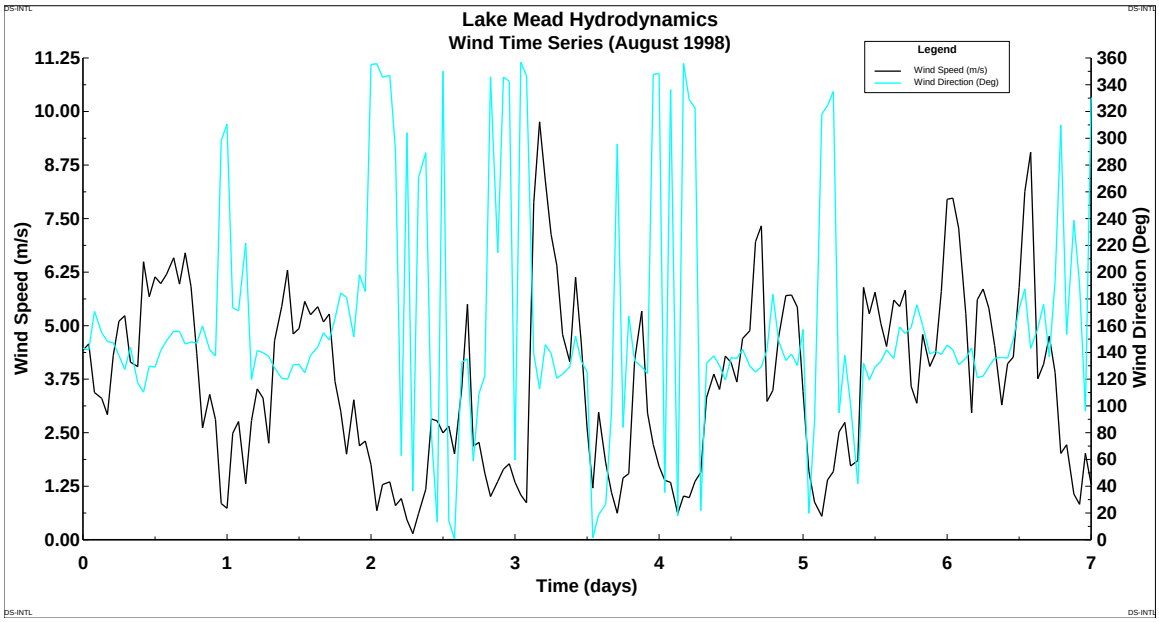

Figure 8. Time series of wind speed and direction (August 2007)

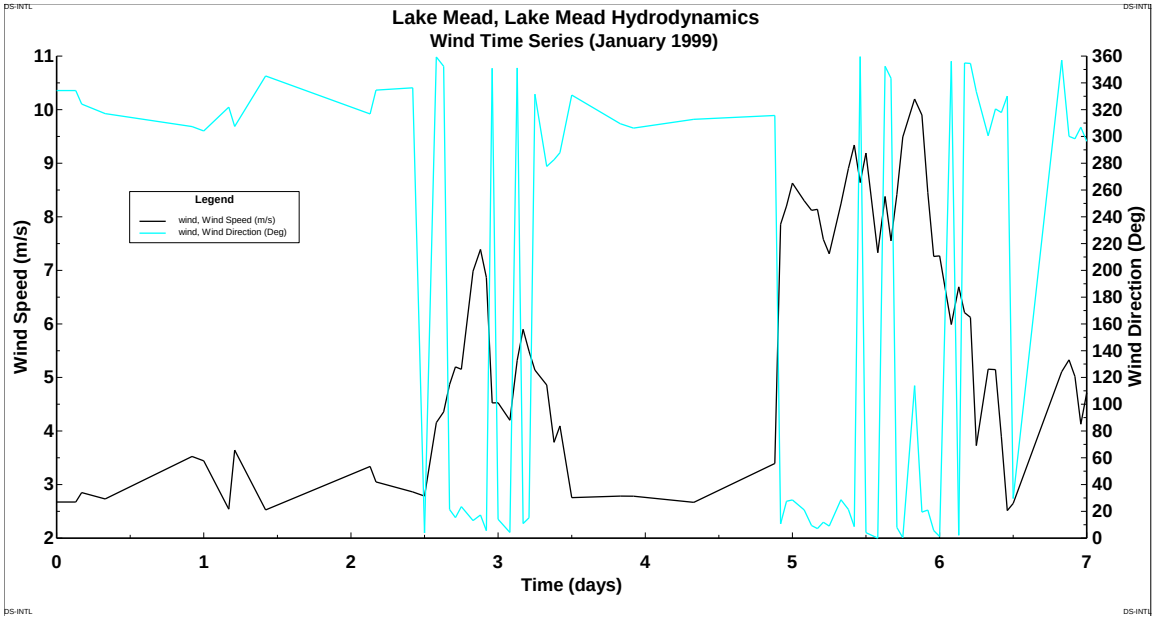

Figure 9. Time series of wind speed and direction (January 2008)

4.5 Turbulent Parameters and other Input Data

Turbulence in the lake leads to mixing. The formulation of the governing equations for ambient environmental flows characterized by horizontal length scales which are orders of magnitude greater than their vertical length scales begins with the vertically hydrostatic, boundary layer form of the turbulent equations of motion for an incompressible, variable density fluid. More details regarding the turbulent equations and the external mode solutions (used in this study) could be found in EFDC manual (Hamrick 1992), while determination of several import turbulent parameters in this study are addressed in the present section.

Those parameters include horizontal eddy viscosity, dimensionless horizontal momentum diffusivity, vertical eddy viscosity, and vertical molecular diffusivity. The horizontal eddy viscosity, AH, is determined as suggested by Smagorinsky (1963) when the AH is used to represent subgrid scale mixing. The classical Smagorinsky eddy viscosity turbulence model for the incompressible NS equations is obtained by replacing the given constant viscosity by the artificial turbulent eddy viscosity which depends on the local velocity. Figure 12 shows an example of AH distribution in the 10^{th} layer (top) at T = 0 (initial). As shown in Figure 12, AH values range from 1.0 m^2/s to 3.2 m^2/s.

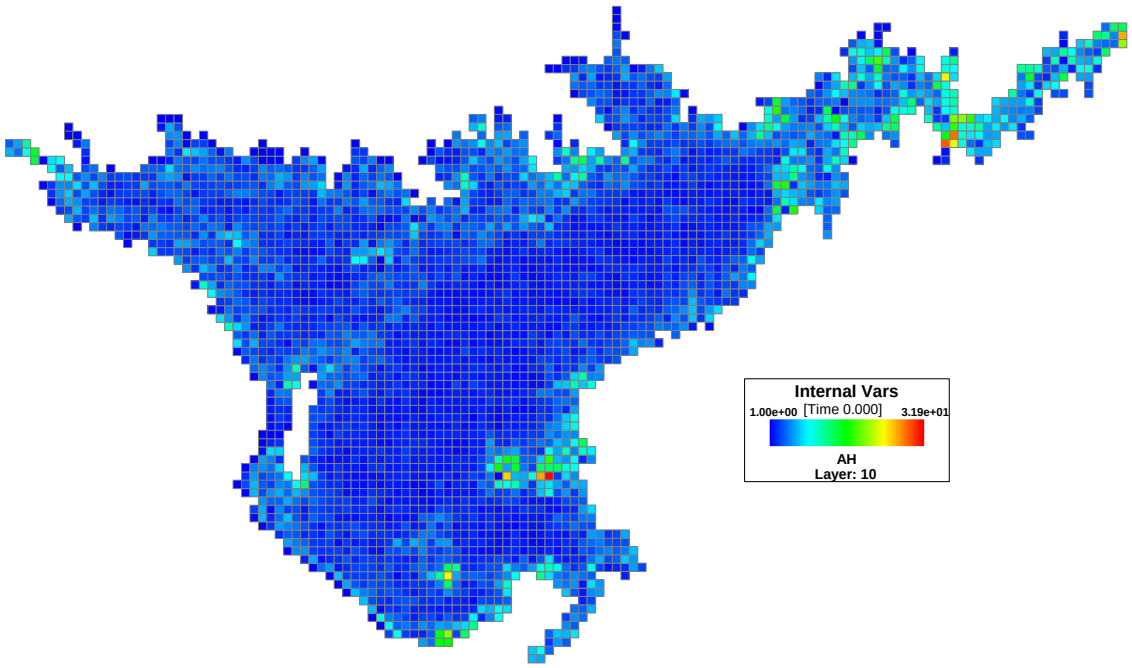

Figure 10. Distribution of AH values of the 10^{th} layer at T = 0 (Aug. 1998)

Because the lake has stratification, vertical displacement must work against the buoyancy force. Therefore, vertical mixing requires more energy than horizontal mixing; horizontal mixing along surfaces of constant density is much larger than vertical mixing across surfaces of constant density. In this study the vertical eddy viscosity was set to 0.0001 m^2/s. Table 5 summarized several other parameters used in the model.

Table 5. Values of several parameters used in the model

Parameter	Description	Unit	Value
ΔT	Adaptive time step	Second	1-15
HDRY	Critical dry water depth	m	0.5
HWET	Critical wet water depth	m	0.51
AHO	Constant horizontal momentum and mass diffusivity	m2/s	1.0
AHD	Dimensionless horizontal momentum diffusivity	Dimensionless	0.2
AVO	Background kinematic eddy viscosity	m2/s	0.001
ABO	Background molecular diffusivity	m2/s	1E-09
AVMN	Minimum kinematic eddy viscosity	m2/s	1E-04
ABMN	Minimum eddy viscosity	m2/s	1E-08
Z0	Bottom roughness height	m	0.02
SWRATNF	Extinction coefficient for pure water	m-1	0.45
DABEDT	Thickness of active bed temperature layer	m	5
TBEDIT	Initial bed temperature	ºC	12
WSC	Wind sheltering coefficient	Dimensionless	1.0
FSWRATF	Solar radiation absorbed in surface layer	Dimensionless	0.45
HTBED1	Convective heat transport coefficient between bed and bottom water layer	Dimensionless	0.003
HTBED2	Heat transport coefficient between bed and bottom water layer	Wm-2 ºC -1	0.3

5. Model Calibration

Lake stage and temperature profiles at Sentinel Island between 1 March and 31 October 2005 were used to calibrate the EFDC. The main calibrated parameters included horizontal and vertical eddy viscosities and diffusivities, bottom roughness height, wind sheltering coefficient (which affects the hydrodynamic process) and several parameters related to temperature simulation. The turbulence parameters related to the Mellor-Yamada turbulence model (Mellor and Yamada 1982, Galperin et al. 1988) were treated as constants and their values were the same as the ones used in other hydrodynamic models, such as the Princeton Ocean model (Mellor 1990) and the Estuary, Coastal and

Ocean model (HydroQual 1991). A stepping time step, usually ranging from 1.0 to 15.0 seconds, was used in this study rather than a fixed time step. To adapt to the rapid decline and fluctuation of water levels, a moving water surface boundary was applied in the model by assigning a critical dry water depth (0.5m) and a wetting/drying procedure proposed by Hamrick (1994). Bottom roughness height (z0) is often adjusted for water level calibration; in this study, it was set as a typical value of 0.02 meters (HydroQual 2001, Hamrick 1992).

The comparison of time series of lake water levels between observed values and calibrated results at Sentinel Island illustrated that calculated lake water levels presented greater fluctuation than observed values because the observed values were daily averages (Fig. 13). The calibrated and monitored temperature time series at the surface, middle and bottom water layers at Sentinel Island (Fig. 14) showed that an apparently strong agreement was achieved for the calibrated temperature time series at the top and median water layers. However, the calibrated temperature time series at the bottom water layer diverged to a certain extent from the observation. The error is believed to be from the pressure gradient error caused by the sigma coordinate transformation. Detailed discussion regarding the sigma pressure gradient error is discussed in the section 5.2.
To quantify the errors and assess the calibration performance, the Absolute Mean Error (AME) and Mean Absolute Relative Error (MARE) were used to assess the performance of the model due to its direct interpretability.

$$AME = \frac{\sum |Modeled - Observed|}{number\ of\ observations} \tag{4}$$

$$MARE = \frac{\sum (|Modeled - Observed| / Observed)}{number\ of\ observations} \times 100\% \tag{5}$$

The calculated AME and MARE for water level errors was 0.084 m and 0.02%, respectively, which indicates that the calibration results are accurate enough to set up model parameters. The AMEs for surface, middle and bottom water temperatures were 1.51 ºC, 1.04 ºC and 1.42 ºC, respectively. Correspondingly, the MAREs for them were 7.3%, 6.9% and 10.9%.

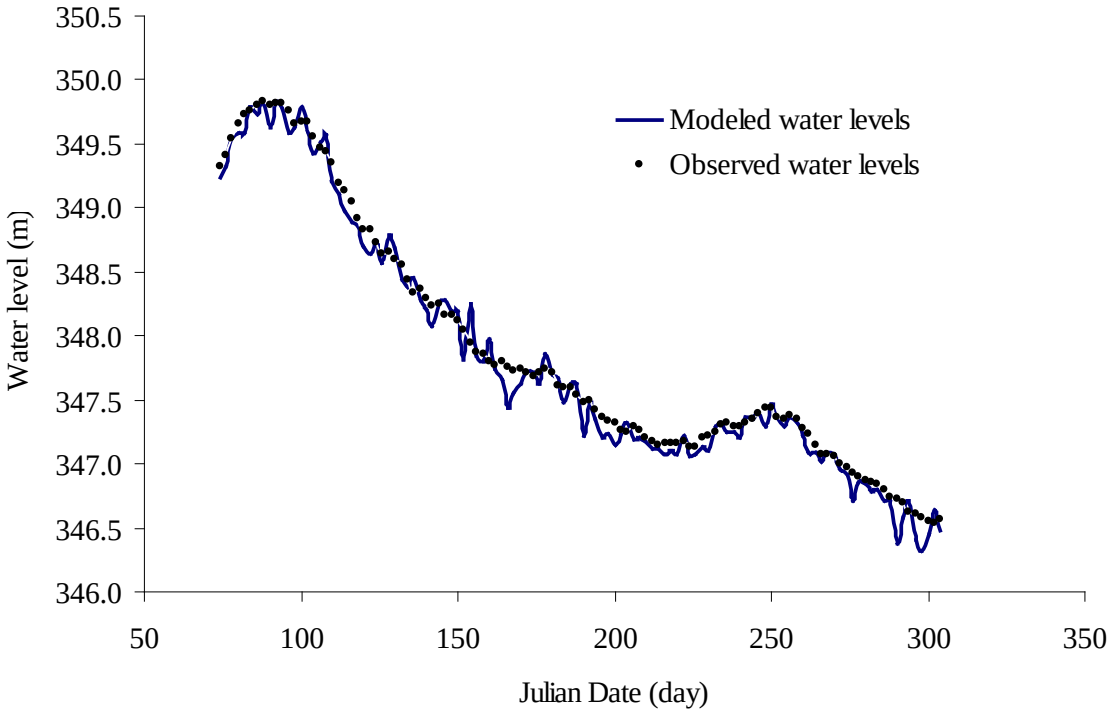

Figure 13 Time series of the simulated water level (solid line) and the observed data (dotted points) at Sentinel Island

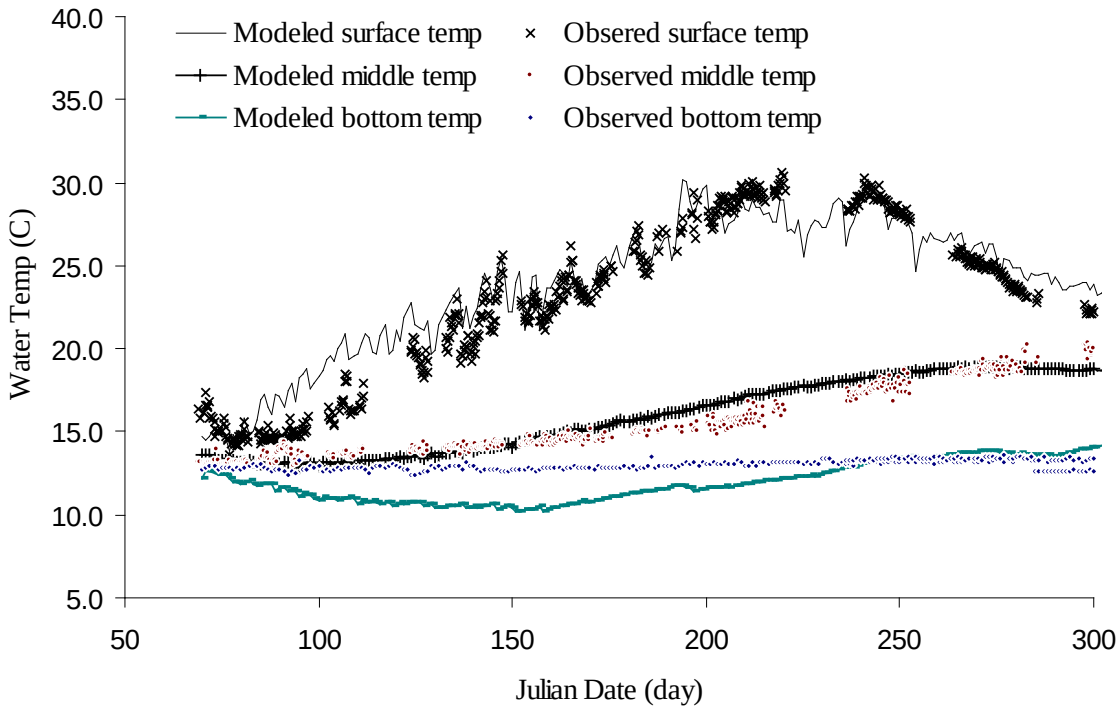

Figure 14 Time series of temperature calibration results at surface, middle and bottom water column from March 1 to October 31, 2005 at Sentinel Island

6. Computational Results of Water Age and Thermal Structures

The calibrated model was applied to calculate water ages and thermal structures in Lake Mead under two scenarios: 1) a high-stage situation in the year 2000 with an initial water level of 370.0 m (LMWD 2009) and 2) a drawdown scenario in the year 2017 with an initial water level 320.0 m, which is the minimum power pool level for Lake Mead (Barnett and Pierce 2008). This condition represents one possible scenario should the current drought condition on the Colorado River continue into the next decade. The total drop of water level is approximately 50 m between the two scenarios, and the water volume decrease is 18.5 km3 (from 30.8 to 12.3 km3) from year 2000 to 2017 (LMWD 2009). The maximum water depth would drop to 100 m in 2017 from 150 m in 2000 (Fig. 5). Thus, the decline in water depth, volume and water surface area would be approximately 35%, 50% and 40%, respectively, between the two scenarios. To assess the sole impact of water level drawdown, other boundary conditions (i.e., meteorology, discharge and initial water temperature) were assumed to be the same for the 2017 condition as those used in the calibration scenario. Each model was simulated for 365 days.

6.1 Characteristics of temperature and water age in Lake Mead

Temperature and water age were selected to study the impact of water level drawdown as indicative parameters of thermal regime and hydrodynamic processes. The temporal distributions of these two parameters were investigated over the 2000 simulation at two representative locations in a shallow region (site A) and a deep region (site B) (Fig. 15). Site A (36.47472° N; 114.80889° W) is located near the center of Las Vegas Bay and site B (36.06194° N; 114.74200° W) is located off the northeast corner of Saddle Island. Water depths at sites A and B were 88 m and 150 m at the initial day of the 2000 simulation and 38.0 m and 100 m for the initiation of the 2017 simulation. The results showed that lake temperature profiles changed seasonally, with warm and thermally stratified conditions in the summer and cool isothermal conditions in the winter (Fig. 16). The stratification duration was approximately 220 days in 2000. Minimum temperatures of approximately 11 ºC were generally found in December–February, while temperatures exceeding 28 ºC were persistent through much of the summer. The maximum temperature differences between surface and bottom layers during thermal stratification were approximately 18 ºC in deep regions and 12 ºC in shallow regions. The time series of water temperature in different layers of the water column (surface, middle and bottom) demonstrated the close relationship between surface water temperatures and air temperature, whereas the bottom water temperatures varied spatially amongst the lake regions. During the thermal stratification period, the bottom temperatures in shallow regions (site A) were 5–8 ºC higher than that of deep regions, while the surface temperatures were fairly uniform across the lake. It can also be seen that the duration of thermal stratification in shallow regions (~200 days) was 50 days shorter than that of deep regions (~260 days).

To improve understanding of transport in this complex hydrodynamic system, the water age was considered as an indicator of the transport timescales of dissolved substances. The water age in Lake Mead illustrated high spatial and temporal heterogeneity. The time series of water age profiles for shallow conditions (site A) (Fig. 17a) indicated that water age increased throughout the simulation, suggesting minimal interaction with incoming flow from the Colorado River over the simulation period. For site B (Fig. 17b), water ages of the surface and middle layers appeared to approach their maximum values, whereas the bottom layer water age continued to increase throughout the simulation period. In general, the maximum depth-averaged water age was 220 days for the shallow region (site A) and 190 days for the deep region (site B) during the year 2000 simulation period. By comparing the vertical distribution of water age (Fig. 17), it was found that the vertical distribution of water age was quite uniform for the shallow condition whereas significant variations were found in the deep region. For example, water age at Day 365 in the surface, middle and bottom layers of the deep region (site B) were 178 days, 211 days and 266 days, respectively, suggesting that a higher degree of water exchange occurs in the surface water than in the bottom water.

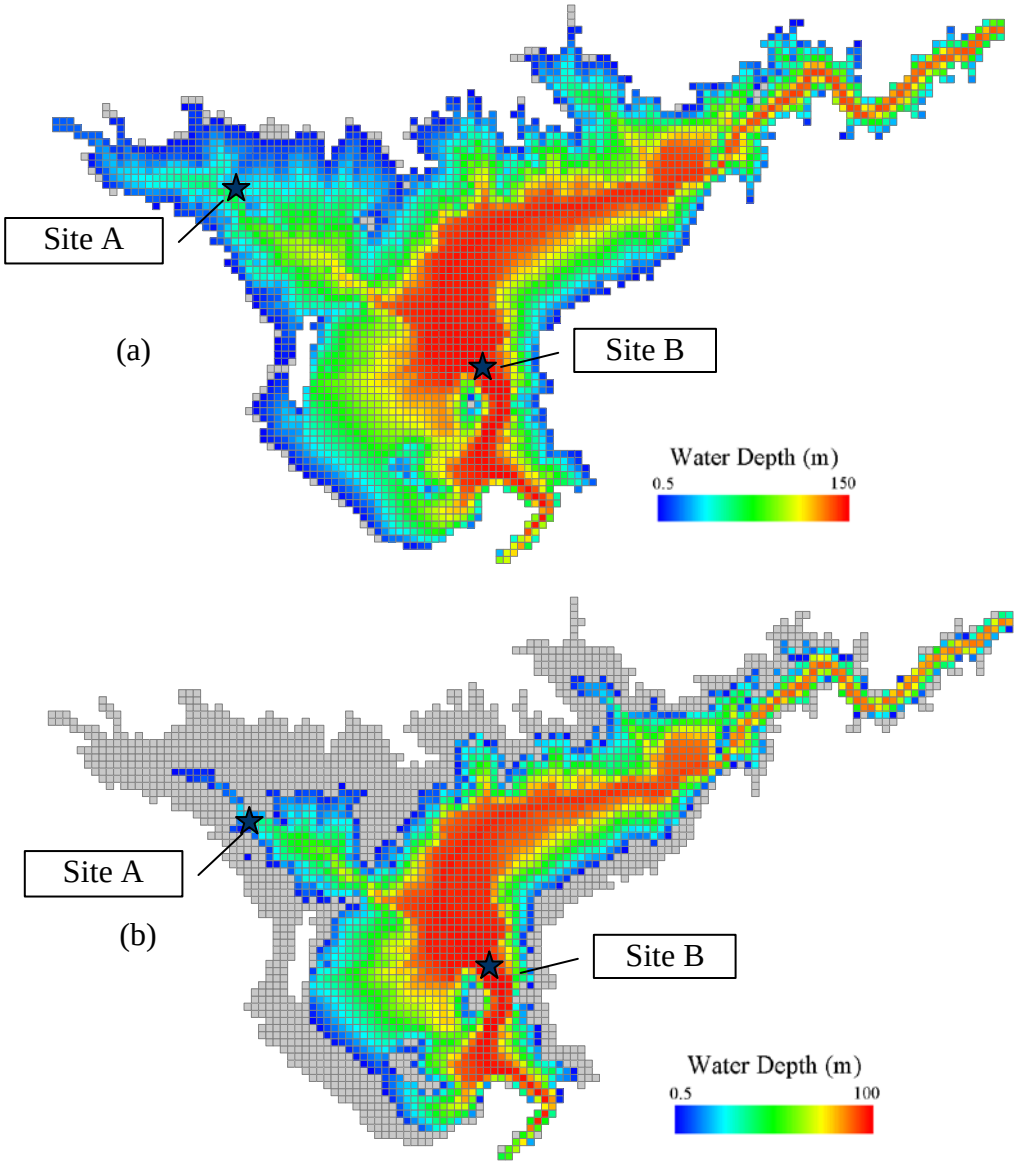

Figure 15 Water depths in the 1st day of 2000 (a) and 2017 (b)

Sites A (36° 6'28.80"N, 114°48'31.99"W), B (36° 3'43.02"N, 114°44'31.21"W) are used in Figs.6, 7 &8 for analysis

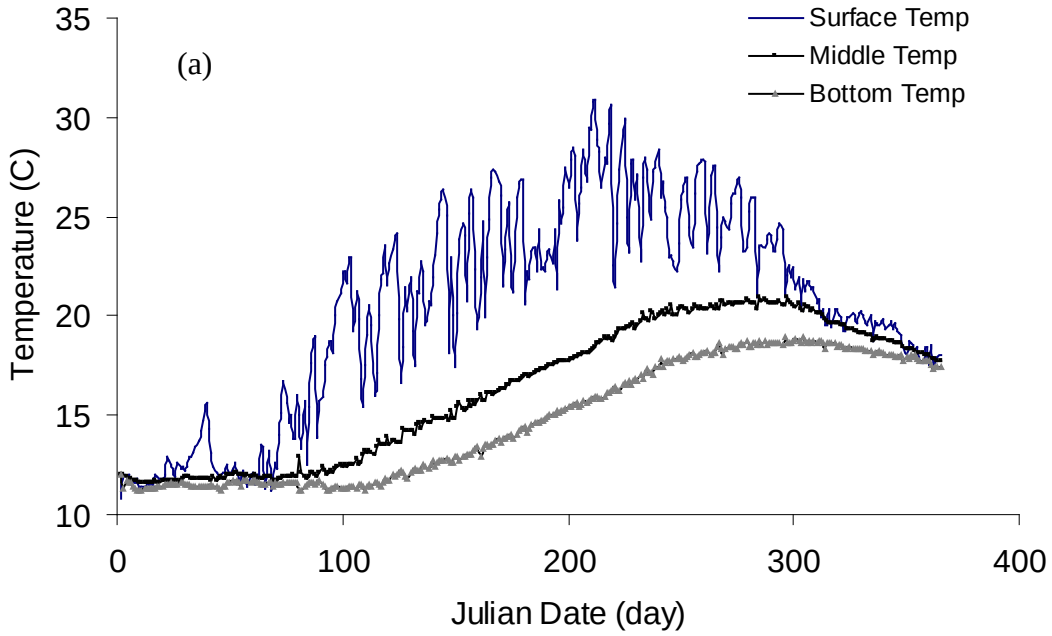

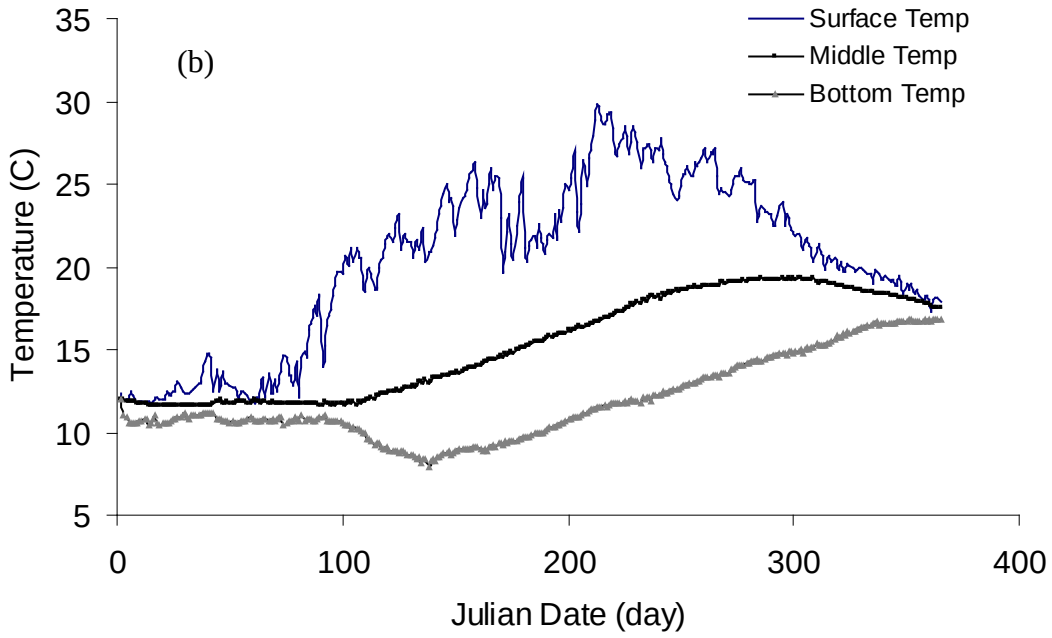

Figure 16 Calculated time series of temperature at Site A (a) and B (b) in 2000

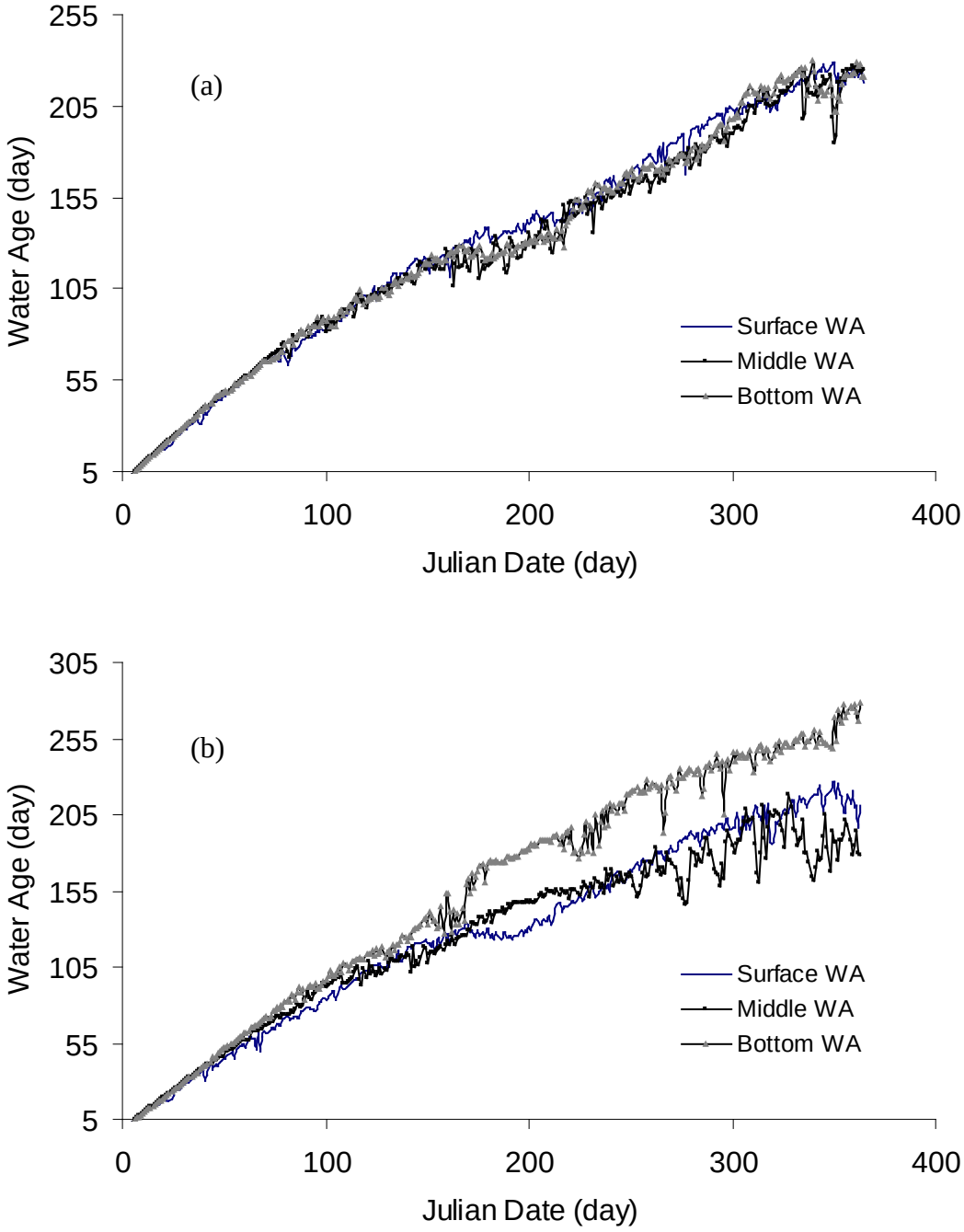

Figure 17 Calculated time series of water age at Site A (a) and B (b) in 2000

6.2 Impact of water level drawdown on temperature stratification

Temporal patterns of water temperature were investigated over the entire 2000 and 2017 simulations at sites A and B. The results indicated that the extent and duration of thermal stratification were strongly influenced by declining water levels (Fig. 18a). Although the depth-averaged temperatures changed only slightly during winter months (December–February), there was a progressive increase in depth-averaged temperature differences from March through August (from Day 90 to Day 250 in Julian Date) due to the reduced water surface. The maximum depth-averaged temperature difference (ΔT between the years 2000 and 2017) at sites A and B were 4.3 ºC on 26 July (Day 208) and 2.5 ºC on 21 August (Day 234), respectively.

Changes in temperature (ΔT) between 2000 and 2017 at the water surface, lake bottom and the depth-averaged condition were investigated during the periods with strong thermal stratification (Fig. 9). The results indicated large ΔTs in shallow regions. For instance, the depth-averaged water temperature increased by 4–7 ºC for shallow regions versus 2–4 ºC for deep regions. Temperature shifts were influenced by location in the water column. For example, for the depth-averaged water temperatures (Fig. 19a), the regions with $\Delta T > 2$ºC and with $\Delta T > 5$ ºC accounted for 99.9% and 15.7% of the total water surface area, respectively. However, for the water surface layer (Fig. 19b), the percentages of the water surface area with $\Delta T > 2$ºC and > 5 ºC were 30.1% and 0.2%, respectively. The corresponding values for the bottom water layer (Fig. 19c) were 76.9% and 30.4%, respectively. In other words, the water in deeper layers displayed greater warming under low water levels than did the water higher in the water column. The water surface is more strongly influenced by the atmospheric boundary conditions, which were considered to be the same in this study.

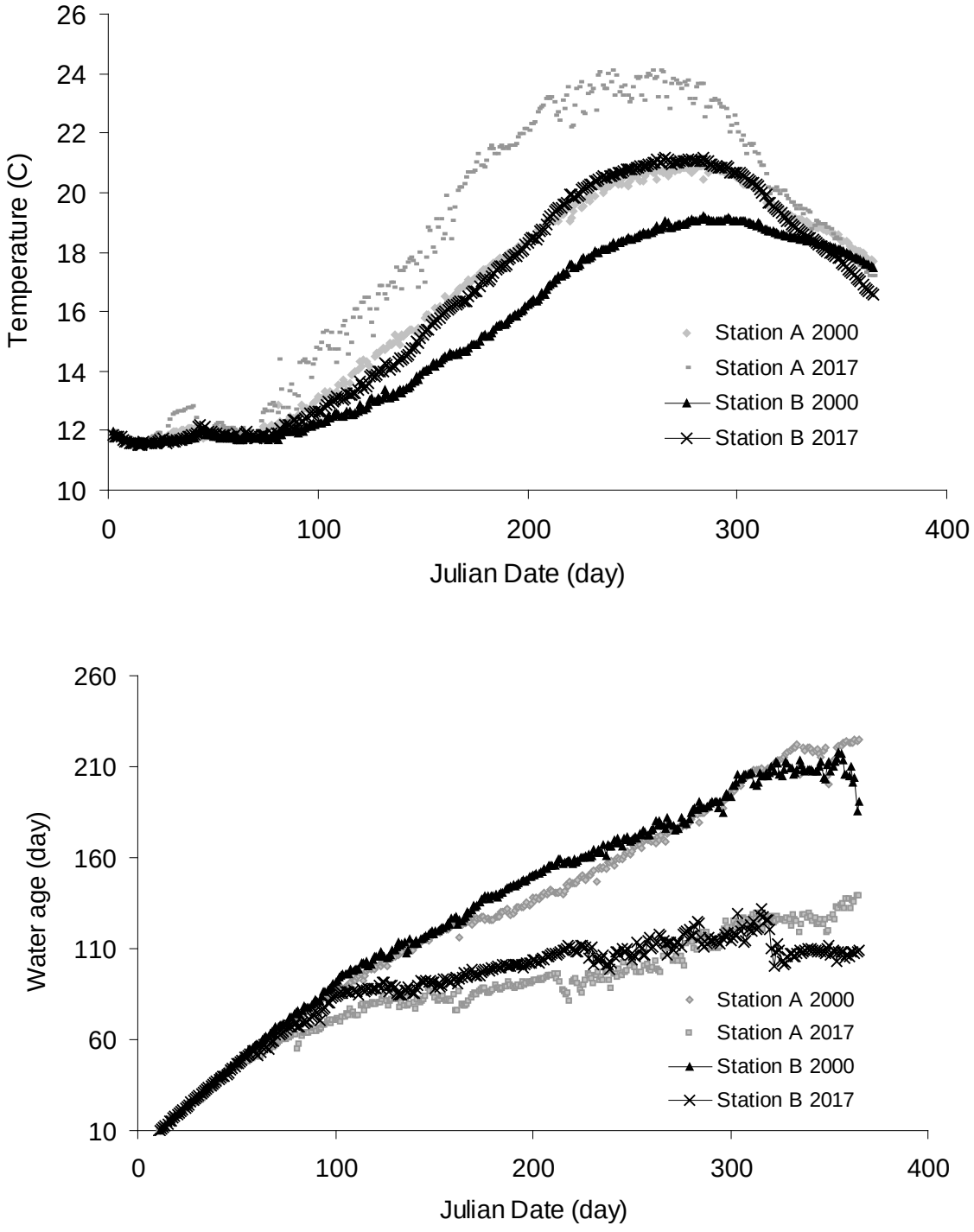

Figure 18 Comparison of calculated time series of depth averaged temperature (a) and water age (b) at Site A and B

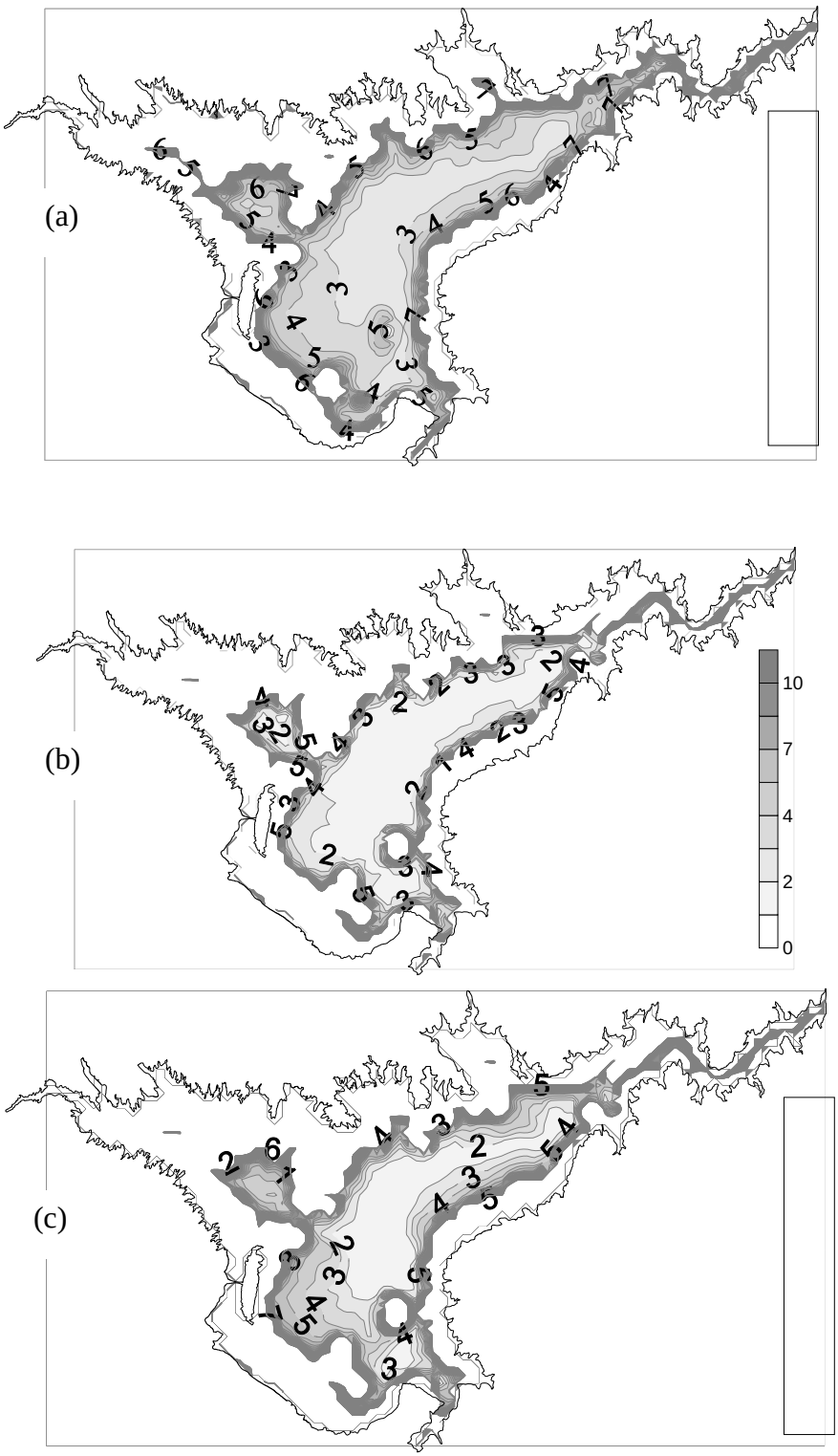

Figure 19 The spatial distribution of calculated temperature differences (ΔT) between year 2000 and 2017 at Day 219. ΔT means temperature in 2017 subtract temperature in 2000. (a) Depth averaged ΔT, (b) Surface ΔT, (c) Bottom ΔT.

6.3 Impact of water level drawdown on water age

The daily variation of depth-averaged water age at sites A and B over the 2000 and 2017 simulations showed that the differences in water age were notable during the simulation period (Fig.18b). The maximum change in water age (ΔWA) for site A was found at the end of the simulation period (Day 365), with a ΔWA of 84 days; while the maximum ΔWA for site B was found at Day 357 at 105 days. These results suggest that the declining water levels for Lake Mead will greatly accelerate the transport and discharge of dissolved substances from the lake.

To study the changes of the extent of horizontal and vertical water ages, the depth-averaged, surface water and bottom ΔWA between years 2000 and 2017 at Day 365 were investigated (Fig. 20), and the percentages of water column with different ΔWA at Day 365 between the two years at various water depths were compared (Tab. 2). The results showed that for the surface layer, the variation in ΔWA throughout the lake was relatively uniform, with ΔWA between 80 and 90 days for 55% of the lake. However, in the bottom layer, ΔWA was more evenly distributed between 70 and 150 days. The depth-averaged ΔWA showed an intermediate level of variability. These results also suggest that water level drawdown will have a stronger effect on the bottom water and deep lake regions than on the surface water and shallow regions in terms of water exchange (Fig.20).

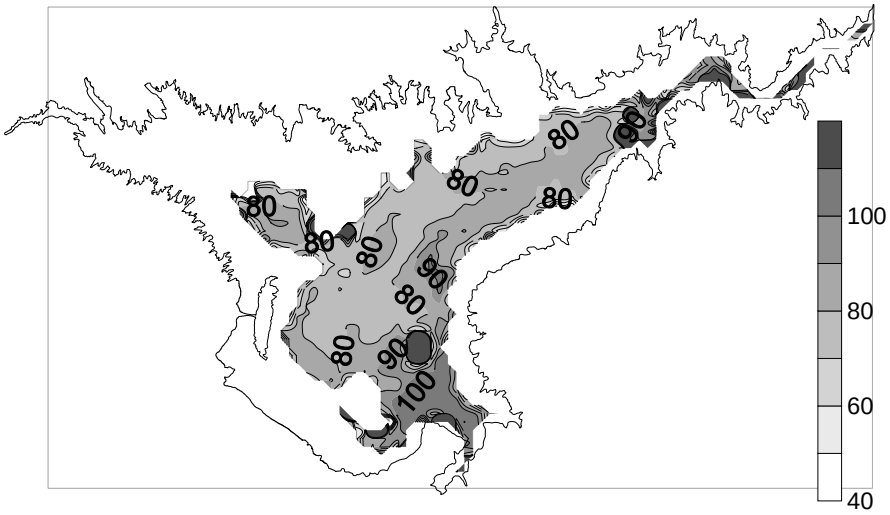

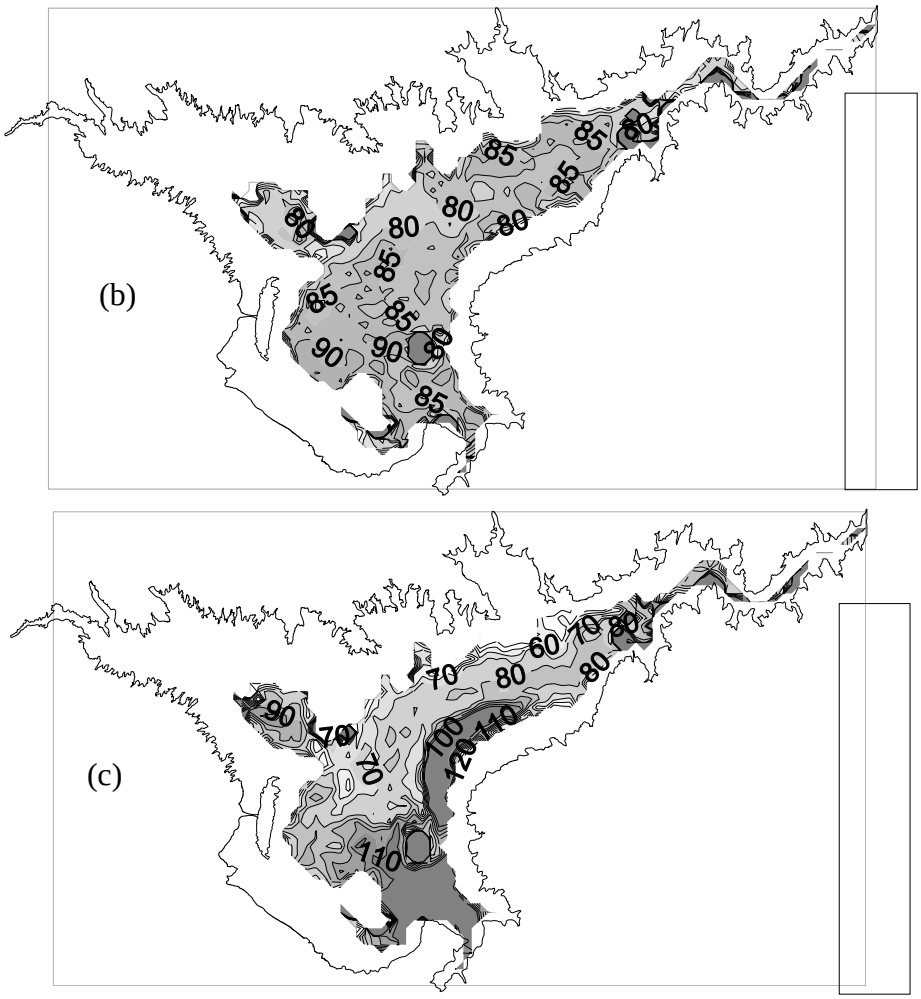

Figure 20 The spatial distribution of calculated water age differences (ΔWA) at Day 365 between year 2000 and 2017. ΔWA represent water age of 2000 subtract that of 2017(a) Depth averaged ΔWA, (b) Surface ΔWA, (c) Bottom ΔWA,

6.4 Discussions on the impact of water level drawdown

The simulation results suggest that the thermal stratification and water age of Lake Mead will be significantly influenced by water level drawdown. During the summer thermal stratification period, depth-averaged temperature increased by 4–7 ºC in shallow regions and 2–4 ºC in deep regions, between to the two simulated conditions. Such temperature changes would likely have a notable impact on the lake's aquatic habitat and food web (Pauly 1980). Particularly, the composition and distribution of fish species in the lake would be changed under the new temperature environment. Usually, each fish species exhibits a characteristic preferred temperature based on its thermal guild. For cold-water fish, when the water temperatures exceed their preferred temperature by 2 to 5 ºC, the fish will actively select and rapidly change their living area (Gunn 2002). Lake Mead provides habitat for one endangered fish species, the razorback sucker (*Xyrauchen texanus)* and several other game fish including largemouth bass (*Micropterussalmoides*) and striped bass (*Morone saxatilis*) (Martin et al. 1982). The preferred temperatures are 13–20 ºC for striped bass (Kellogg and Gift 1983), 22–25 ºC for razorback sucker (Bulkley and Pimentel 1983) and 26.5–30.9 ºC for largemouth bass (Cincotta1 and Stauffer 1983). The simulation results showed surface water temperatures changing from 28–30 ºC in 2000 to 30–32 ºC in 2017 and the bottom temperatures changing from 12–15 ºC in 2000 to 15–20 ºC in 2017. The changes of water temperature will force fish to move away from their existing habitat and seek out refuge areas elsewhere. Due to the extreme water level drawdown, the water volume is diminishing rapidly, resulting in the reduction of habitat and an increase in competition for resources such as food, oxygen and spawning areas. Additionally, the increasing water temperature will likely depress the dissolved oxygen concentration, degrade water quality and promote the growth of harmful algae species, which will have notable negative impacts on the fish as well as on overall ecosystems of the lake (Sloman et al. 2002).

By comparing the air temperature and surface temperature for the 2000 simulation (Fig. 4), we can conclude that there is a strong correlation between air and surface water temperatures in Lake Mead, particularly in the shallow regions. Therefore, water temperatures in Lake Mead will likely warm even further in response to climate change. It was reported that surface air temperatures around the globe have increased by approximately 0.6 °C over the last several decades (Hansen et al. 2006) and will potentially continue to increase by 1.1–6.4 °C by the year 2100 as reported by the Intergovernmental Panel on Climate Change (IPCC) (Andrady et al. 2008). Warming trends in lake temperature have been found in Lake Superior and Lake Tahoe in the U.S. (Coats et al. 2006, Austin and Colman 2007) and Lake Malawi in East Africa (Vollmer et al. 2005). Therefore, the double threats of water level drawdown and potential global warming could seriously affect the ecosystem of Lake Mead.

In view of the quite complex problem of investigating the internal hydrodynamic processes of Lake Mead under declining water levels, the concept of water age was implemented. The decrease in depth-averaged water age by 80–100 days in 2017 compared to 2000 (Fig. 20) means that the water exchange will become more intense after the water level drawdown seriously modifying lake's thermal stratification period

and turn over processes which could lead to new ecosystem equilibrium. The relatively younger water at the lake surface compared to the older water at the lake bottom suggests that distinct vertical patterns exist in the lake's circulation processes. By comparing the differences in water age at the surface and bottom of the lake between 2000 and 2017, it was revealed that the water age changed faster for the bottom water than it did for the surface water, suggesting that water level drawdown could accelerate the bottom water's movement. This could subsequently affect the transfer and transport of pollutants. Thus, water age provides a useful tool to describe the complex hydrodynamic processes and substance transport properties.

6.5 Discussions on pressure gradient error

The abilities of sigma coordinate models to resolve the bottom and surface layers is an attractive feature of this class of models. Unfortunately, this model of Lake Mead with sigma coordinate transformation has suffered from numerical errors while calculating horizontal pressure gradients (PG) over steep topography. The source of the problem is that in sigma coordinates, the *x* components of the internal pressure are written

$$\frac{\partial \rho}{\partial x}\Big|_z = \frac{\partial \rho}{\partial x} - \frac{\sigma}{H}\frac{\partial H}{\partial x}\frac{\partial \rho}{\partial \sigma} \tag{3}$$

where ρ is the density, H is the water depth, and $\sigma \equiv z / H$. Near steep topography the two terms on the right may be large, comparable in magnitude and typically opposite in sign. In such cases, a small truncation error can result in a large error in the pressure gradient force. These errors can be of the same order of the expected flow (Song 1998). This error caused severe instability in the Lake Mead model. For example, the calibration results (Fig. 4) indicate that the modeled bottom temperature at Sentinel Island for the calibration scenario first decreased for a significant period and then later increased (Fig. 4), whereas the observed bottom temperature varied throughout the simulation period.

Much attention has been paid to the errors in computing horizontal pressure gradients in the region of steep topography, and many alternative PG schemes have been proposed to reduce the errors, including vertical interpolation schemes, higher-order methods and methods retaining integral properties and subtracting reference state (Mellor et al. 1998, Berntsen and Furnes 2005, Marsaleix et al. 2009). Further, methods associated with the specific characteristics of a study area have been suggested to find suitable model parameters to reduce errors to an acceptable level including grid characteristics, horizontal and vertical resolution, and horizontal viscosity and smoothing topography (Berntsen and Furnes 2005, Berntsen and Thiem 2007). Berntsen and Thiem (2007) described that the erroneous flows may be reduced considerably by using higher values of horizontal viscosity in areas where there is a combination of stratification and varying topography. The formulation of Smagorinsky method (Smagorinsky, 1963) for calculating horizontal viscosity is shown as below

$$A_M = C_M \Delta x \Delta y \left[\left(\frac{\partial U}{\partial x} \right)^2 + \frac{1}{2}\left(\frac{\partial V}{\partial x} + \frac{\partial U}{\partial y} \right)^2 + \left(\frac{\partial V}{\partial y} \right)^2 \right]^{1/2} \tag{4}$$

where A_M is horizontal viscosity, C_M is a nondimensionless viscosity parameter. And it was recommended that CM would multiply by approximately a factor of 100 on the basis of usually recommended value, 0.2 (Berntsen and Thiem 2007).

For this study, two methods were investigated to reduce the PG errors to an acceptable level, including increasing the vertical resolution and applying large horizontal viscosity by using a large CM value. For the first method, the PG error on three vertical resolutions, 14, 20 and 30 vertical levels, were investigated. The AMEs of bottom temperatures with 14, 20 and 30 vertical layers were 2.47 ºC, 2.05 ºC and 1.37 ºC at site B (Fig. 21), respectively. As expected, the higher the vertical resolution, the lower the PG errors. However, the higher vertical resolution requires a longer CPU calculation time. For example, during the simulation period from 1 March to 31 October 2005, the case with 30 vertical layers required approximately 120 CPU hours (Dell, Intel Core 4-CPU processor, 2.6 GHz), whereas the case with 14 vertical layers required only 40 CPU hours. For the second method, different multiples of the recommended CM value (0.2) were applied to investigate the PG error. To test the impact of the C_M value, a comparison between the time series of bottom temperatures at site B (Fig. 5a) with C_M ranging from 0.2 to 1.0 was conducted (Fig. 22). The mean values and standard deviations of errors of calculated A_M values at Site B for two cases during the simulation time were 1.28±0.24 (C_M=0.2) and 3.35± 2.59 (C_M=1.0) m^2/s, respectively. The AMEs of the bottom temperatures were 2.46 ºC (C_M=0.2) and 2.30 ºC (C_M=1.0) at site B (Fig. 15a). The results indicated that the model is not highly sensitive to moderate changes to C_M. However, the model was unstable under larger adjustments to C_M. Thus, the present study did not verify Berntsen and Thiem's (2007) finding that it is possible to reduce the PG errors by using C_M by a factor of 100 from the typically recommended value of 0.2 due to model instability.

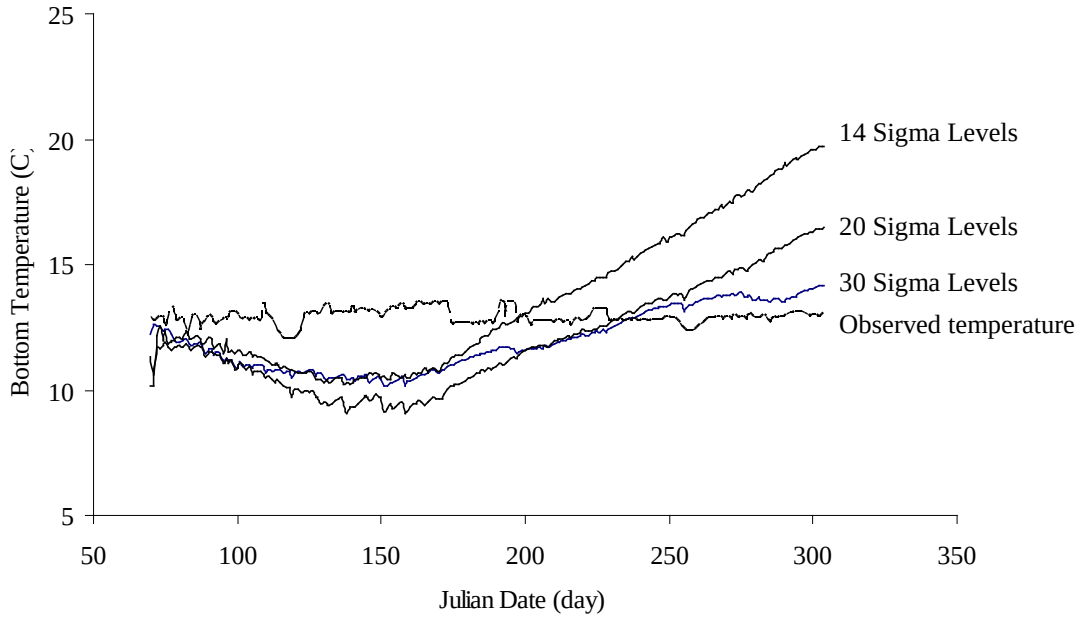

Figure 21 Time series of bottom temperature at Site B using three different vertical resolutions: 14, 20 and 30 levels from March 1 to October, 2005

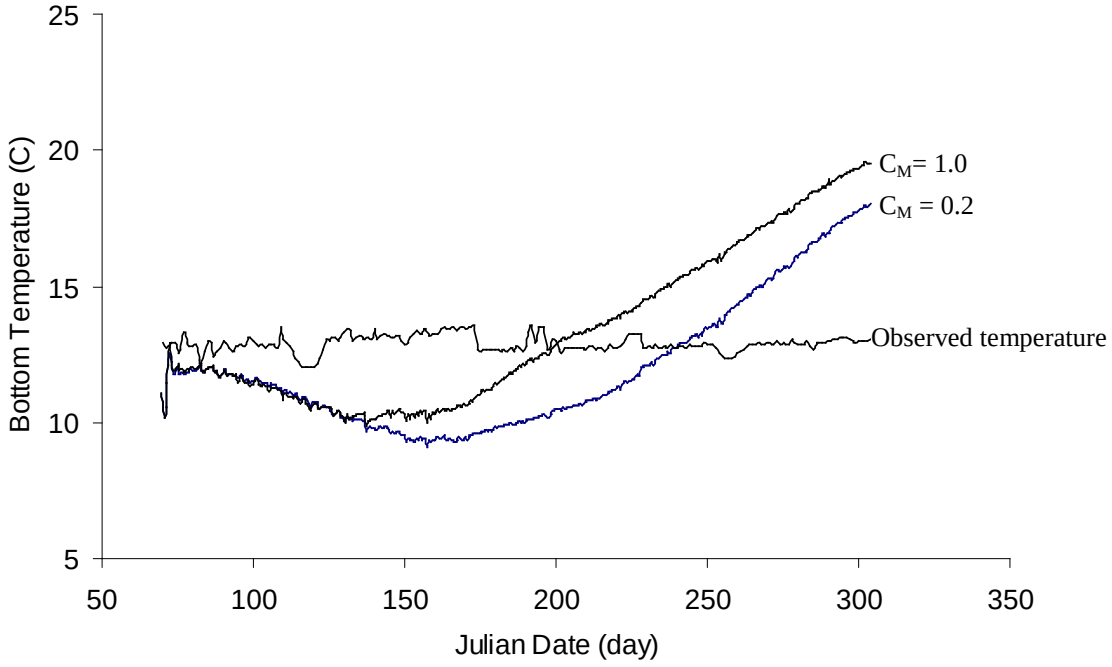

Figure 22 Time series of bottom temperature at Site B using two CM values: 0.2 and 1.0 with 14 sigma layers from March 1 to October, 2005

6.6 Water Quality and Eutrophication Modeling Results

There are four simulated cases for water quality modeling: (1) high-stage simulation (August 1998) with a lake stage of 370.12 m; (2) high-stage simulation (January 1999) with a lake stage of 369.69 m; (3) drawdown simulation (August 2007) with a lake stage of 338.39 m; and (4) drawdown simulation (January 2008) with a lake stage of 340.30 m. The high-stage simulations described the pre-drought lake mixing processes while the drawdown simulations shed light on the drawdown impact on such processes.

Eighteen water quality state variables have been simulated in this study as shown in Table 6. The unit of nutrient concentration is mg/L. The calculation results were plotted in the Appendix due to the size limitation of Microsoft Word. In the figures of Appendix, the X and Y coordinates are grid numbers as shown in Fig. 23.

Table 6. Values of several parameters used in the model

Parameter	Description
BC	Cyanobacteria
BD	Diatom Algae
BG	Green Algae
RPOC	Refractory particulate organic carbon
LPOC	labile particulate organic carbon
DOC	dissolved carbon
RPOP	refractory particulate organic phosphorus
LPOP	labile particulate organic phosphorus
DOP	dissolved organic phosphorus
PTO4	total phosphate, refractory part
RPON	organic nitrogen, labile part
LPON	organic nitrogen
DON	dissolved organic nitrogen
NH4	ammonia nitrogen
NO3	nitrate nitrogen
DO	dissolved oxygen

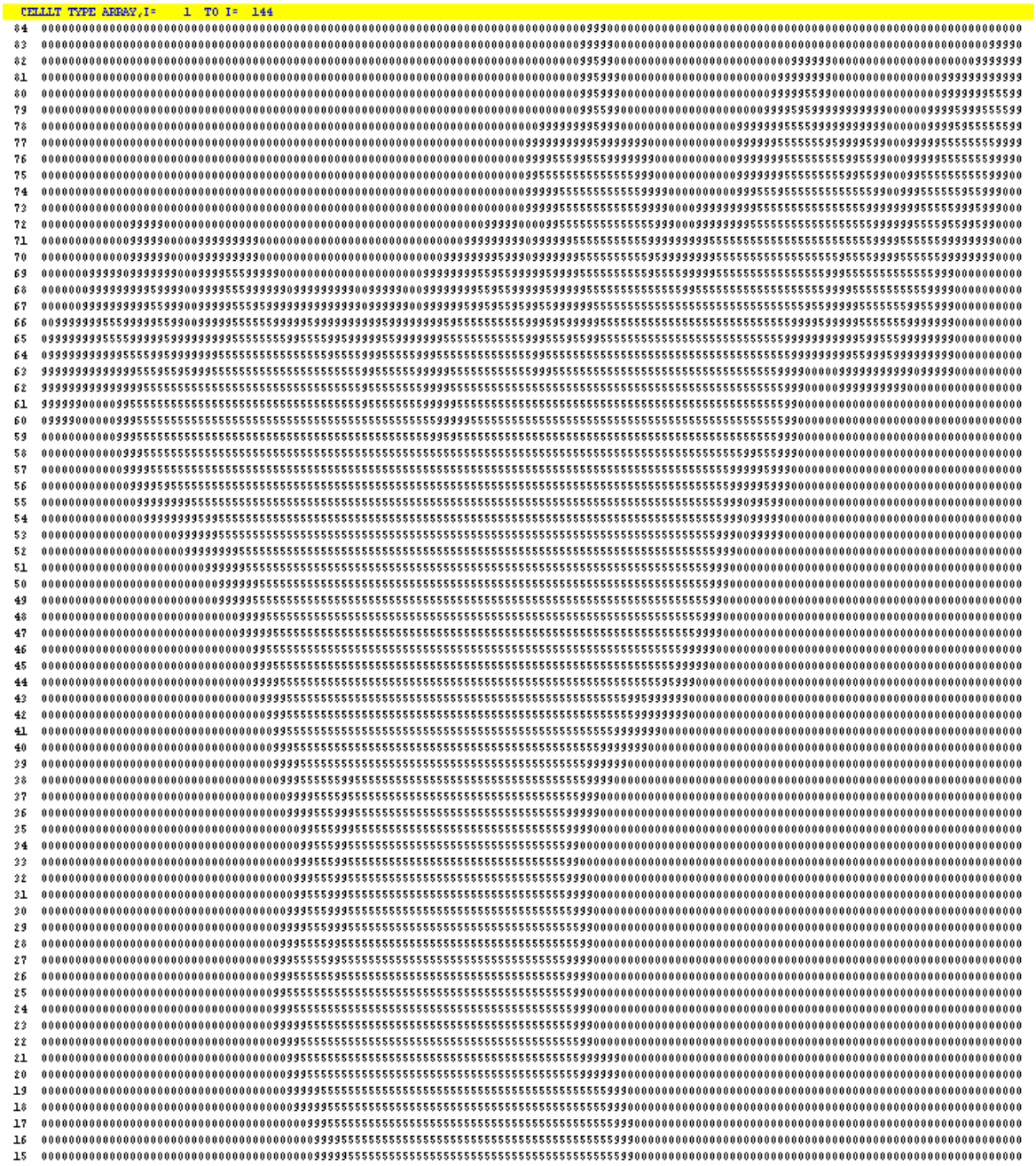

Figure 23 Grid index in figures of Appendix

7. Conclusions

A three-dimensional numerical model, EFDC, was calibrated for Lake Mead based on observed data from 2005, and was applied to study the impacts of water level drawdown on thermal structure and hydrodynamic processes of the lake. The model results indicated that water level decline from the year 2000 to a projected scenario in 2017 would have a stronger impact on temporal stratification in the shallow regions of the lake than in the deeper regions. Further, depth-averaged temperatures increased by 4–7 ºC for shallow regions and 2–4 ºC for deeper regions during the summer thermal stratification period. However, water level drawdown may have a stronger effect on the bottom water and deep lake regions than on the surface water and shallow regions in terms of water exchange. Depth-averaged water age decreased by approximately 70–90 days for shallow regions and 90–120 days for deep regions. Such changes in the thermal regime and water ages of the lake would likely have a significant impact on the fishery and ecosystem of Lake Mead. Additionally, application of the widely used EFDC model required careful attention to account for the pressure gradient error in the presence of steep bottom slopes in Lake Mead. An increase in the vertical resolution of the model reduced the error to an acceptable level for the Lake Mead model. In general, this work provides useful information for understanding the thermal and hydrological processes in Lake Mead under extreme water level drawdown.

8. Acknowledgments

The research is funded by the Nevada Institute of Water Resources. We would like to thank Ronald Veley with the U.S. Geological Survey (USGS) for providing monitoring data. We wish to especially thank Dr. Sen Bai, Dr. Scott C. James and Dr. Craig Jones for their help in developing the Lake Mead model. My colleagues (or former colleagues), Dr. Kumud Acharya, Dr. Mark Stone, and Dr. Yiping Li have participated in the study. This project has financially supported three months for Naveen Kumar Veeramisti who is a graduate student from University of Nevada, Las Vegas.

9. References

Algae Task Force. 2004. Blue-Green algal toxins monitoring and reporting plan. Prepared by the Algae Task Force a subcommittee of the Lake Mead Water Quality Forum.

Andrady A, Aucamp PJ, Bais AF, Ballare CL, Bjorn LO, Bornman JF, et al. 2008. Environmental effects of ozone depletion and its interactions with climate change: Progress report, 2007. Photoch Photobio Sci. 7:15–27.

Austin JA, Colman SM. 2007. Lake Superior summer water temperatures are increasing more rapidly than regional air temperatures: A positive ice-albedo feedback. Geophys Res Lett. 34:1–5.

Barnett TP, Pierce DW. 2008. When will Lake Mead go dry? Water Resour Res. 44.

Berntsen J, Furnes G. 2005. Internal pressure errors in sigma-coordinate ocean models-sensitivity of the growth of the flow to the time stepping method and possible non-hydrostatic effects. Continental Shelf Research. 25:829–848.

Berntsen J,Thiem O. 2007. Estimating the internal pressure gradient errors in a sigma-coordinate ocean model for the Nordic Seas. pp. 417–429.

Brauns M, Garcia XF, Pusch MT. 2008. Potential effects of water-level fluctuations on littoral invertebrates in lowland lakes. Hydrobiologia. 613:5–12.

Brennwald MS, Peeters F, Imboden DM, Giralt S, Hofer M, Livingstone DM, Klump S, Strassmann K, Kipfer R. 2004. Atmospheric noble gases in lake sediment pore water as proxies for environmental change. Geophysical Research Letters 31: L04202.

Bourne JK, Joel K, Ludwig G. 2005. Eccentric Salton Sea. National Geographic Magazine. 07: 88–107.

Bulkley RV, Pimentel R. 1983. Temperature Preference and Avoidance by Adult Razorback Suckers. T Am Fish Soc. 112:601–607.

Caliskan A, Elci S. 2009. Effects of Selective Withdrawal on Hydrodynamics of a Stratified Reservoir. Water Resour Manag. 23:1257–1273.

Chen, D., K. Acharya, M. Stone, and J.G.. Duan (2007). Suspended sediment transport study in the Las Vegas Wash. Technical Report of Desert Research Institute.

Chen, D., M. Stone, Y. Li (2009). Hydrodynamic modeling of Lake Mead under Changing Water Levels. Technical Report of Desert Research Institute.

Cincotta DA, Stauffer Jr. JR. 1983.Temperature preference and avoidance studies of six North American freshwater fish species. Hydrobiologia. 109(2): 173–177.

Coats R, Perez-Losada J, Schladow G, Richards R, Goldman C. 2006. The warming of Lake Tahoe. Climatic Change. 76:121–148.

Coe MT, Foley JA. 2001. Human and natural impacts on the water resources of the Lake Chad basin. J Geophys Res-Atmos. 106:3349–3356.

Cole T, Wells SA. 2005. CE-QUAL-W2: A two-dimensional laterally averaged, hydrodynamic and water quality model, version 3.2. Instructional Report EL-03-01. U. S. Army Corps of Engineers, Waterway Experiment Station, Vicksburg, MS.

Delhez EJM, Campin JM, Hirst AC, Deleersnijder E. 1999. Toward a general theory of the age in ocean modeling. Ocean Modelling. 1:17–27.

Dynesius M, Nilsson C. 1994. Fragmentation and flow regulation of river systems in the northern third of the World. Science 266: 753–762.

Elci S, Bor A, Caliskan A. 2009. Using numerical models and acoustic methods to predict reservoir sedimentation. Lake Reserv Manage. 25:297–306.

Galperin B, Kantha LH, Hassid S, Rosati A. 1988. A Quasi-Equilibrium Turbulent Energy-Model for Geophysical Flows. Journal of the Atmospheric Sciences. 45:55–62.

Gong W, Shen J, Hong B. 2009. The influence of wind on the water age in the tidal Rappahannock River. Marine Environmental Research. 68(4):203–216.

Greene, J. C., W. E. Miller, et al. (1986). "The Effect of Secondary Effluents on Eutrophication in Las-Vegas Bay, Lake Mead, Nevada." Water Air and Soil Pollution **29**(4): 391-402.

Gunn JM. 2002. Impact of the 1998 El Nino event on a lake charr, Salvelinus namaycush, population recovering from acidification. Environ Biol Fish 64, 343–351.

Haney RL. (1991) On the Pressure-Gradient Force over Steep Topography in Sigma Coordinate Ocean Models. J Phys Oceanogr 21, 610–619.

Hamrick JM. 1992. A Three-dimensional Environmental Fluid Dynamics Computer Code: Theoretical and Computational Aspects. Special Report in Applied Marine Science and Ocean Engineering, No. 317 College of William and Mary, VIMS, p.63.

Hamrick JM. 1994. Application of the EFDC, environmental fluid dynamics computer code to SFWMD Water Conservation Area 2A.J. M. Hamrick and Associates, Report JMH-SFWMD-94-01, Williamsburg, VA, 126 pp.

Hamrick, J.M. 1996. A user's manual for the Environmental Fluid Dynamics Computer Code (EFDC). Virginia Institute of Marine Science. Special Report 331, 234pp.

Hansen J, Sato M, Ruedy R, Lo K, Lea DW, Medina-Elizade M. 2006. Global temperature change. P Natl Acad Sci USA. 103:14288–14293.

Heniche M, Secretan Y, Boudreau P, Leclerc M. 2000. A two-dimensional finite element drying-wetting shallow water model for rivers and estuaries. Adv Water Resour. 23:359–372.

Hoerling M, Eischeid J. 2000. Past peak water in the West. Southwest Hydrol. 6(1):18–19.

Hofmann H, Lorke A, Peeters F. 2008. Temporal scales of water-level fluctuations in lakes and their ecological implications. Hydrobiologia. 613:85–96.

HydroQual Inc. 2001. A Primer for ECOMSED, Version 1.2: User Manual, HydroQual, Inc, 1 Lethbridge Plaza, Mahwah, NJ. 179 pp.

Ji ZG, Hu GD, Shen JA,Wan YS. 2007. Three-dimensional modeling of hydrodynamic processes in the St. Lucie Estuary. Estuar Coast Shelf S. 73:188–200.

Jin KR, Ji ZG, James RT. 2007. Three-dimensional water quality and SAV modeling of a large shallow lake. J Great Lakes Res. 33:28–45.

Junk WJ, Wantzen KM. 2004. The flood pulse concept: New aspects, approaches, and applications—an update. In Welcomme, R. & T. Petr (eds), Proceedings of the 2nd Large River Symposium (LARS), Pnom Penh, Cambodia.Bangkok. RAP Publication: 117–149.

Kellogg RL, Gift JJ. 1983. Relationship between optimum temperatures for growth and preferred temperatures for the young of four Fish species transactions of the American Fisheries Society. 112: 424–430.

Labounty JF, Burns NM. 2007. Long-term increases in oxygen depletion in the bottom waters of Boulder Basin, Lake Mead, Nevada-Arizona, USA. Lake Reserv Manage. 23:69–82.

LaBounty, J.F., G.C. Holdren, and M.J. Horn (2004). The limnology of Boulder Basin, Lake Mead, Arizona-Nevada. U.S. Bureau of Reclamation, Report 8220-04-10.

LaBounty, J. F. and N. M. Burns (2005). "Characterization of boulder basin, Lake Mead, Nevada-Arizona, USA - Based on analysis of 34 limnological parameters." Lake and Reservoir Management **21**(3): 277-307.

Liang QH, Borthwick AGL. 2008. Adaptive quadtree simulation of shallow flows with wet-dry fronts over complex topography. Comput Fluids. 38:221–234.

LMWD. 2009. Lake Mead water database. http://lakemead.water-data.com/index2.php. Accessed 20 December 2009.

Jin, K. R., Z. G. Ji, and R.T. James. (2007). "Three-dimensional water quality and SAV modeling of a large shallow lake." Journal of Great Lakes Research **33**(1): 28-45.

Marsaleix P, Auclair F, Estournel C. 2009. Low-order pressure gradient schemes in sigma coordinate models: The seamount test revisited. Ocean Model. 30:169–177.

Martin WE, Bollman FH, Gum RL. 1982. Economic Value of Lake Mead Fishery. Fisheries. 7:20–24.

Mellor GL. 1990. User's Guide for a Three-dimensional, Primitive Equation, Numerical Ocean Model, Atmospheric and Ocean Sciences Program, Princeton University. 44pp.

Mellor GL, Oey LY, Ezer T. 1998. Sigma coordinate pressure gradient errors and the Seamount problem. J Atmos Ocean Tech. 15:1122–1131.

Mellor GL, Yamada T. 1982. Development of a Turbulence Closure-Model for Geophysical Fluid Problems. Rev Geophys. 20:851–875.

NASA. 2000. EO Study: Drought Lowers Lake Mead, Jesse Allen, National Aeronautics and Space Administration Earth Observatory, 21 February 2008, http://earthobservatory.nasa.gov/Study/LakeMead/lake_mead.html.

Nash L, Gleick P. 1991. The sensitivity of stream flow in the Colorado Basin to climatic changes. J Hydrol. 125:221–241.

Pauly D. 1980. On the Interrelationships between Natural Mortality, Growth-Parameters, and Mean Environmental-Temperature in 175 Fish Stocks. J Conseil. 39:175–192.

Sloman KA, Wilson L, Freel JA, Taylor AC, Metcalfe NB, Gilmour KM. 2002. The effects of increased flow rates on linear dominance hierarchies and physiological function in brown trout, Salmo trutta. Can J Zool. 80:1221–1227.

Smagorinsky J. 1963. General circulation experiments with the primative equations, I. The basic experiment. Mon Weather Rev.91:99–164.

Song YT. 1998. A general pressure gradient formulation for ocean models. Part I: Scheme design and diagnostic analysis. Mon Weather Rev. 126:3213–3230.

Steinberg SM, Nemr EL, Rudin M. 2009. Characterization of the lignin signature in Lake Mead, NV, sediment: comparison of on-line flash chemopyrolysis (600A degrees C) and off-line chemolysis (250A degrees C). Environ Geochem Hlth. 31:339–352.

Sutela T, Vehanen T. 2008. Effects of water-level regulation on the nearshore fish community in boreal lakes.Hydrobiologia. doi:10.1007/s10750-008-9468-z. Intergovernmental Panel on Climate Change. 2008. Summary for policy makers, in Climate Change 2007: Working Group II: Impacts, Adaptation and Vulnerability, edited by N. Adger et al., Cambridge Univ. Press, New York.

Twichell DC, Cross VA, Belew SD. 2003. Mapping the floor of Lake Mead (Nevada and Arizona): Preliminary discussion and GIS data release. USGS Open-File Report 03-32.

Usmanova RM. 2003. Aral Sea and sustainable development. Water Sci Technol. 47:41–47.

Veley, R.J., L.H. Fisher, and D.M. Wiersma (2008). “The U.S. Geological Survey’s lake mead monitoring network”. Lake Mead Science Symposium, January 13-14, 2009, Las Vegas, NV.

Vermeyen TB. 2003. Acoustic Doppler Velocity measurements collected in Las Vegas Bay and Boulder Basin, Lake Mead, Nevada. Technical report. U.S. Department of the Interior, Bureau of Reclamation, Technical Service Center, Denver, CO.

Vollmer MK, Bootsma HA, Hecky RE, Patterson G, Halfman JD, Edmond JM, Eccles DH, Weiss RF. 2005. Deep-water warming trend in Lake Malawi, East Africa. Limnol Oceanogr. 50:727–732.

Walker J. (2008). “2007 Lake Mead limnology program.” Lake Mead Water Quality Forum.

Wang C, Zhang XQ, Sun YL. 2009. Numerical Simulation of Water Exchange Characteristics of the Jiaozhou Bay Based on A Three-Dimensional Lagrangian Model. China Ocean Eng. 23:277–290.

Wantzen KM, Rothhaupt KO, Mortl M, Cantonati M, Laszlo GT, Fischer P. 2008. Ecological effects of water-level fluctuations in lakes: an urgent issue. Hydrobiologia. 613:1–4.

Zou, R., S. Carter, L.Shoemaker, A. Parker, and T. Henry. (2006). "Integrated hydrodynamic and water quality modeling system to support nutrient total maximum daily load development for Wissahickon Creek, Pennsylvania." Journal of Environmental Engineering-Asce **132**(4): 555-566.

10. Appendix

August 1998

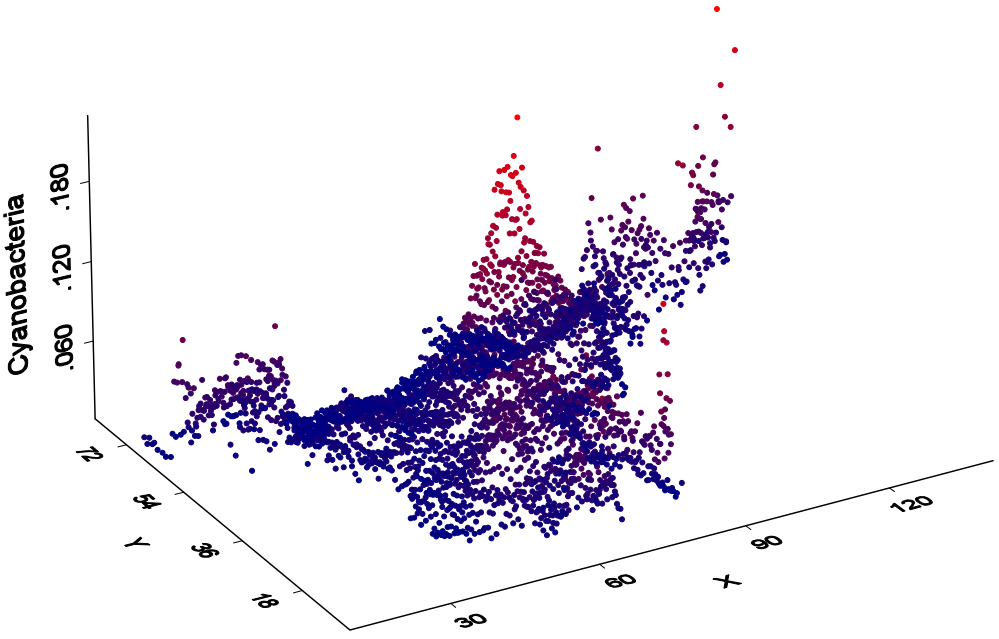

Fig. Cyanobacteria

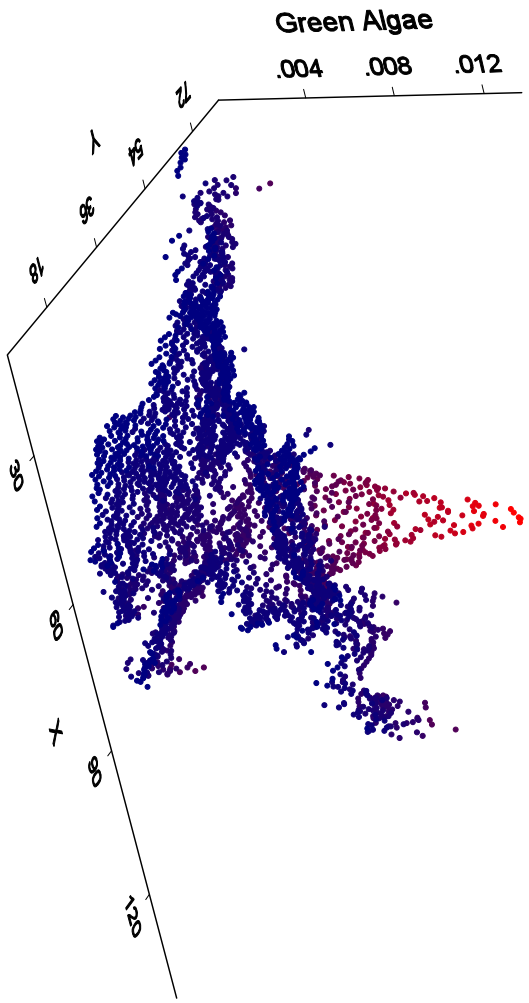
Green Algae
.004
.008
.012
72
54
36
18
0
8
16
24
32
40

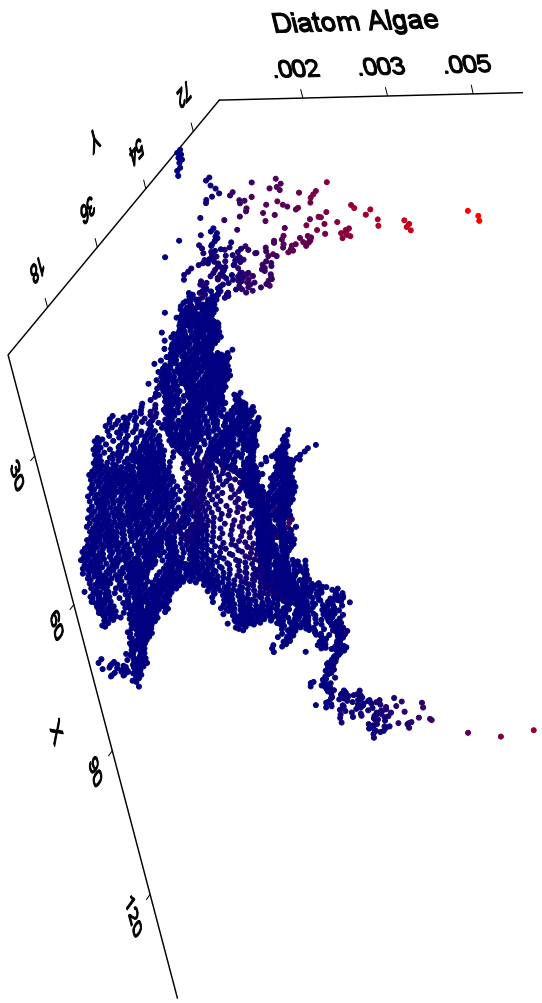
Diatom Algae
.002
.003
.005
72
54
36
18
0
8
16
24
32
40

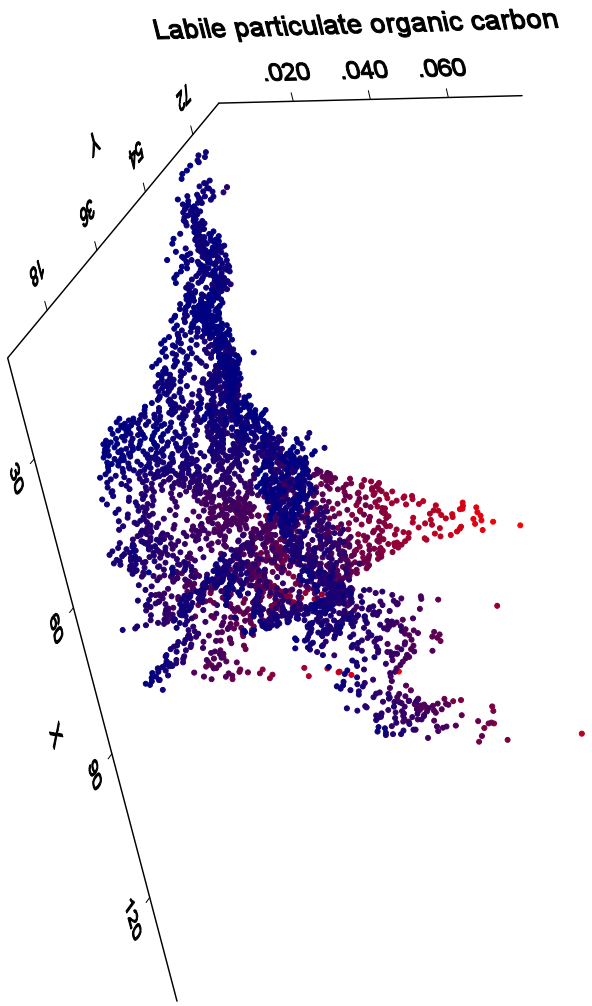
Labile particulate organic carbon
.020
.040
.060
72
54
36
18
0
8
16
24
32
40
Z
Y
X

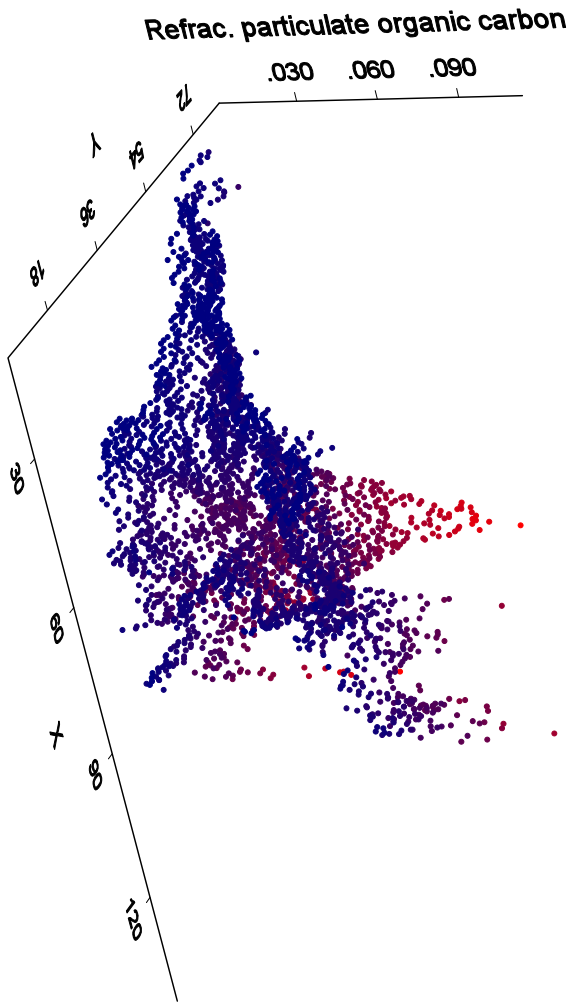
Refrac. particulate organic carbon
.030
.060
.090
72
54
36
18
0
8
16
24
32
40
Z
Y
X

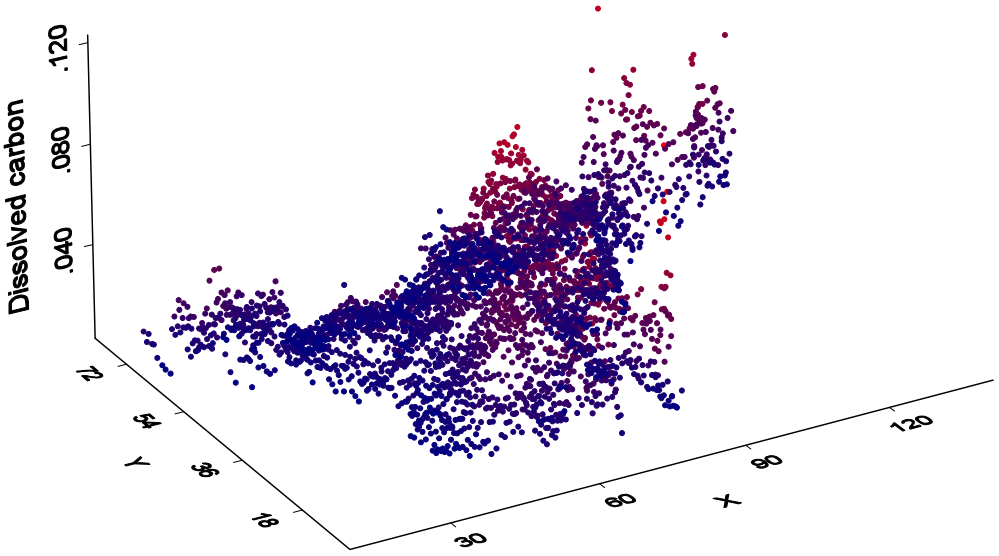
Dissolved carbon
.120
.080
.040
12
24
36
48
Y
30
60
90
120
X

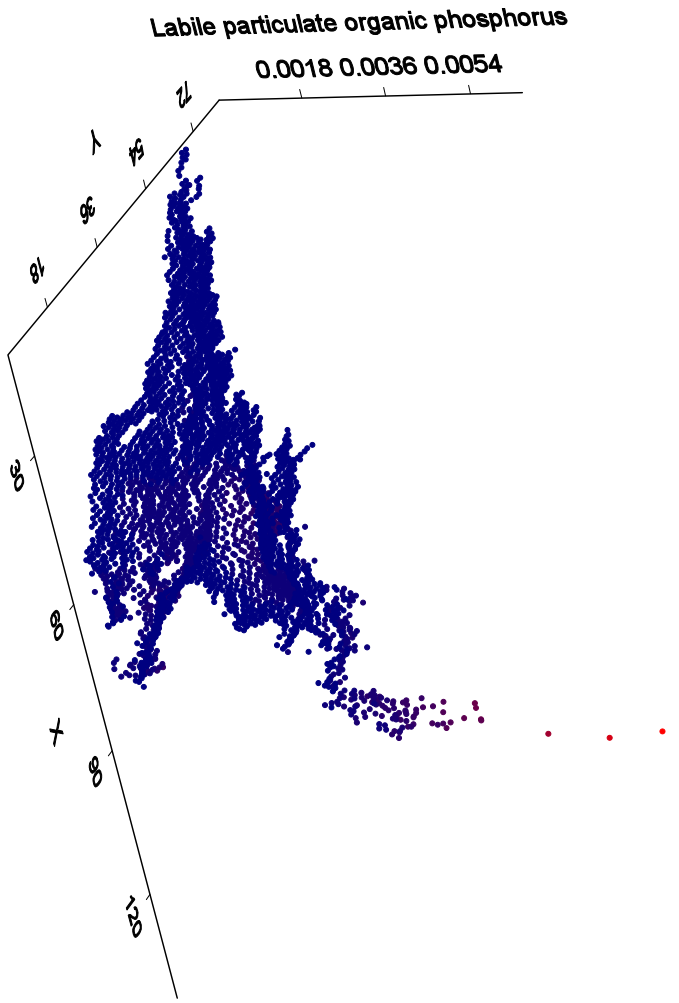
Labile particulate organic phosphorus
0.0018 0.0036 0.0054
Z
54
Y
36
18
36
X
8
12

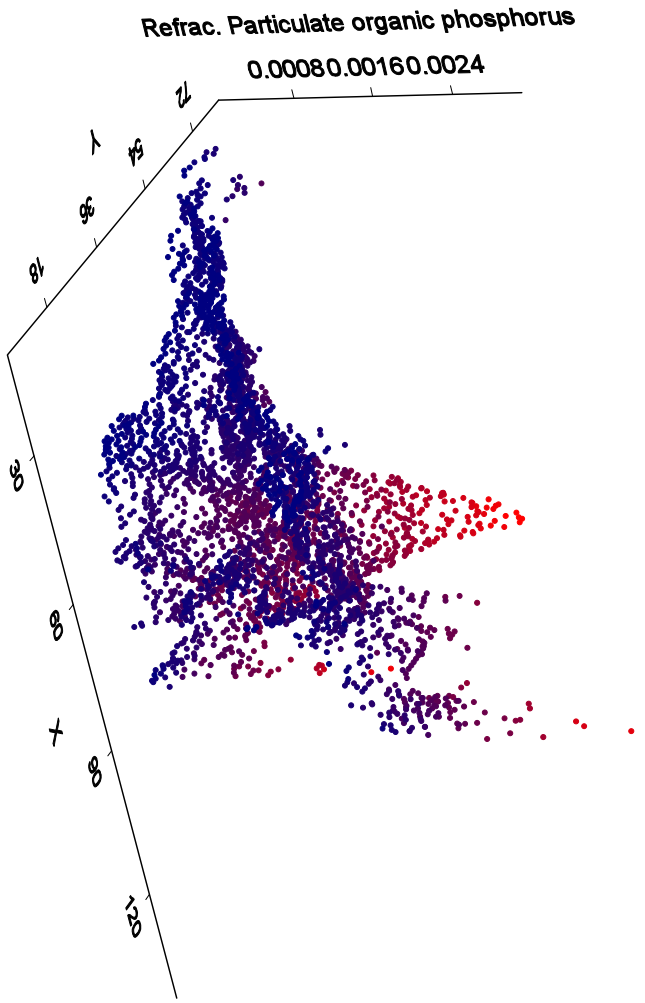
Refrac. Particulate organic phosphorus
0.00080.00160.0024
Z
54
Y
36
18
36
X
8
12

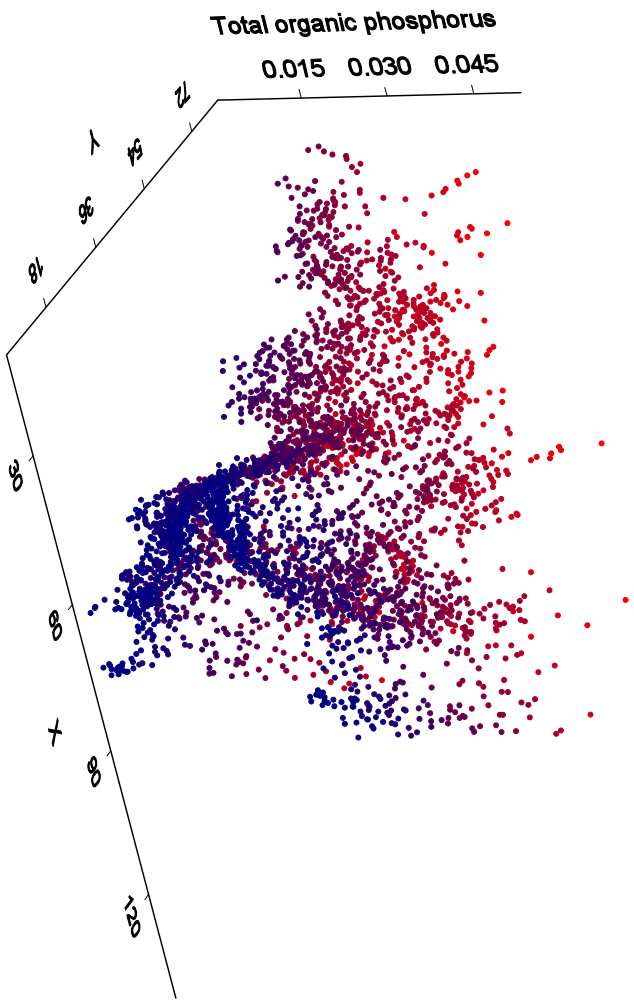
Total organic phosphorus
0.015
0.030
0.045
72
54
36
18
Y
36
18
X
0
18
36

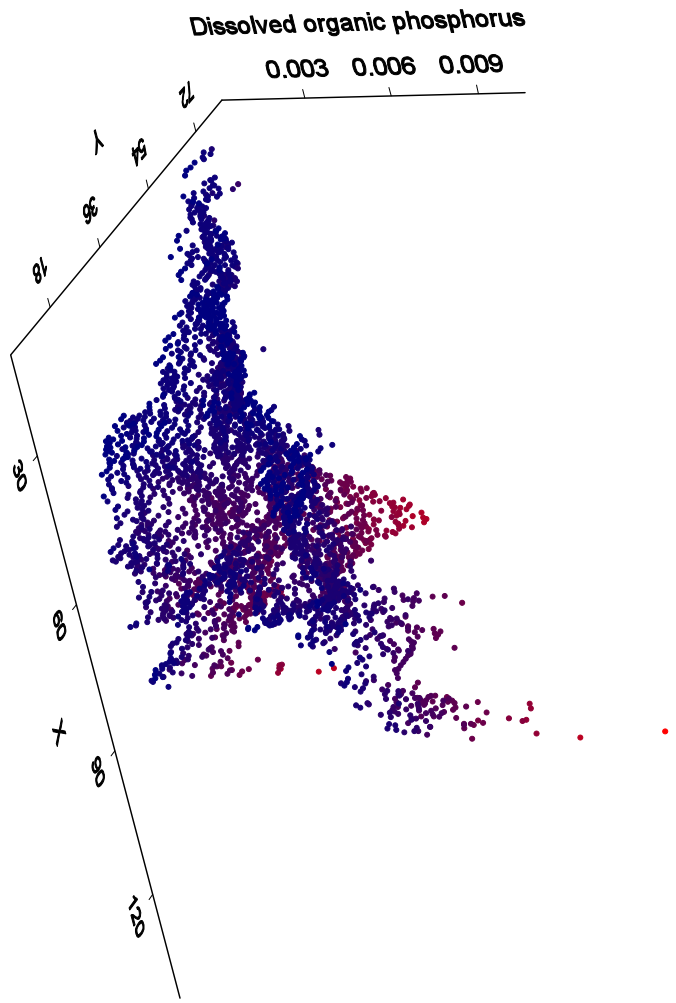
Dissolved organic phosphorus
0.003
0.006
0.009
72
54
36
18
Y
36
18
X
0
18
36

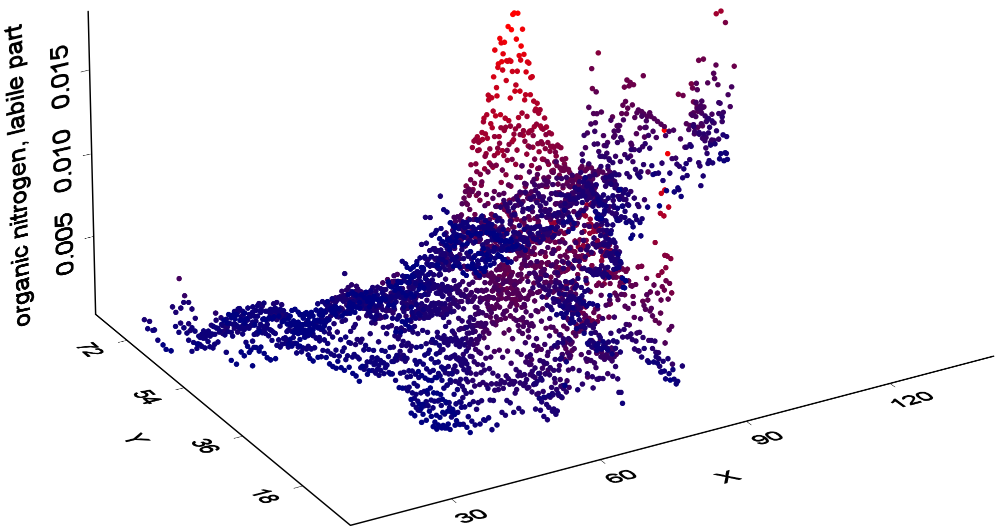
organic nitrogen, labile part
0.005
0.010
0.015
72
54
36
18
Y
30
60
90
120
X

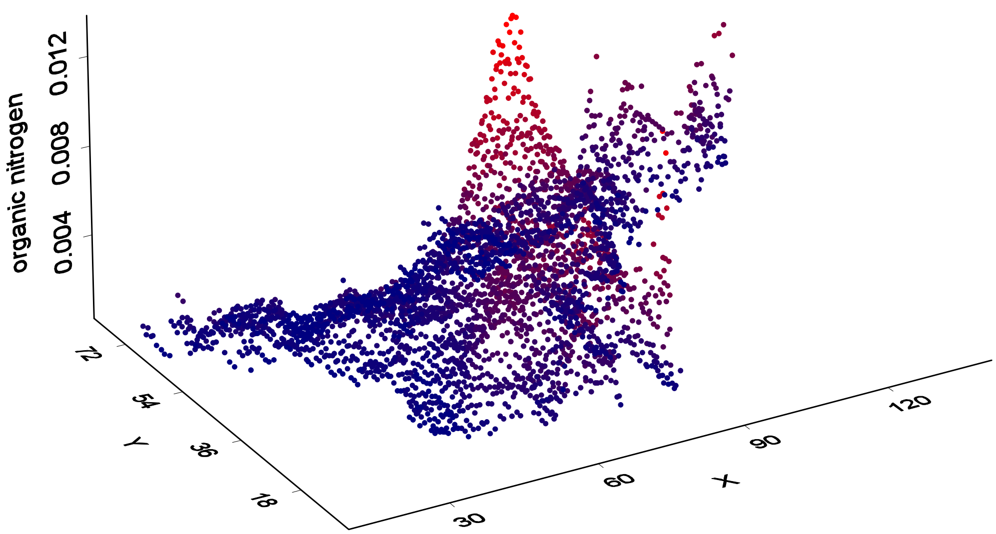
organic nitrogen
0.004
0.008
0.012
72
54
36
18
Y
30
60
90
120
X

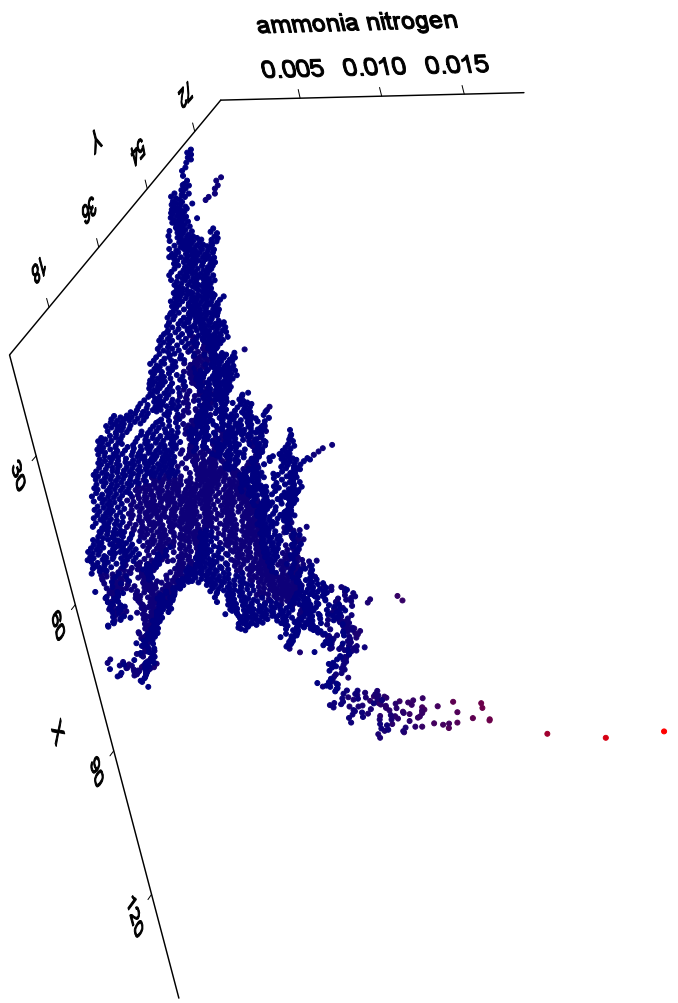
ammonia nitrogen
0.005 0.010 0.015
z
34
y
36
18
36
x
8
120

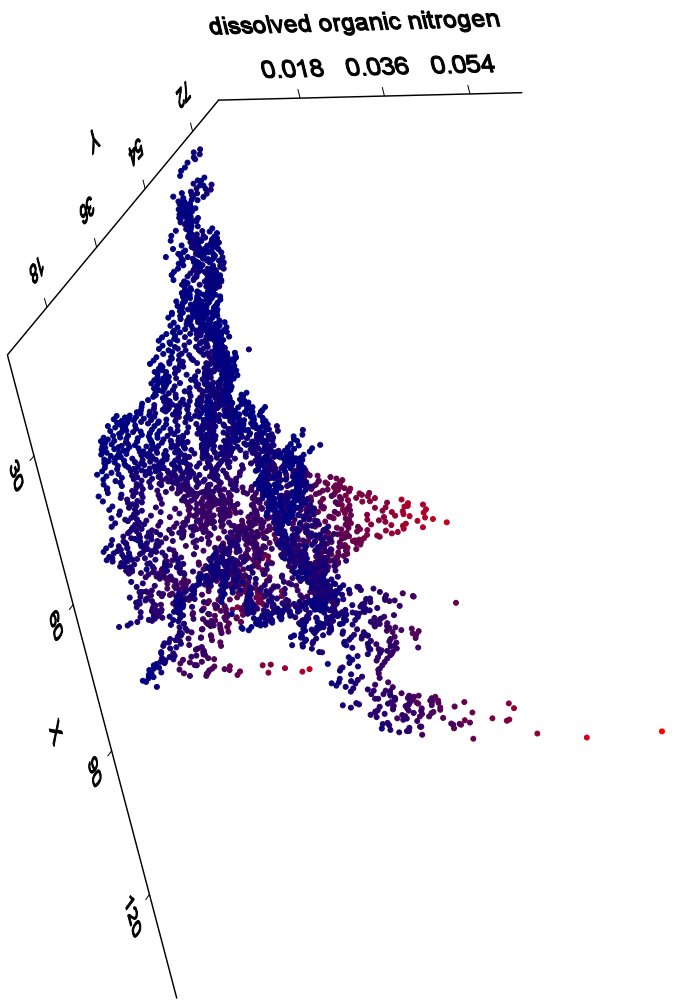
dissolved organic nitrogen
0.018 0.036 0.054
z
34
y
36
18
36
x
8
120

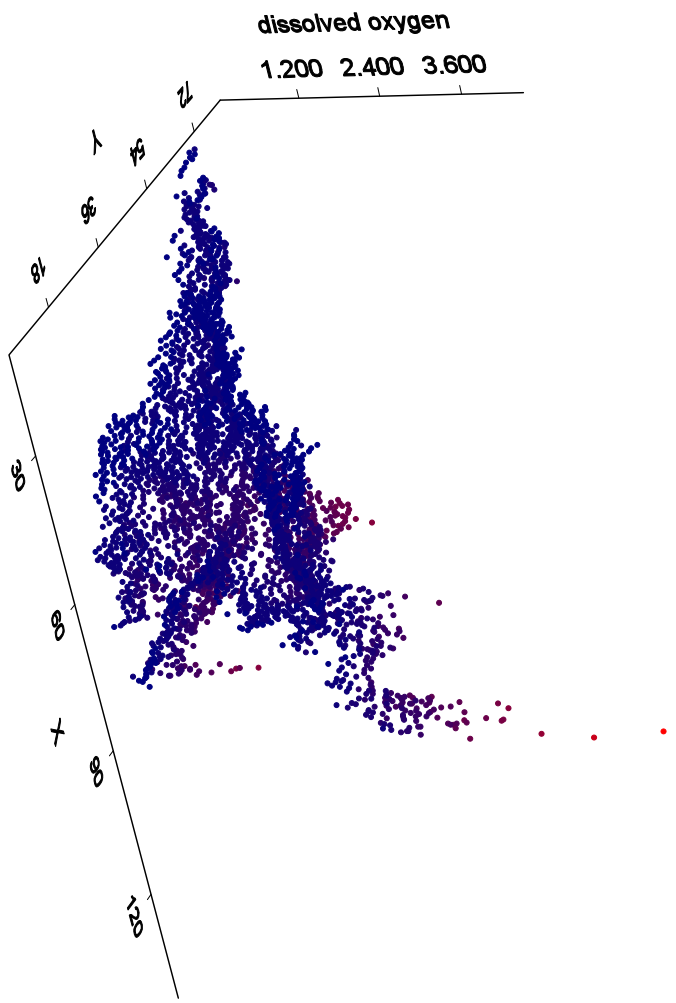
dissolved oxygen
1.200 2.400 3.600
Z
Y
34
36
18
38
X
8
120

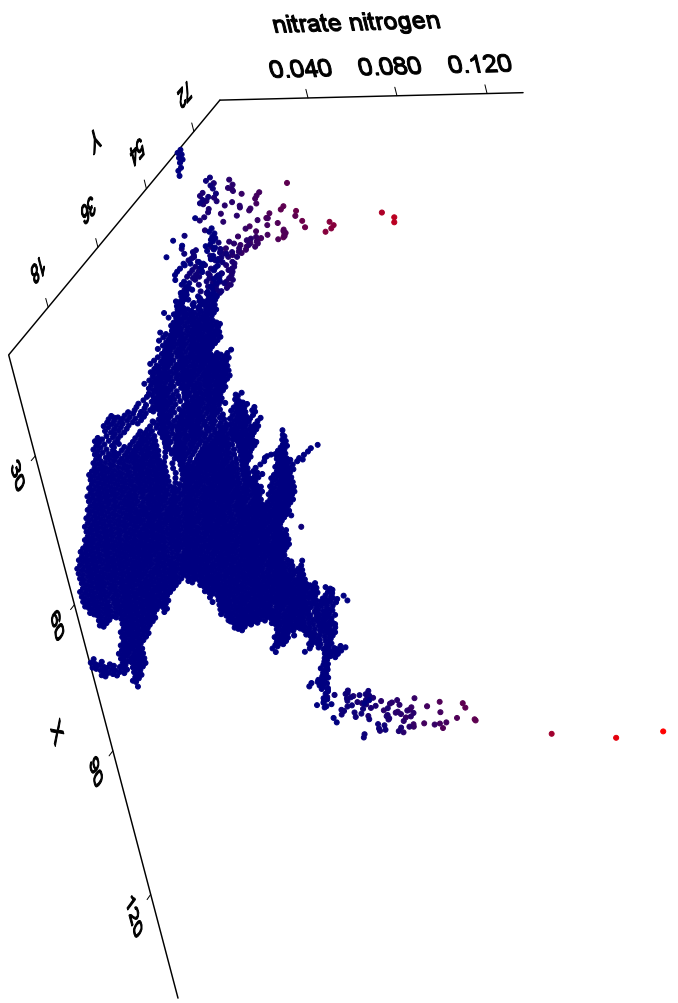
nitrate nitrogen
0.040 0.080 0.120
Z
Y
34
36
18
38
X
8
120

January 1999

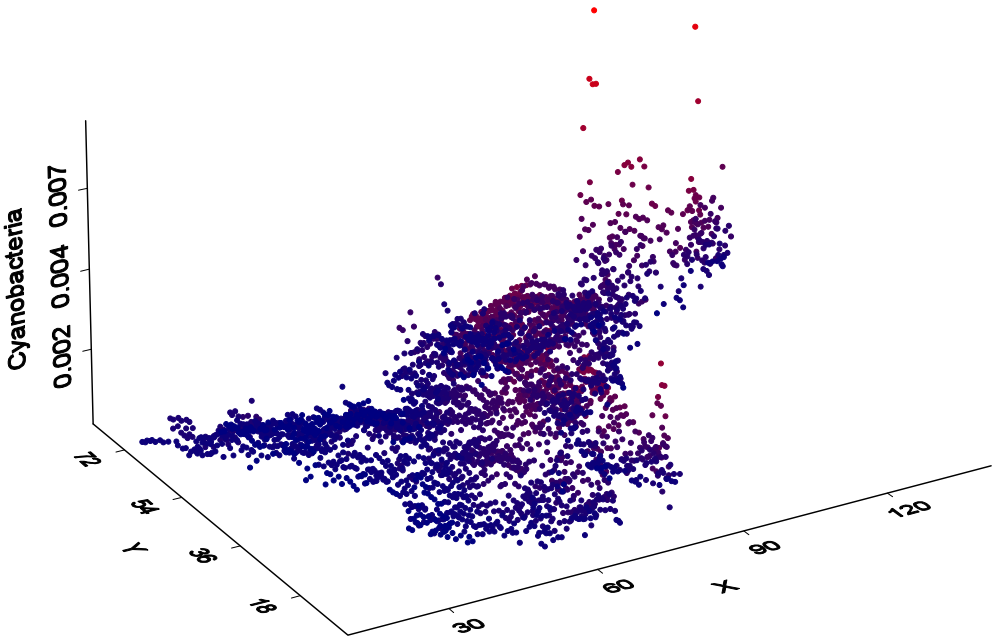

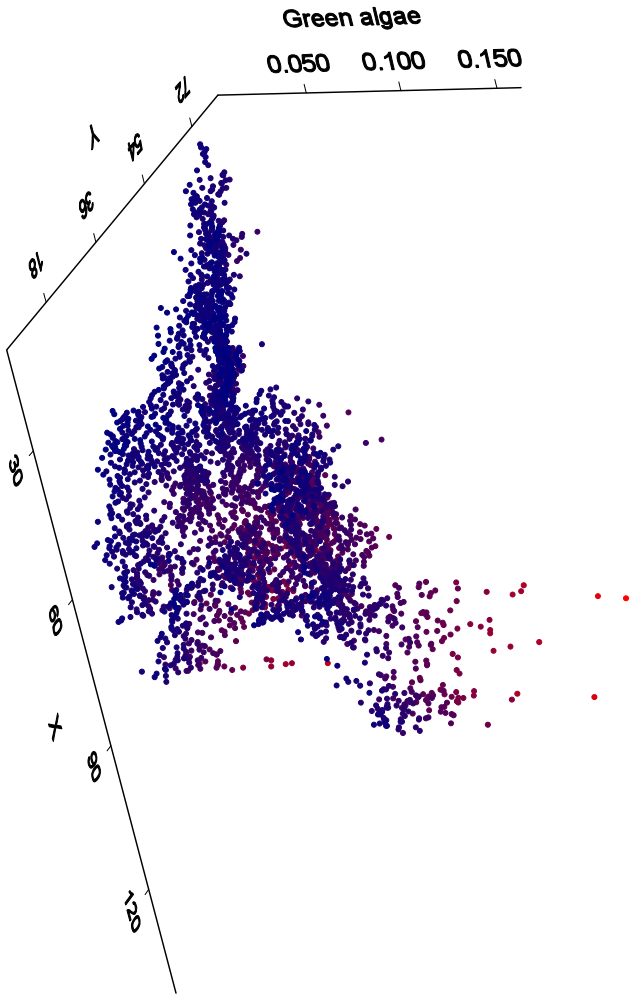
Green algae
0.050
0.100
0.150
z
y
34
36
18
38
8
x
8
12

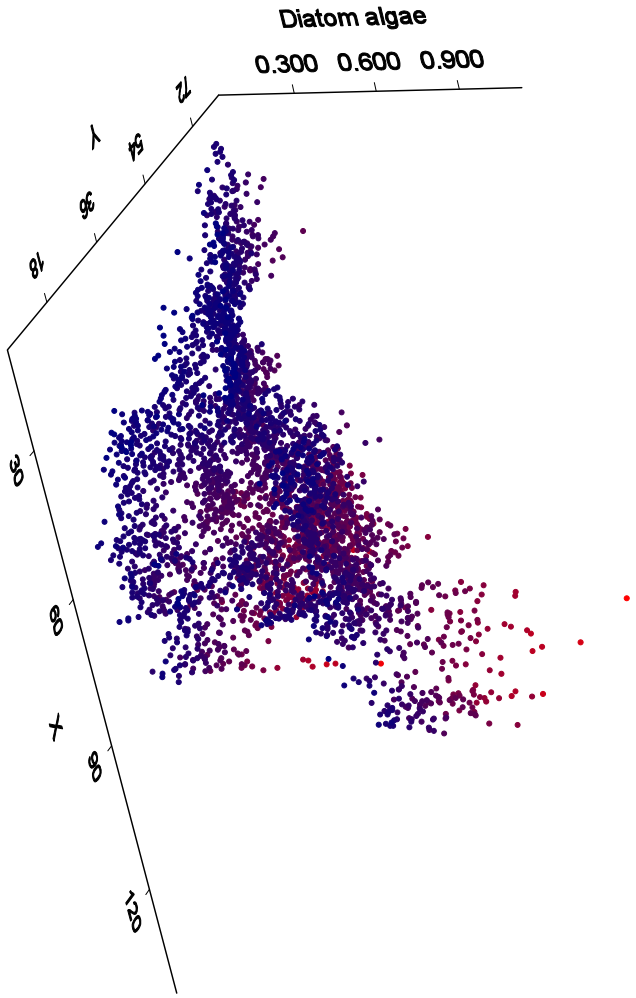
Diatom algae
0.300
0.600
0.900
z
y
34
36
18
38
8
x
8
12

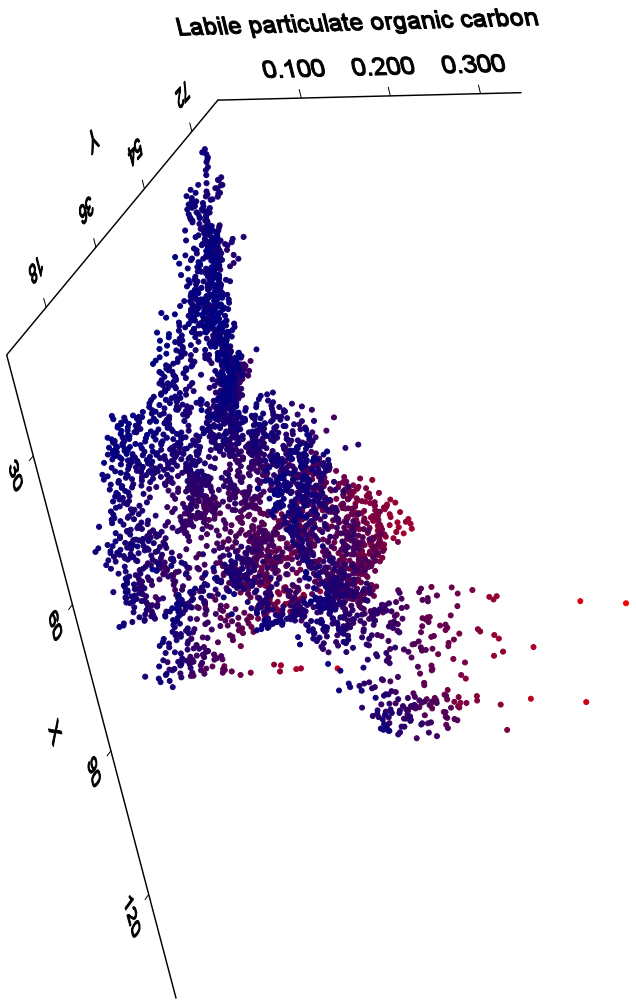
Labile particulate organic carbon
0.100
0.200
0.300
72
54
36
18
Z
90
60
30
0
X

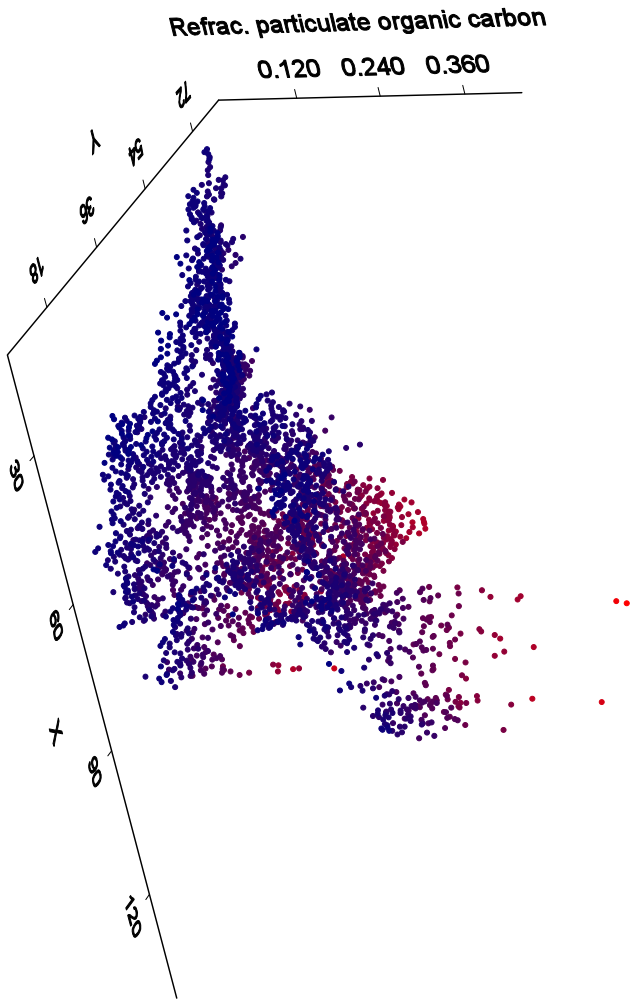
Refrac. particulate organic carbon
0.120
0.240
0.360
72
54
36
18
Z
90
60
30
0
X

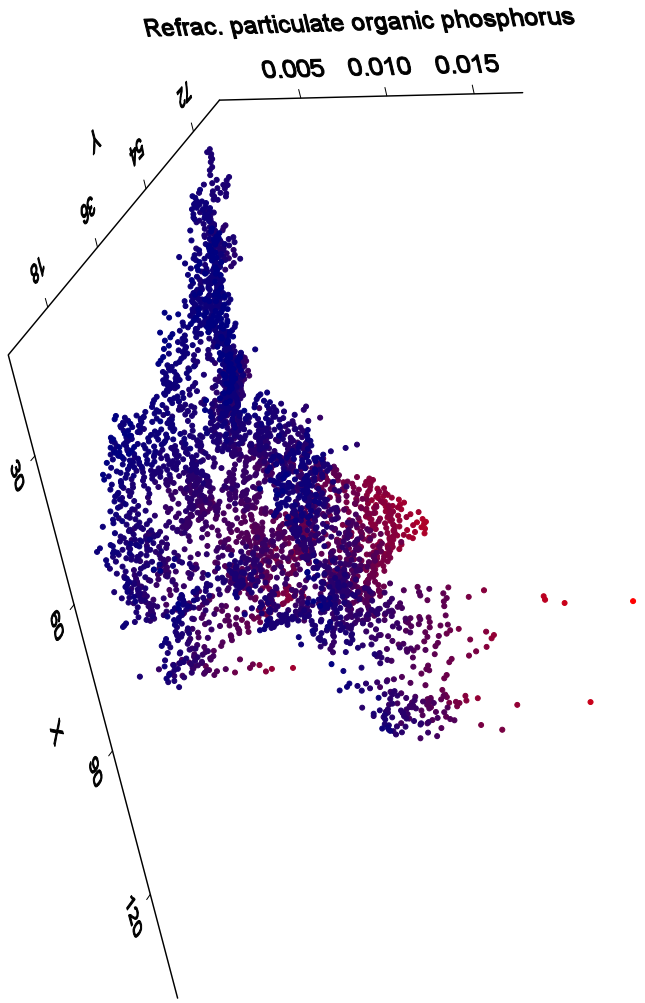
Refrac. particulate organic phosphorus
0.005
0.010
0.015
Z
54
36
18
Y
36
24
12
X

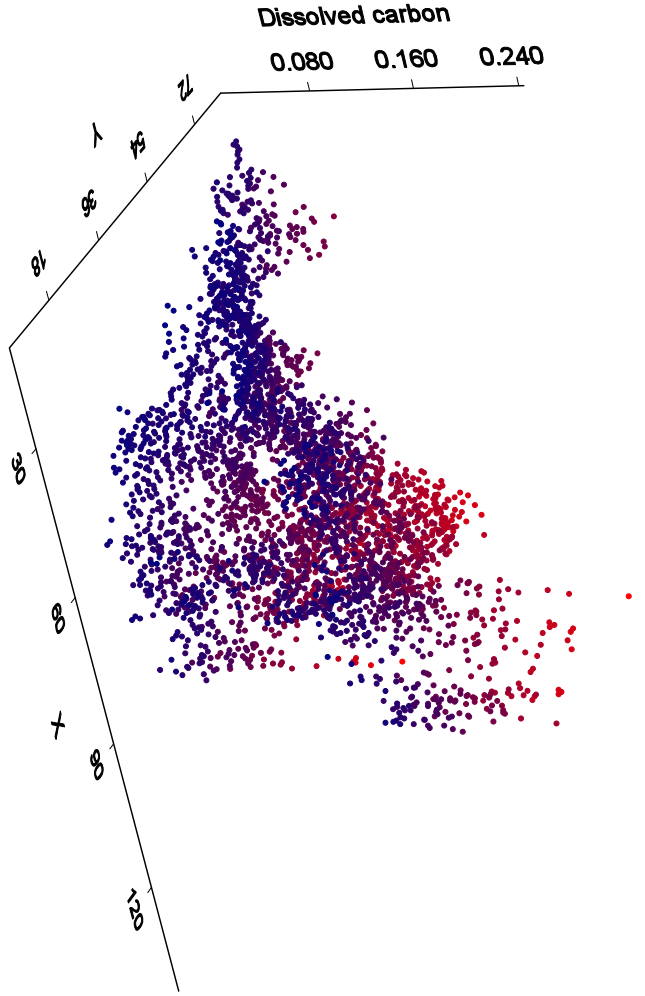
Dissolved carbon
0.080
0.160
0.240
Z
54
36
18
Y
36
24
12
X

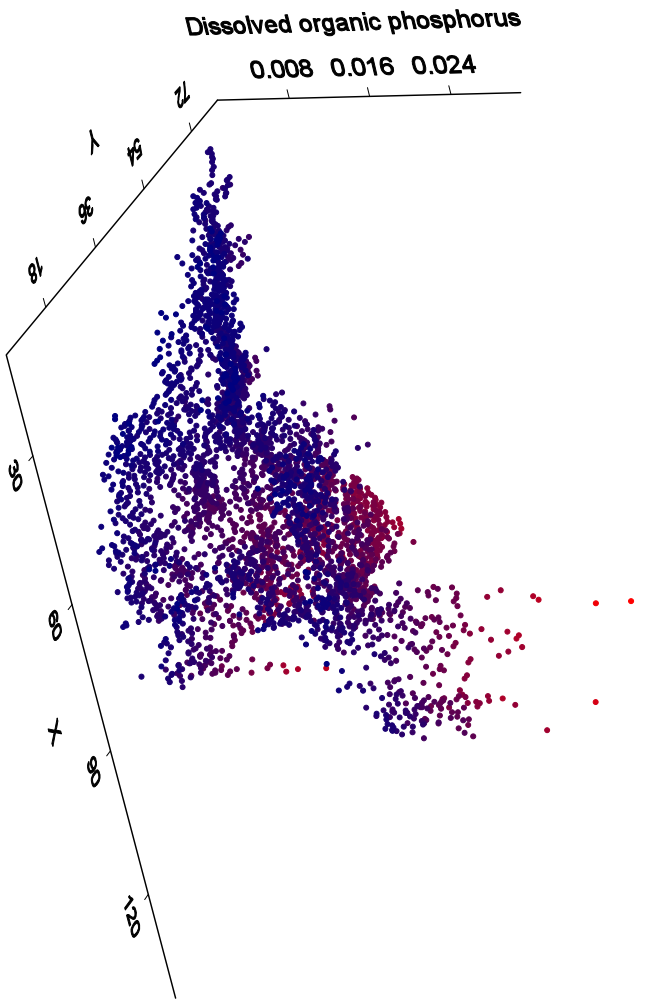
Dissolved organic phosphorus
0.008
0.016
0.024
72
54
36
18
Y
8
8
X
8
12

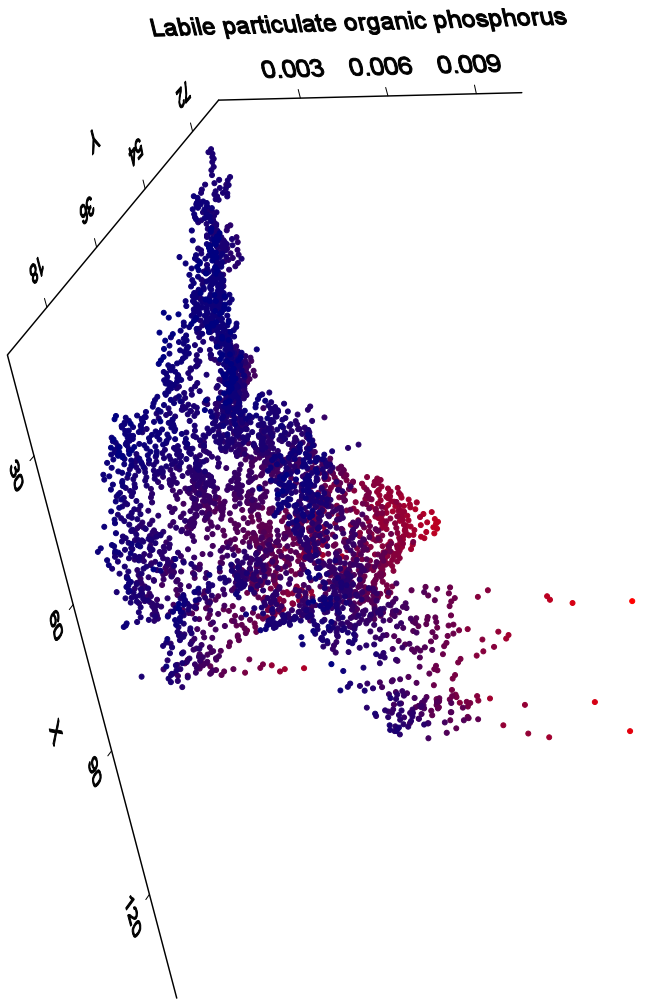
Labile particulate organic phosphorus
0.003
0.006
0.009
72
54
36
18
Y
8
8
X
8
12

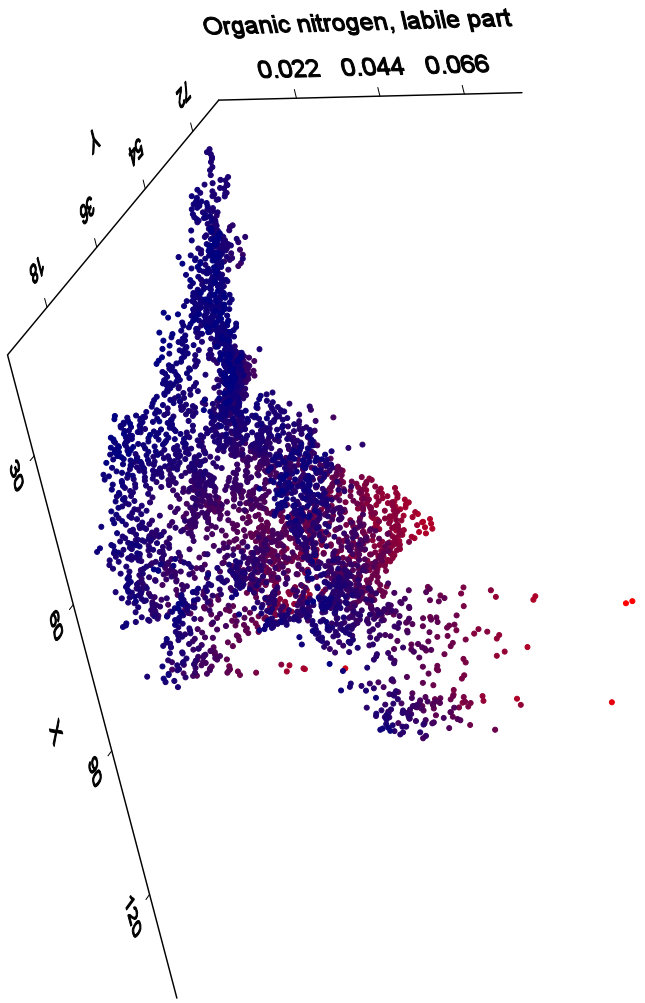
Organic nitrogen, labile part
0.022
0.044
0.066
72
54
36
18
36
24
12

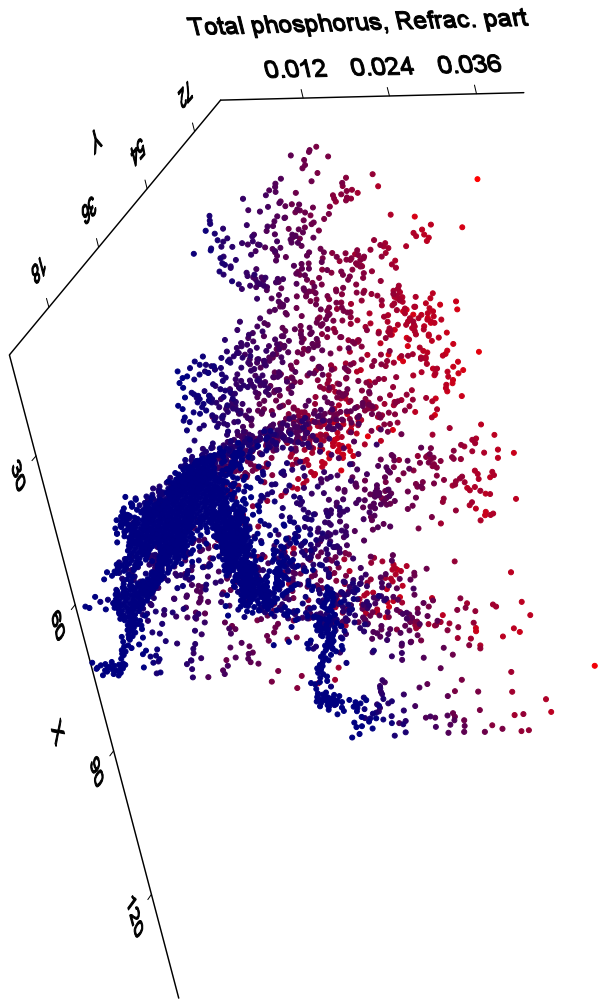
Total phosphorus, Refrac. part
0.012
0.024
0.036
72
54
36
18
36
24
12

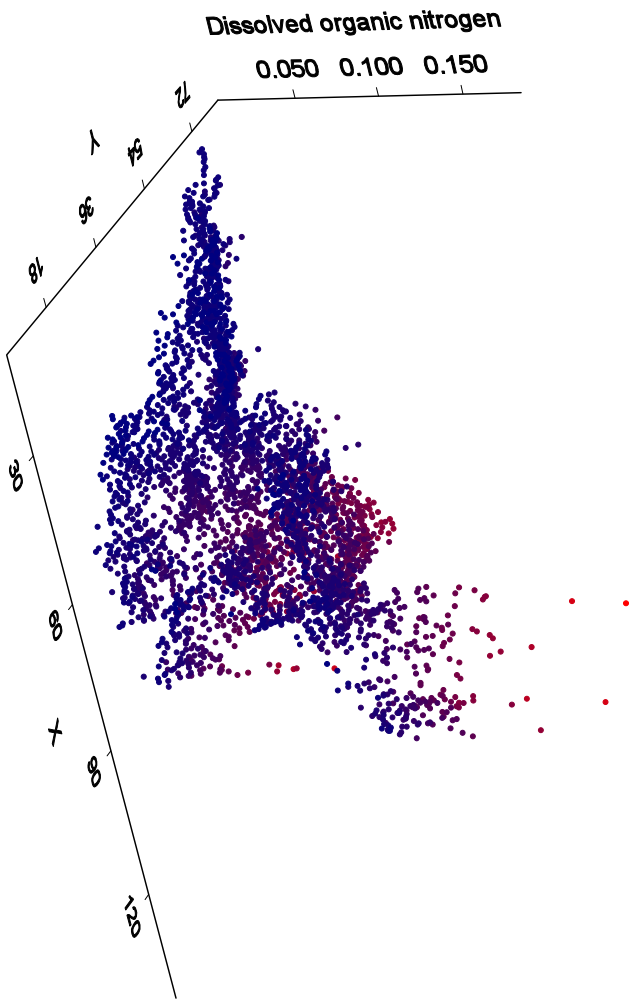
Dissolved organic nitrogen
0.050
0.100
0.150
72
54
36
18
Y
36
18
X
18
36
54

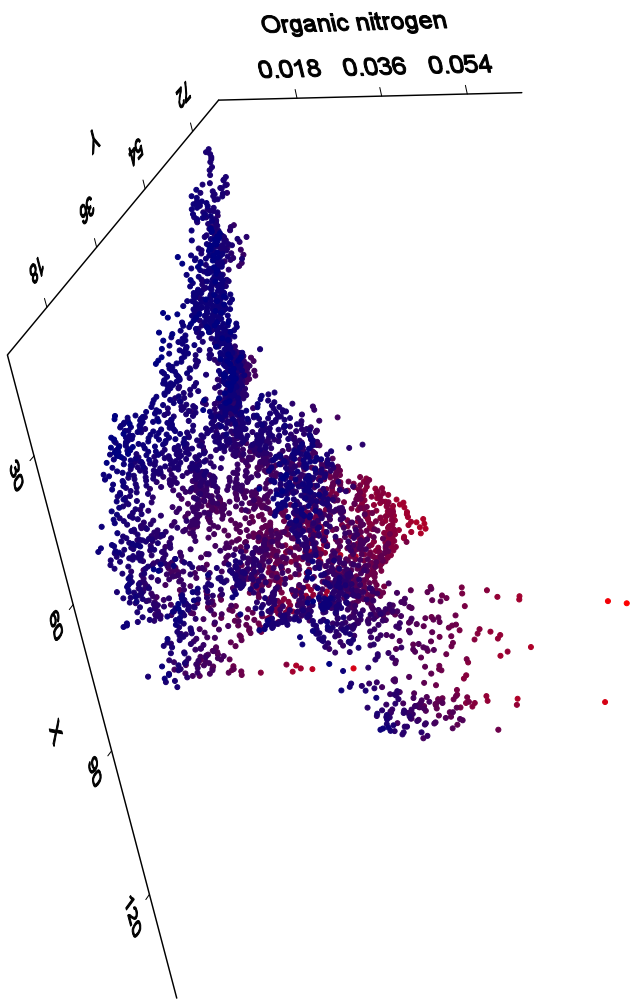
Organic nitrogen
0.018
0.036
0.054
72
54
36
18
Y
36
18
X
18
36
54

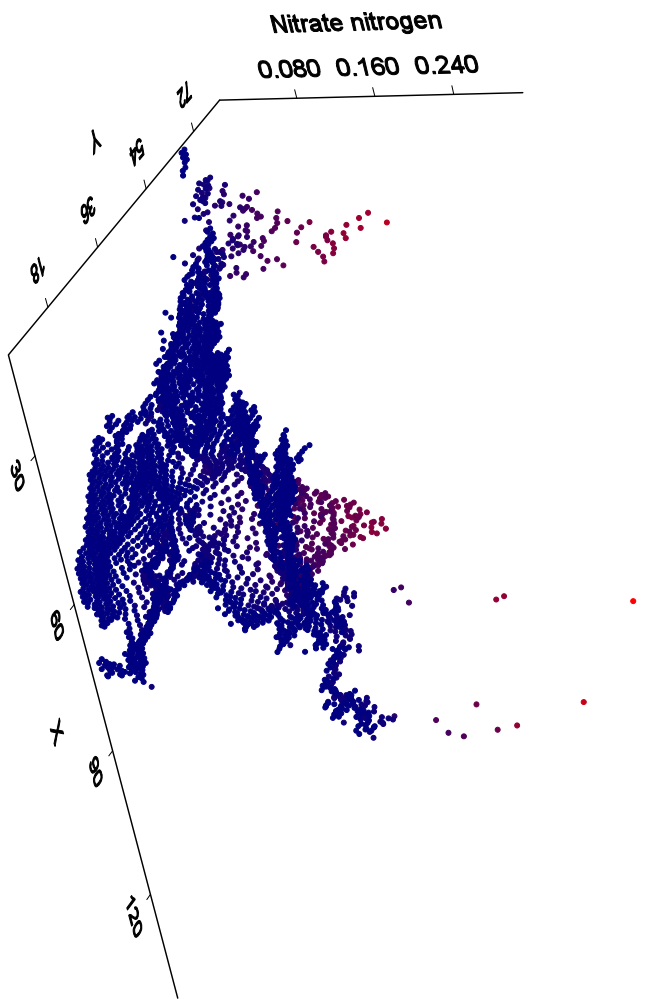
Nitrate nitrogen
0.080 0.160 0.240
Z
Y
54
36
18
36
X
72
108
144

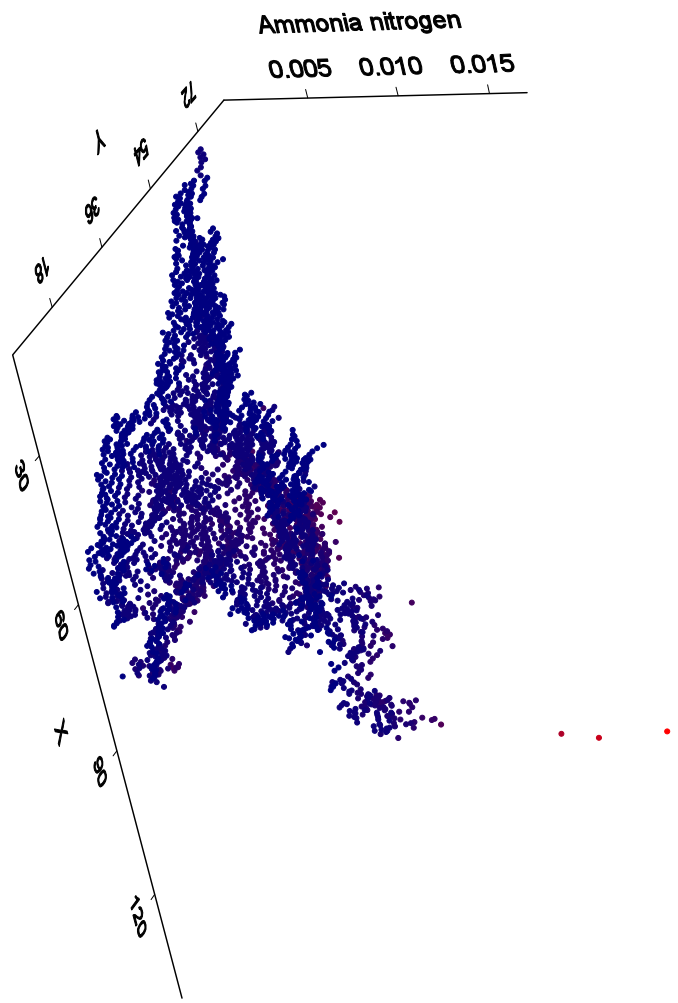
Ammonia nitrogen
0.005 0.010 0.015
Z
Y
54
36
18
36
X
72
108
144

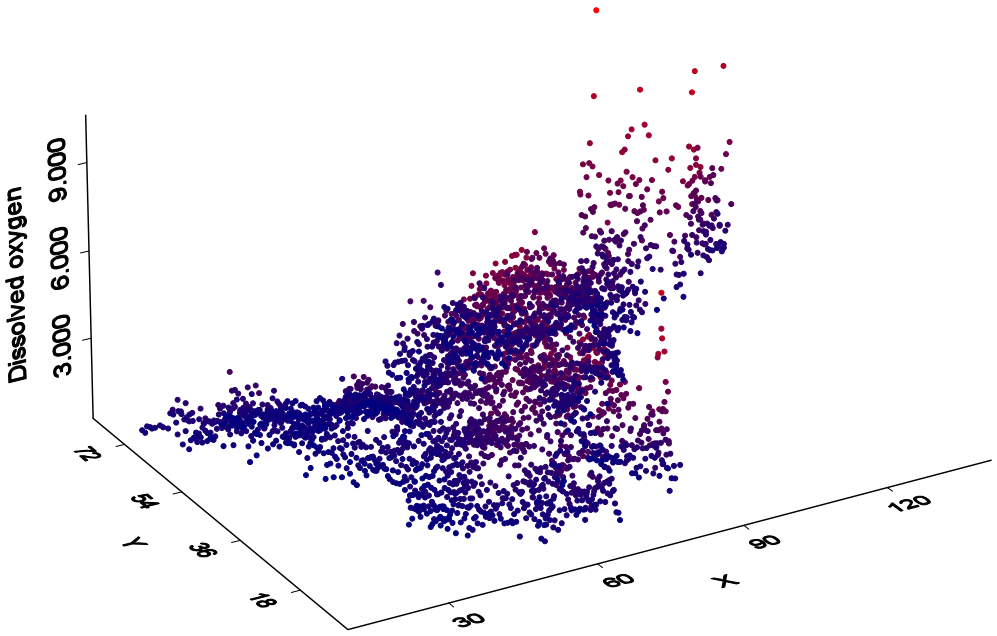
Dissolved oxygen
3.000
6.000
9.000
72
54
36
18
Y
30
60
90
120
X

August 2007

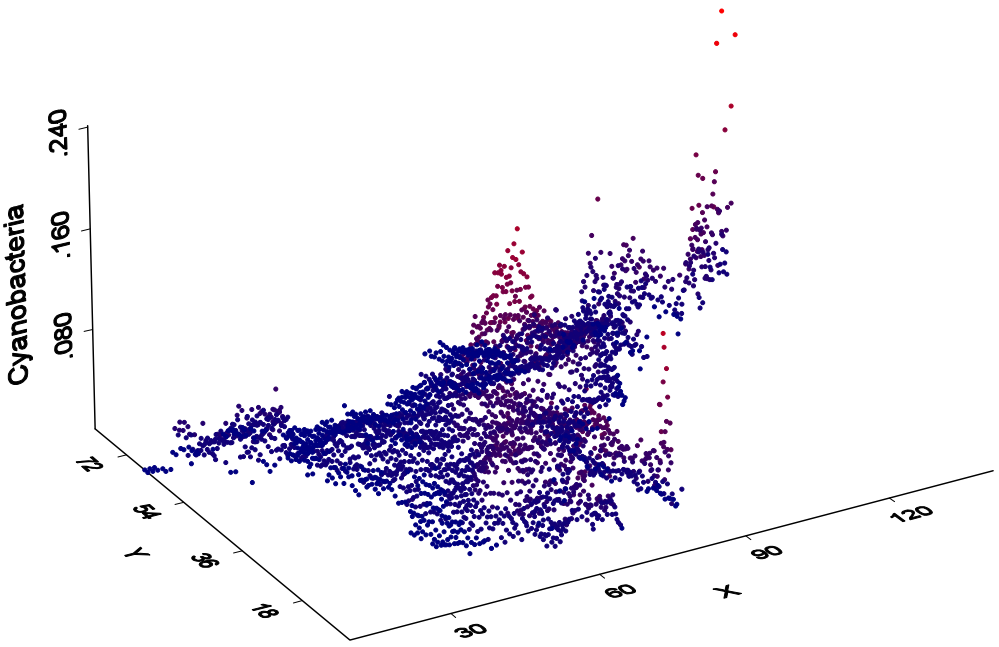
Cyanobacteria
.240
.160
.080
72
54
36
18
Y
30
60
90
120
X

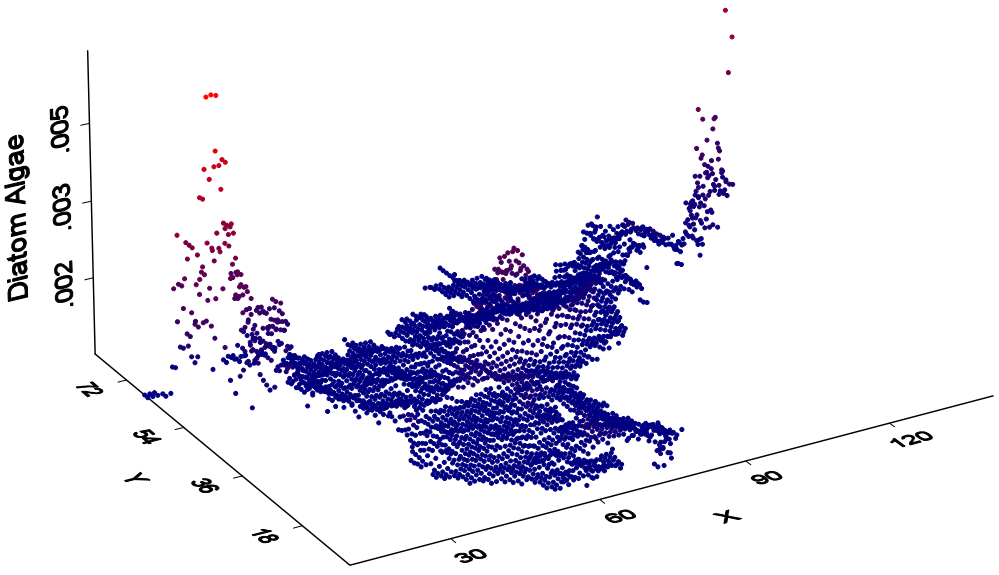
Diatom Algae
.005
.003
.002
72
54
36
18
Y
30
60
90
120
X

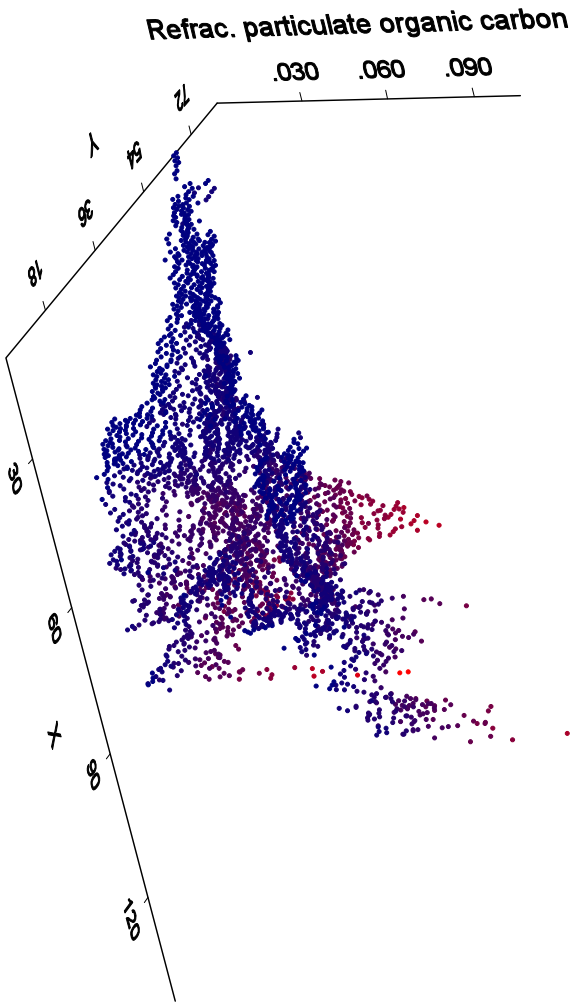
Refrac. particulate organic carbon
.030
.060
.090
z
y
x
18
36
54
38
88
120

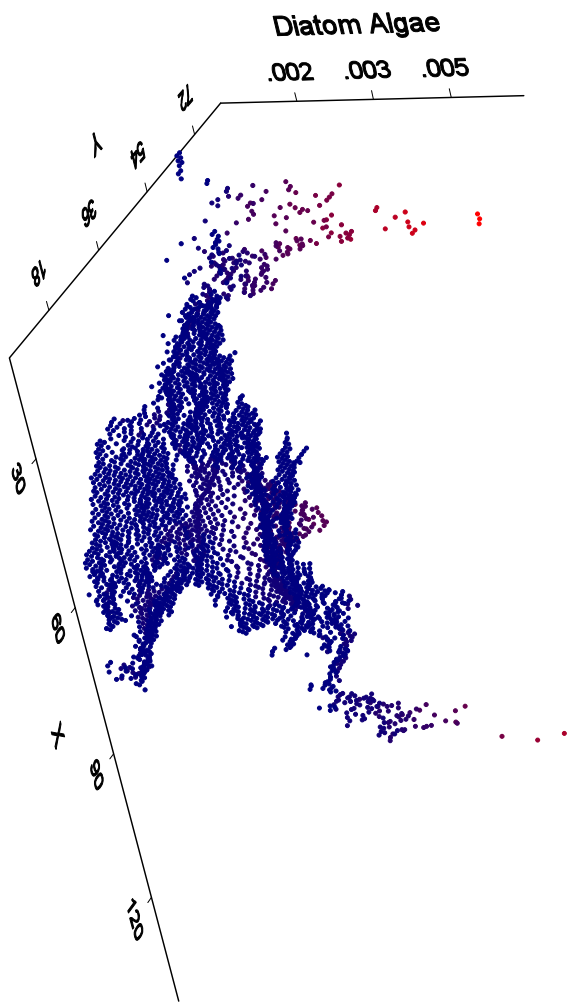
Diatom Algae
.002
.003
.005
z
y
x
18
36
54
38
88
120

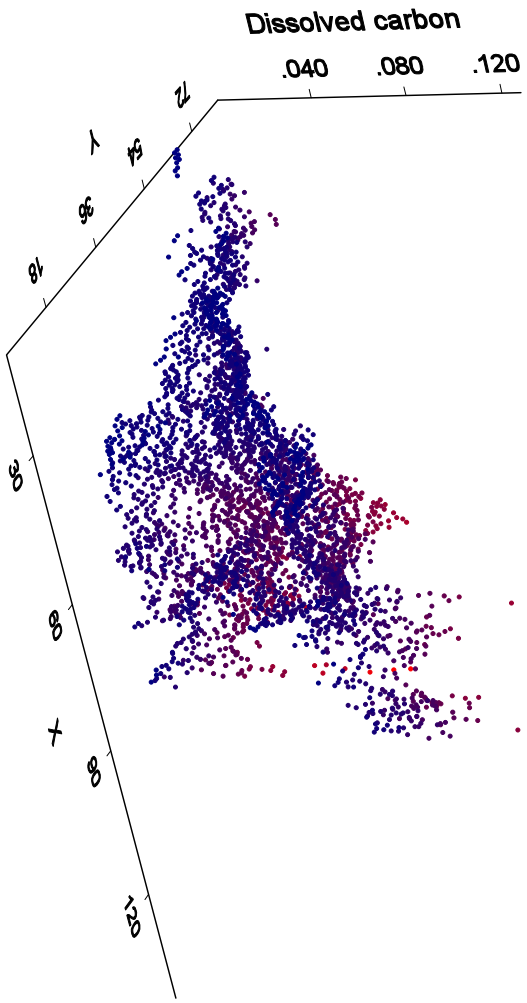
Dissolved carbon
.040
.080
.120
Z
Y
X

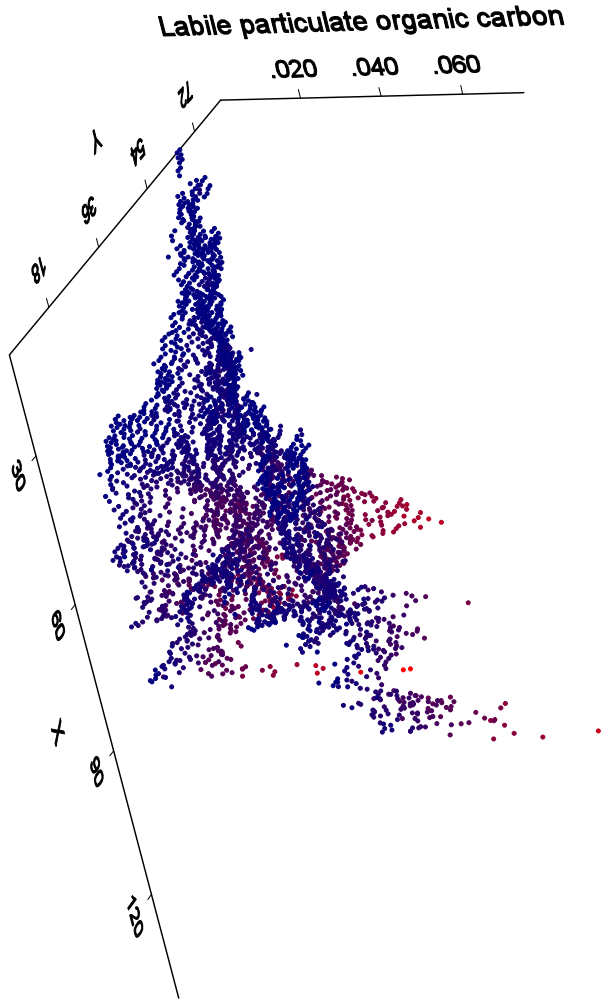
Labile particulate organic carbon
.020
.040
.060
Z
Y
X

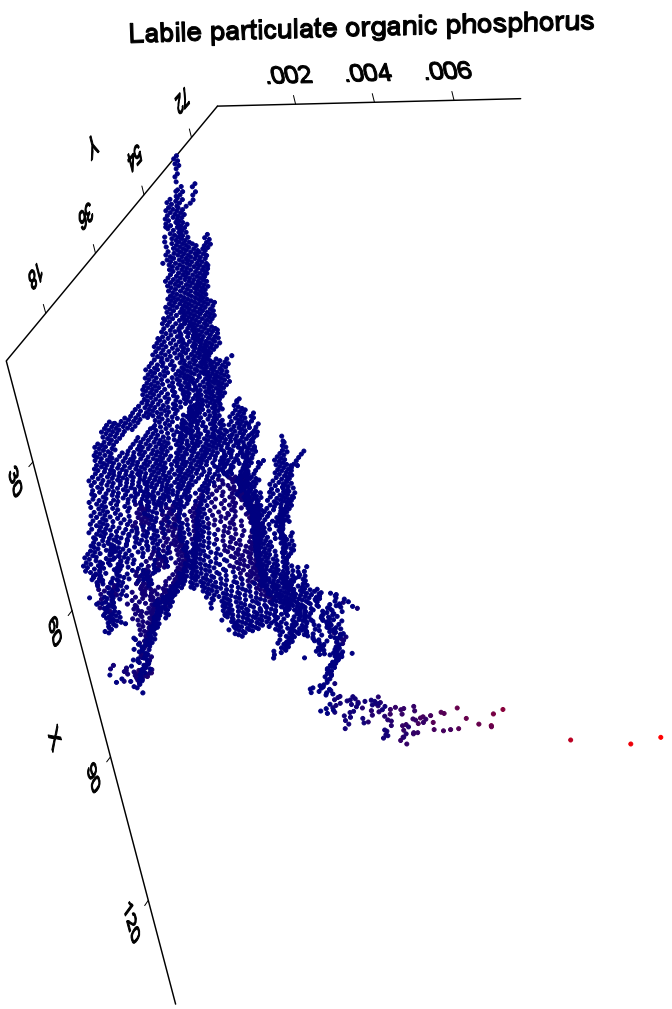
Labile particulate organic phosphorus
.002
.004
.006
Z
Y
34
36
18
38
X
8
12

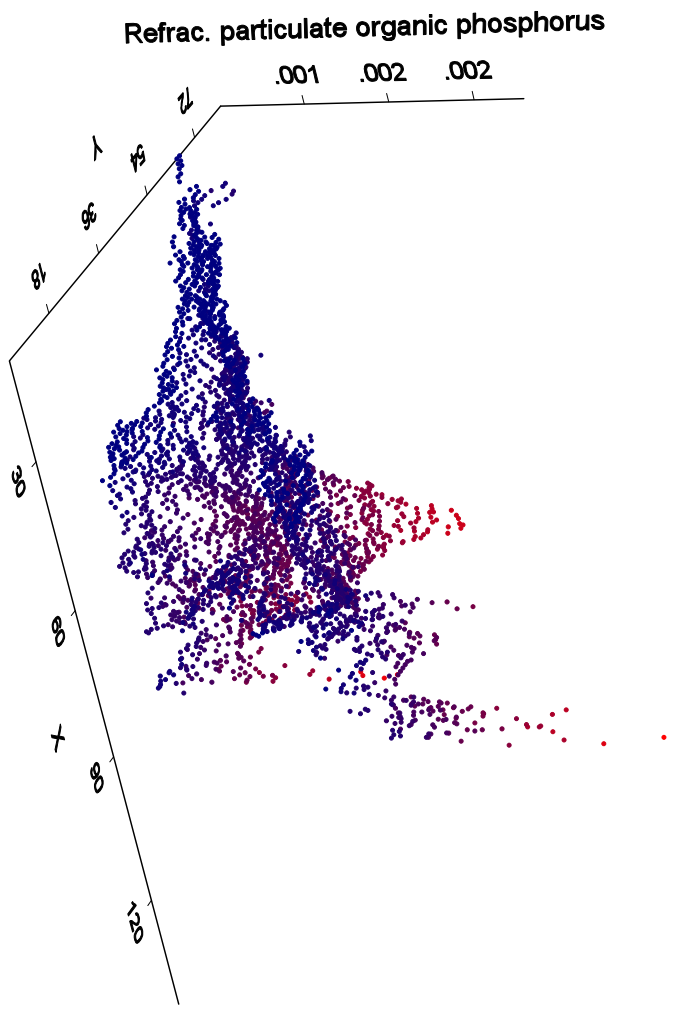
Refrac. particulate organic phosphorus
.001
.002
.002
Z
Y
34
36
18
38
X
8
12

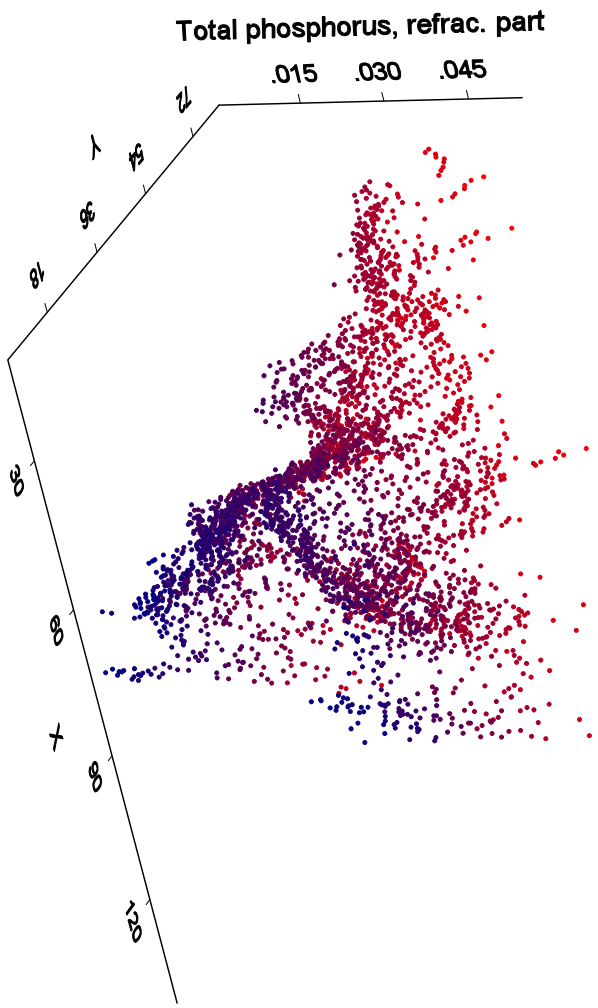
Total phosphorus, refrac. part
.015
.030
.045
Z
Y
34
36
18
38
X
8
120

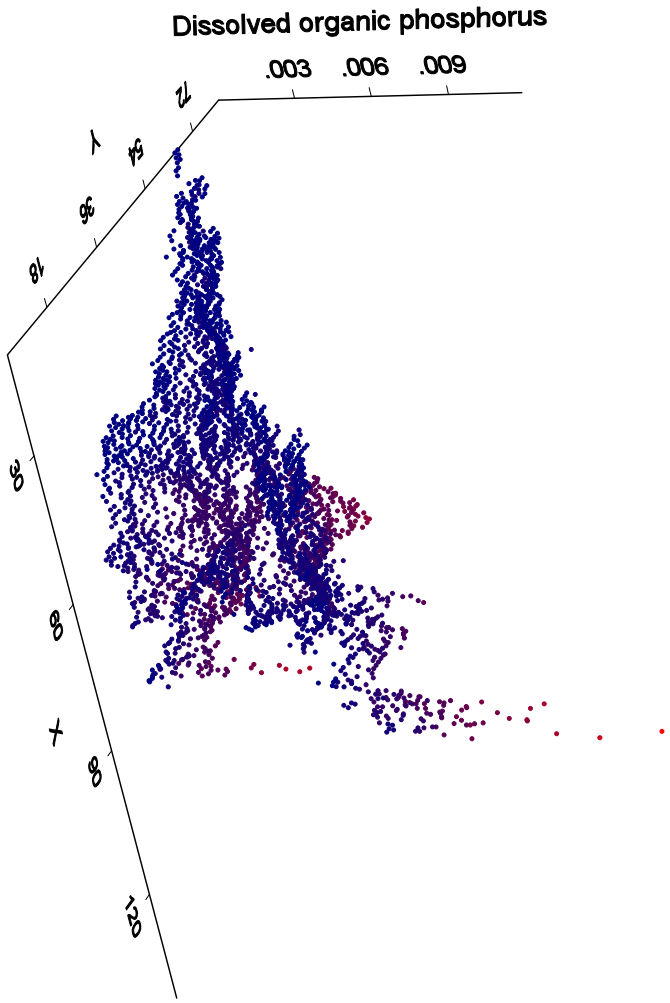
Dissolved organic phosphorus
.003
.006
.009
Z
Y
34
36
18
38
X
8
120

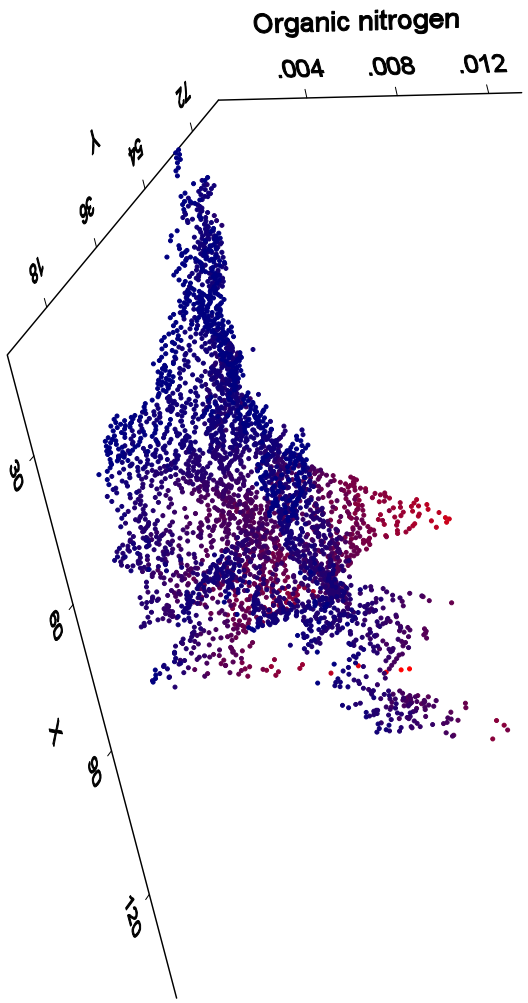
Organic nitrogen
.004
.008
.012
12
24
36
48
Y
8
8
X
8
12

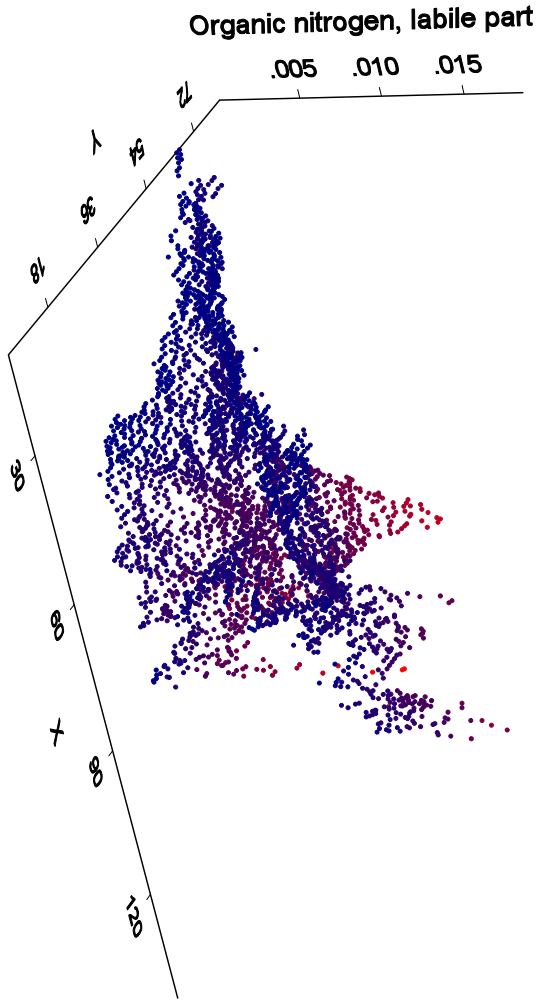
Organic nitrogen, labile part
.005
.010
.015
12
24
36
48
Y
8
8
X
8
12

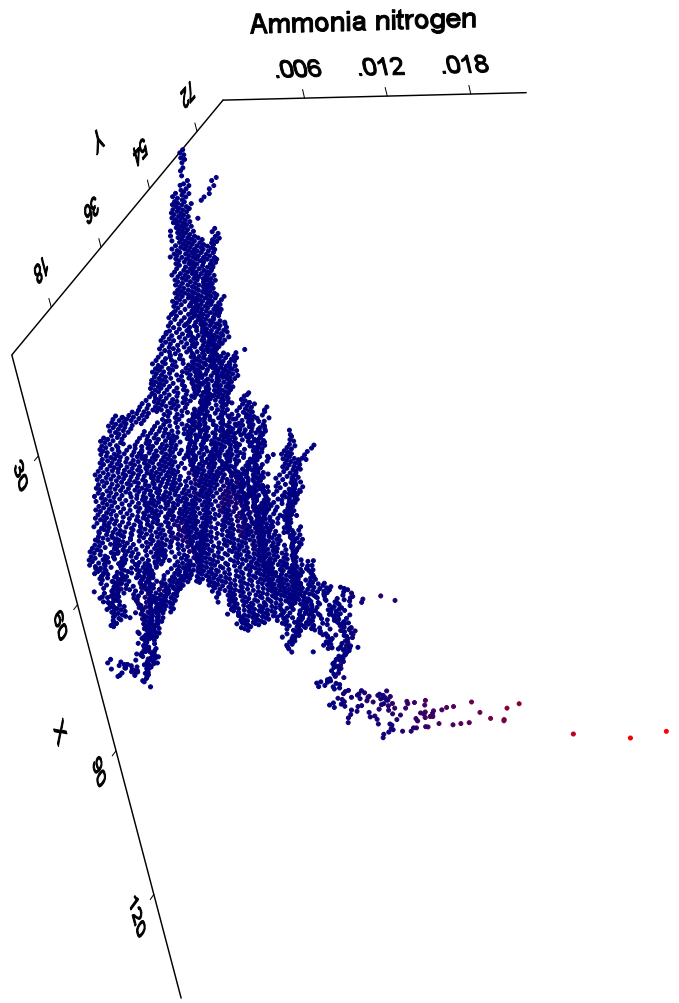
Ammonia nitrogen
.006
.012
.018
Z
Y
X

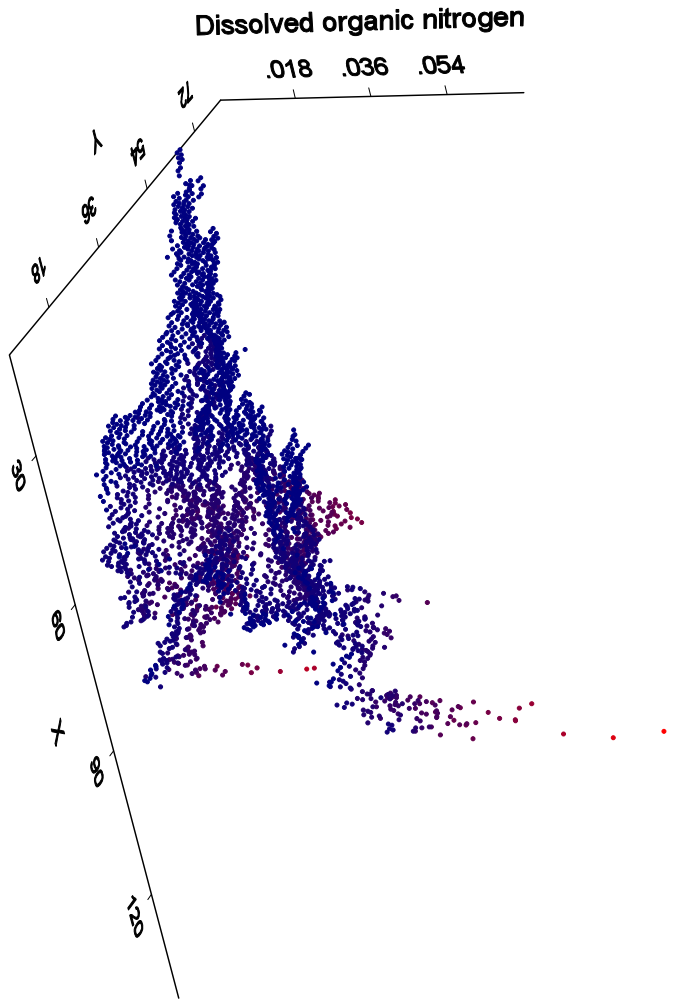
Dissolved organic nitrogen
.018
.036
.054
Z
Y
X

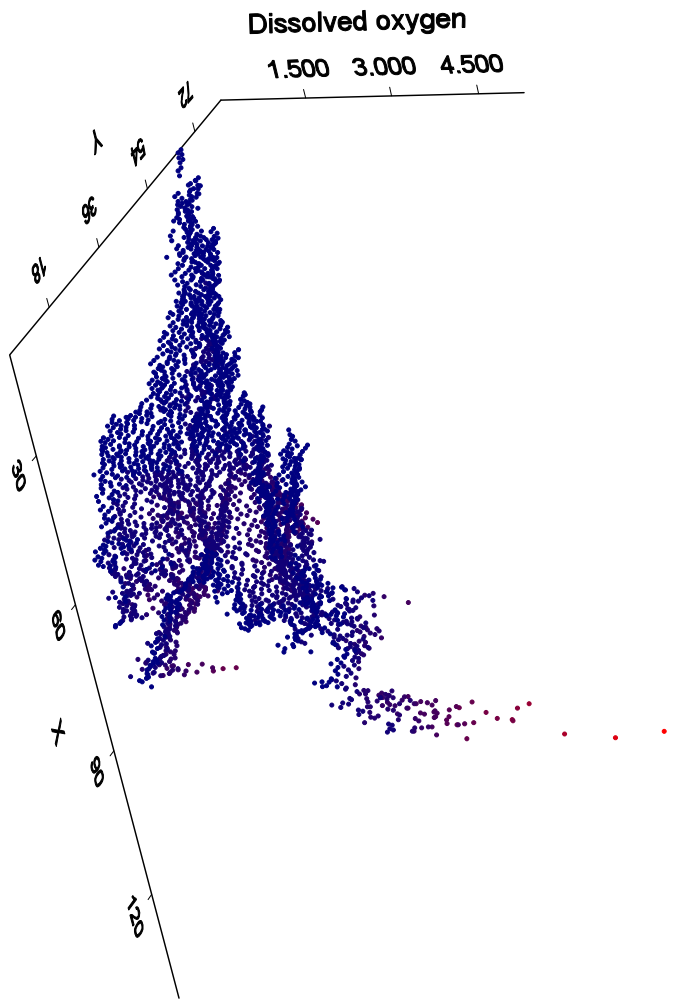
Dissolved oxygen
1.500
3.000
4.500
72
54
36
18
90
80
70
60

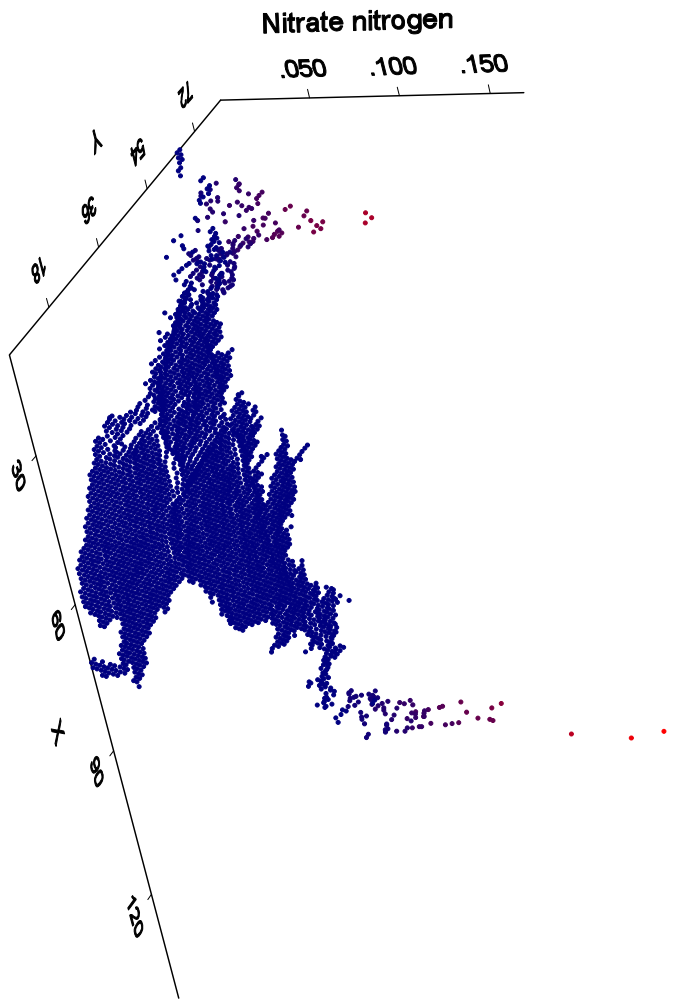
Nitrate nitrogen
.050
.100
.150
72
54
36
18
90
80
70
60

January 2008

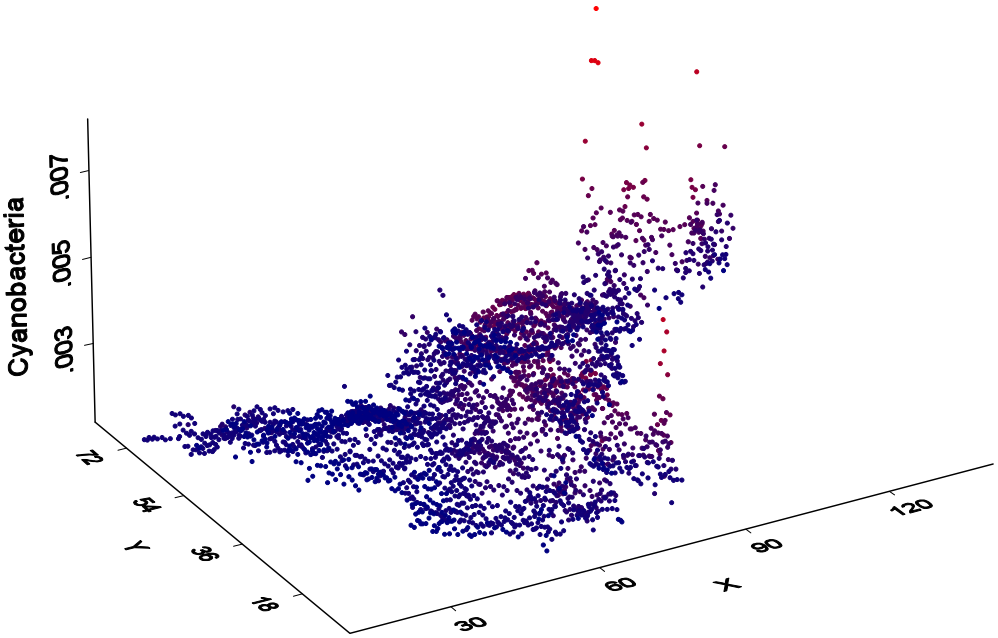

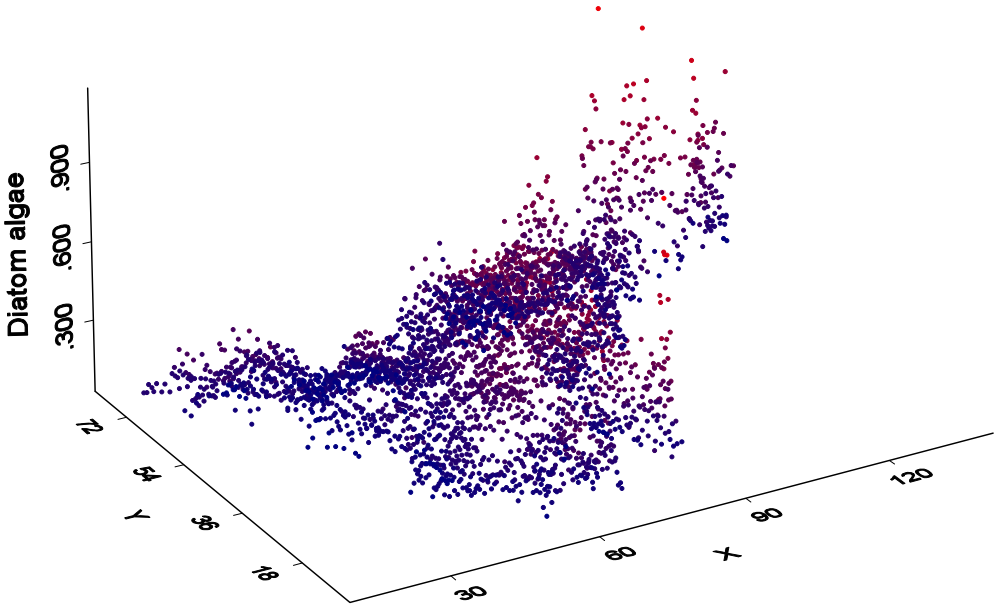

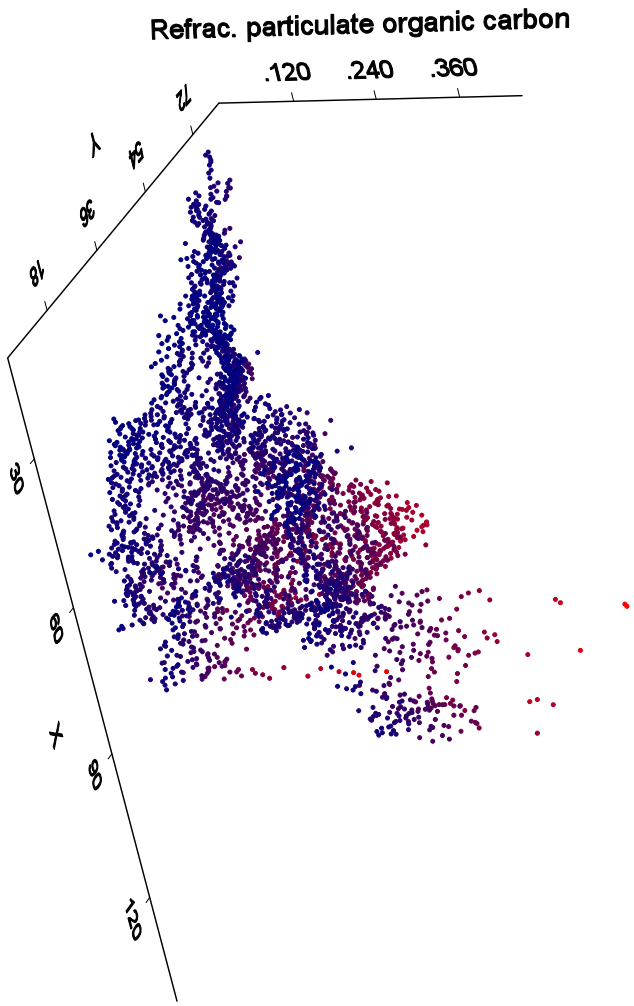
Refrac. particulate organic carbon
.120
.240
.360
Z
Y
18
36
54
Z
72
90
X
90
108
126

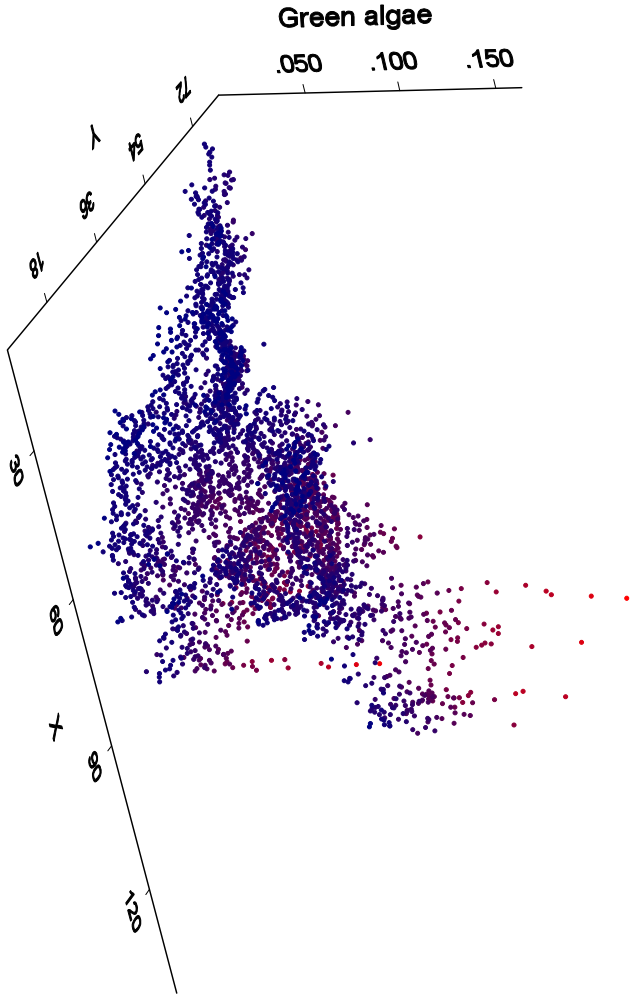
Green algae
.050
.100
.150
Z
Y
18
36
54
Z
72
90
X
90
108
126

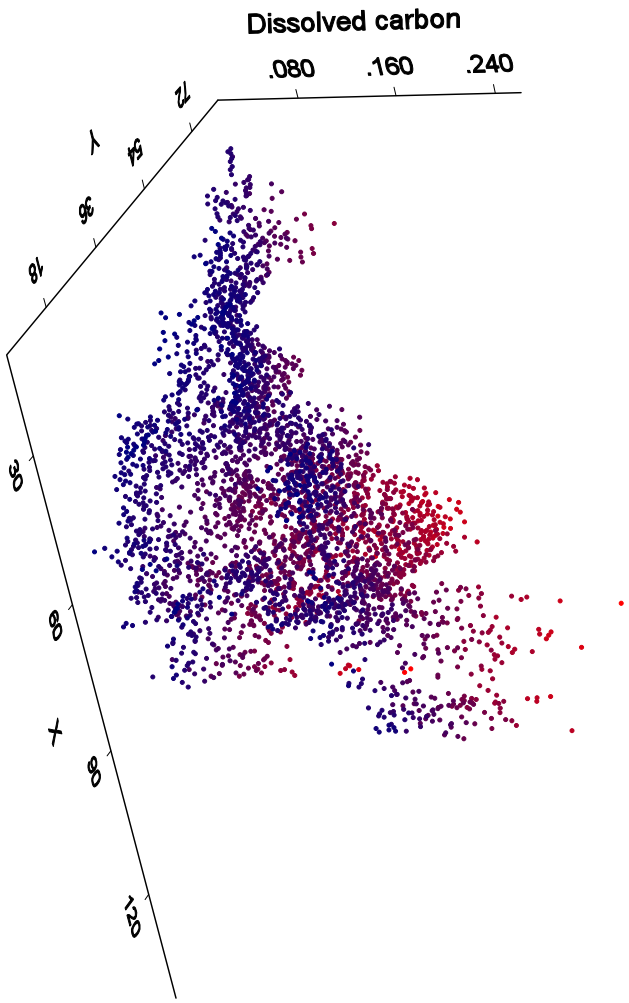
Dissolved carbon
.080
.160
.240
Z
Y
X

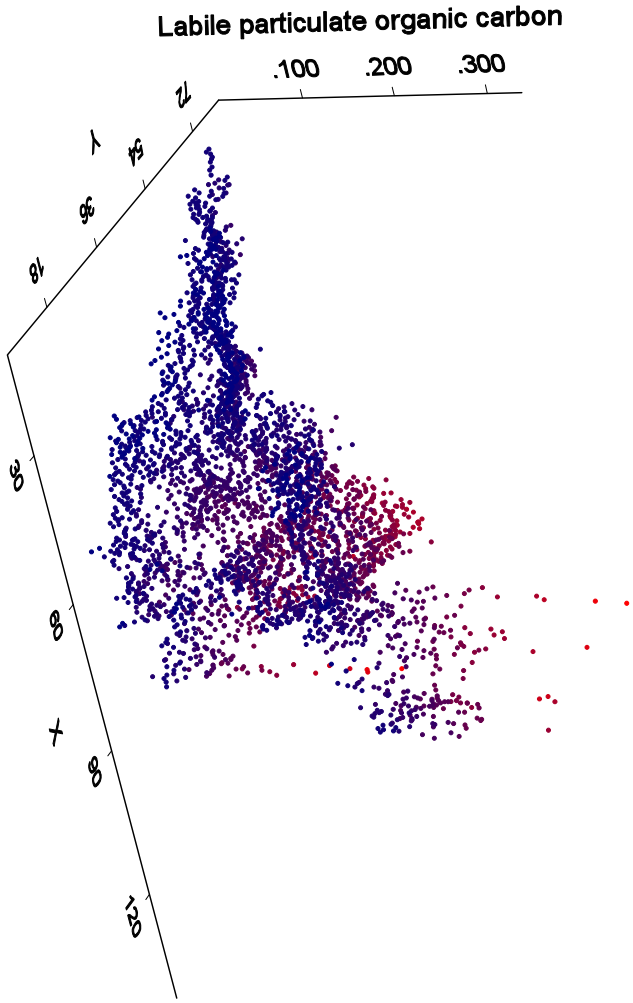
Labile particulate organic carbon
.100
.200
.300
Z
Y
X

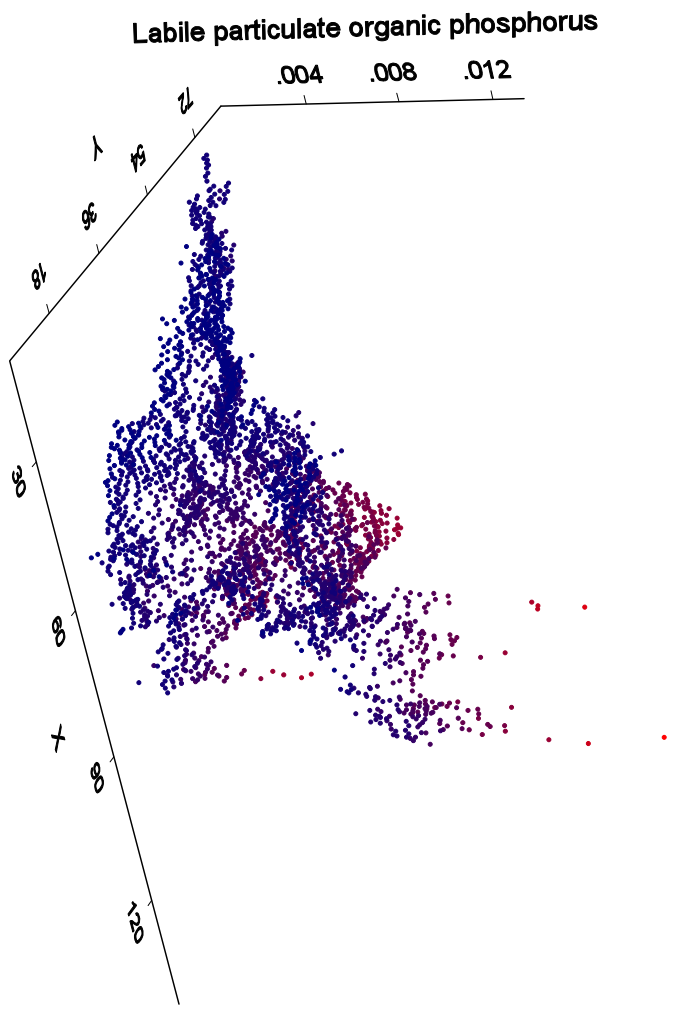
Labile particulate organic phosphorus
.004
.008
.012
72
54
36
18
0
8
16
24
Y
X
Z

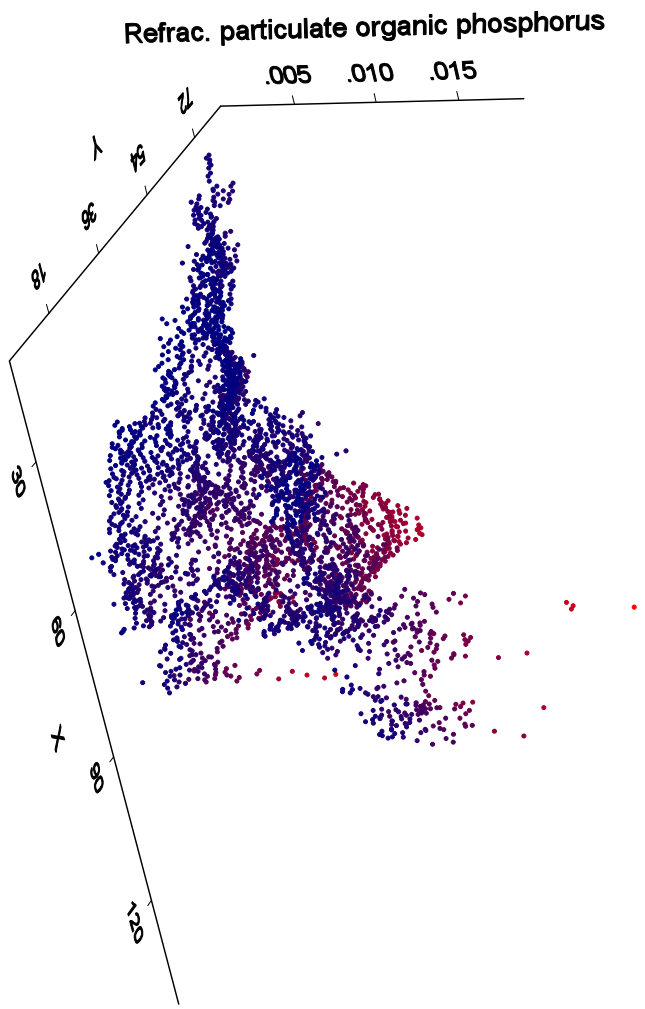
Refrac. particulate organic phosphorus
.005
.010
.015
72
54
36
18
0
8
16
24
Y
X
Z

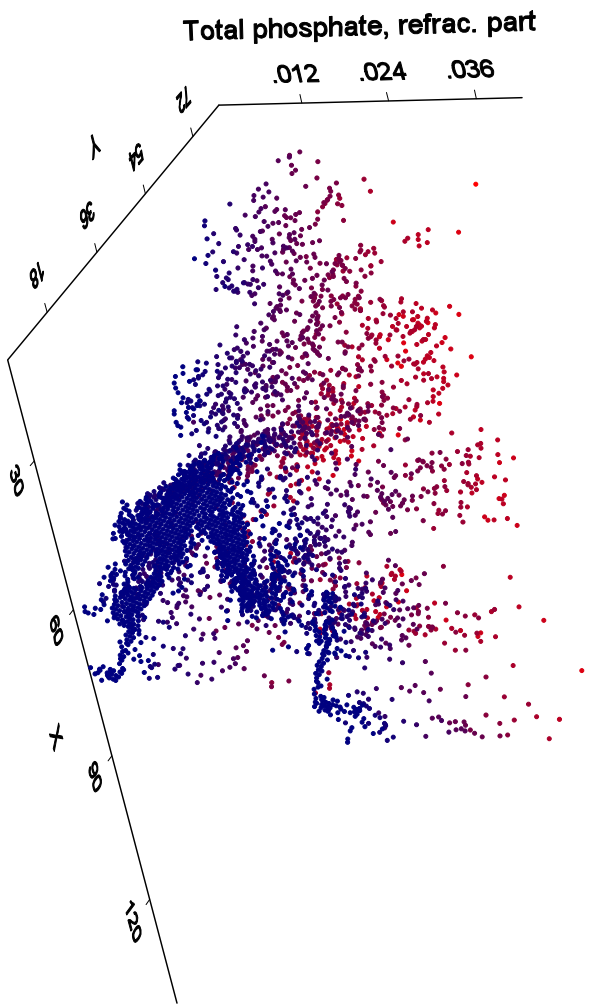
Total phosphate, refrac. part
.012
.024
.036
12
24
36
18
Y
36
18
X
18
12

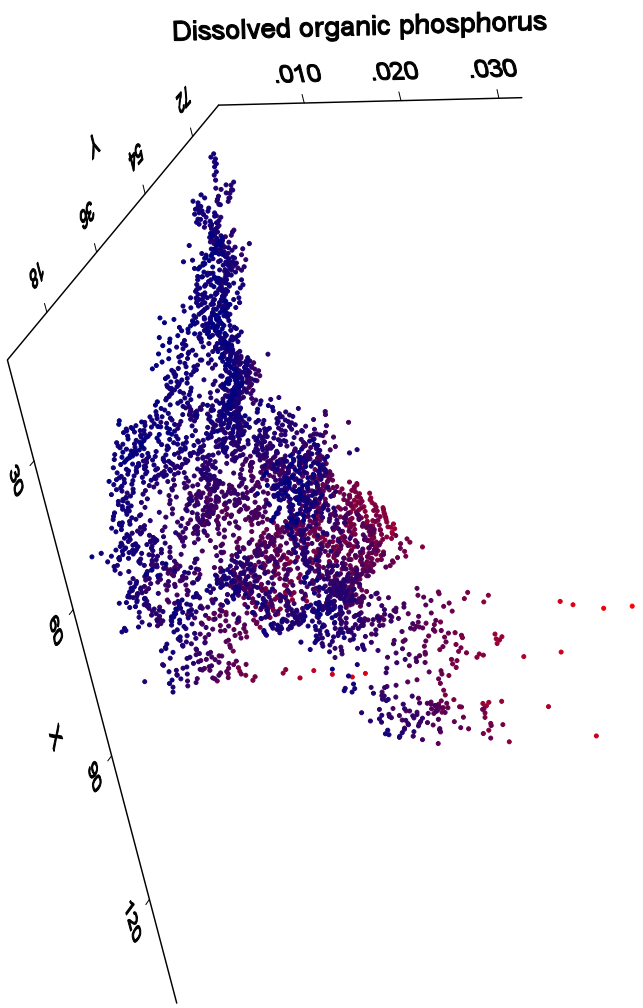
Dissolved organic phosphorus
.010
.020
.030
12
24
36
18
Y
36
18
X
18
12

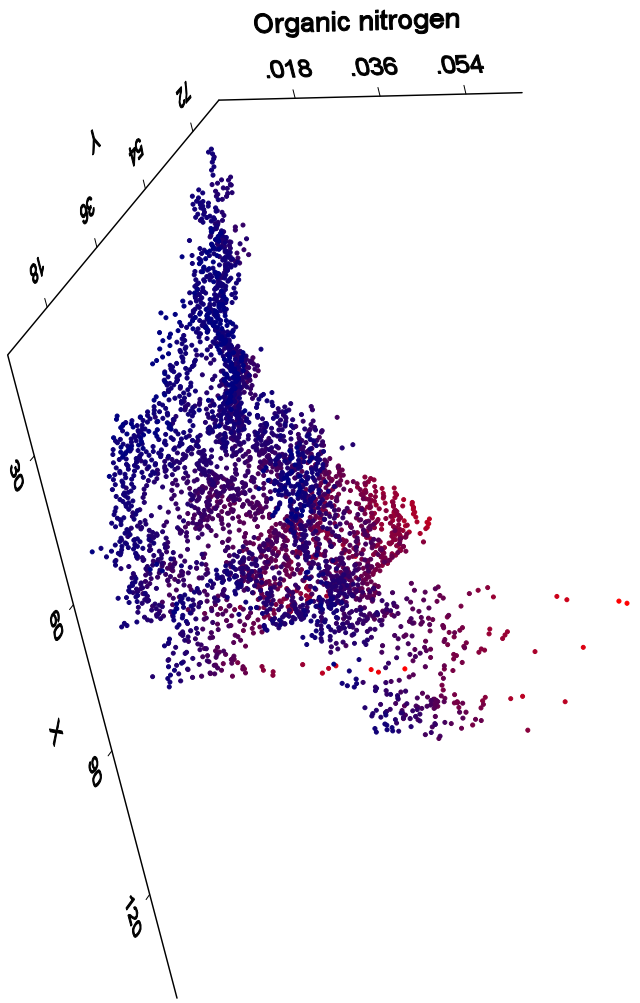
Organic nitrogen
.018
.036
.054
z
y
18
36
54
x
0
40
80
120

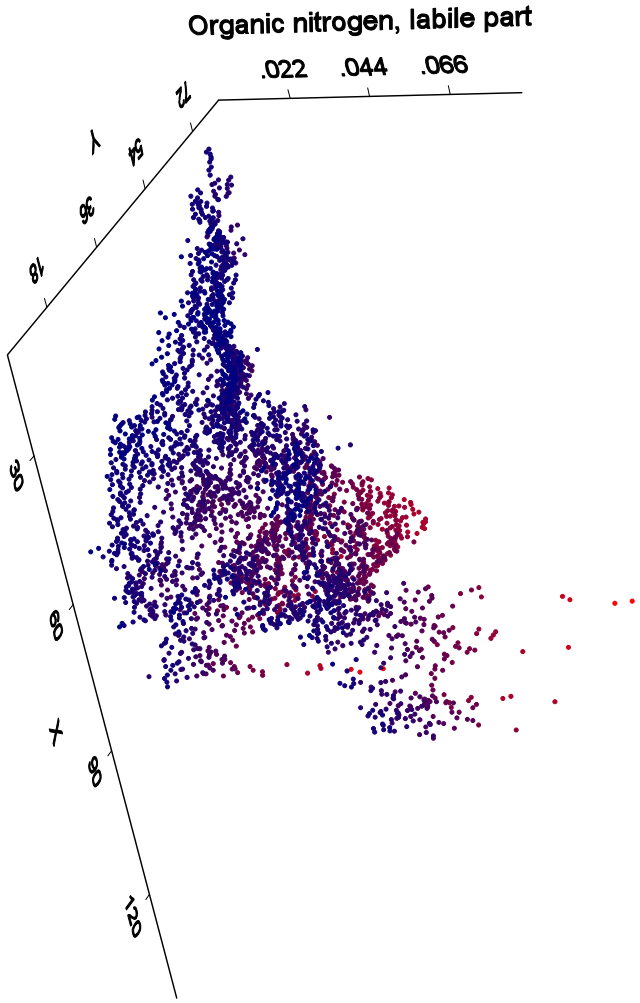
Organic nitrogen, labile part
.022
.044
.066
z
y
18
36
54
x
0
40
80
120

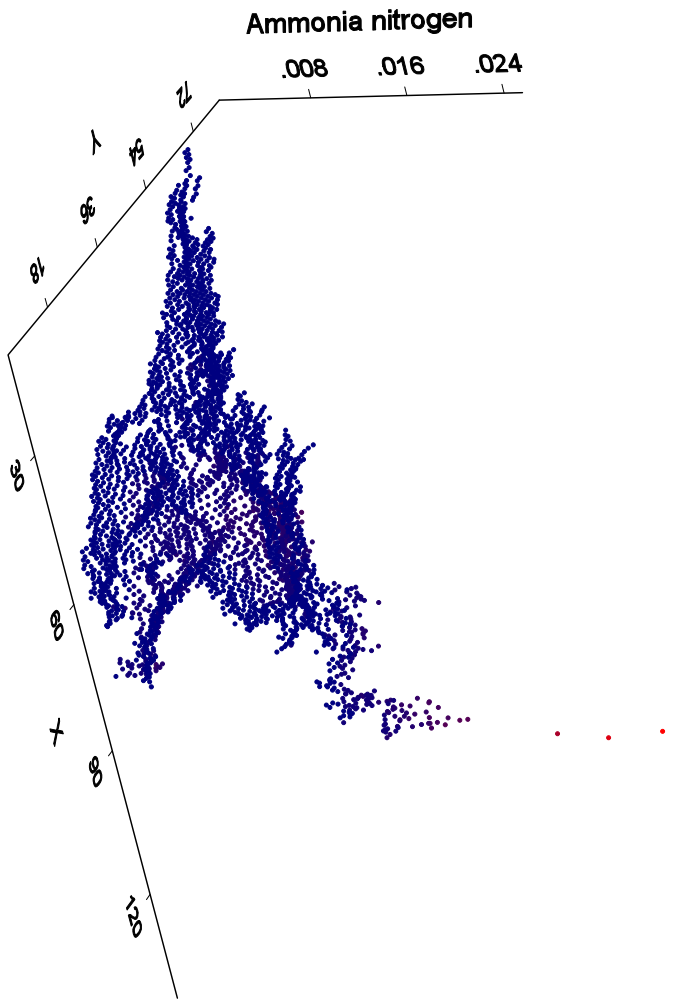
Ammonia nitrogen
.008
.016
.024

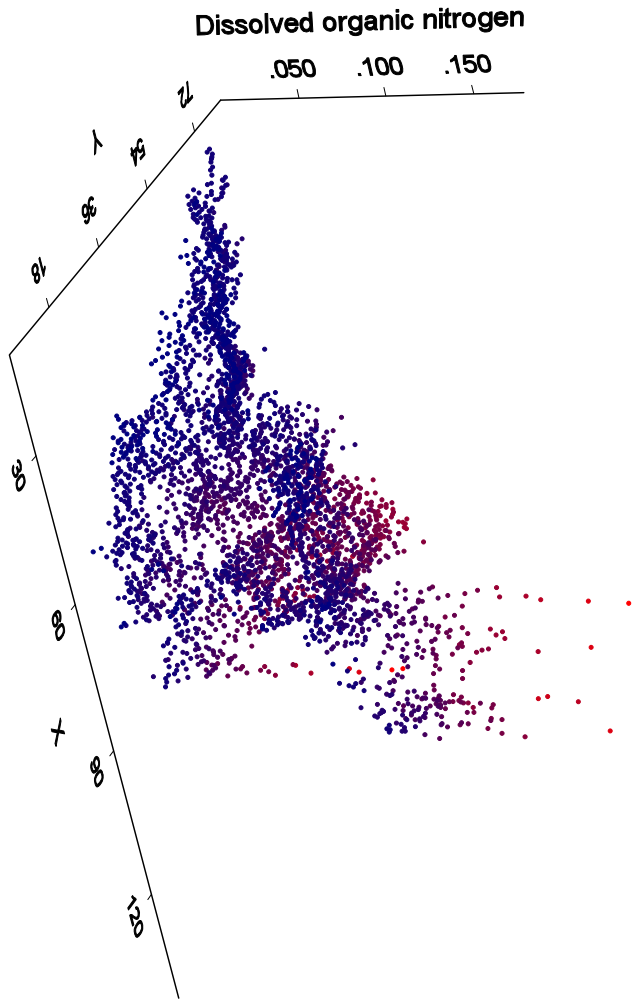
Dissolved organic nitrogen
.050
.100
.150

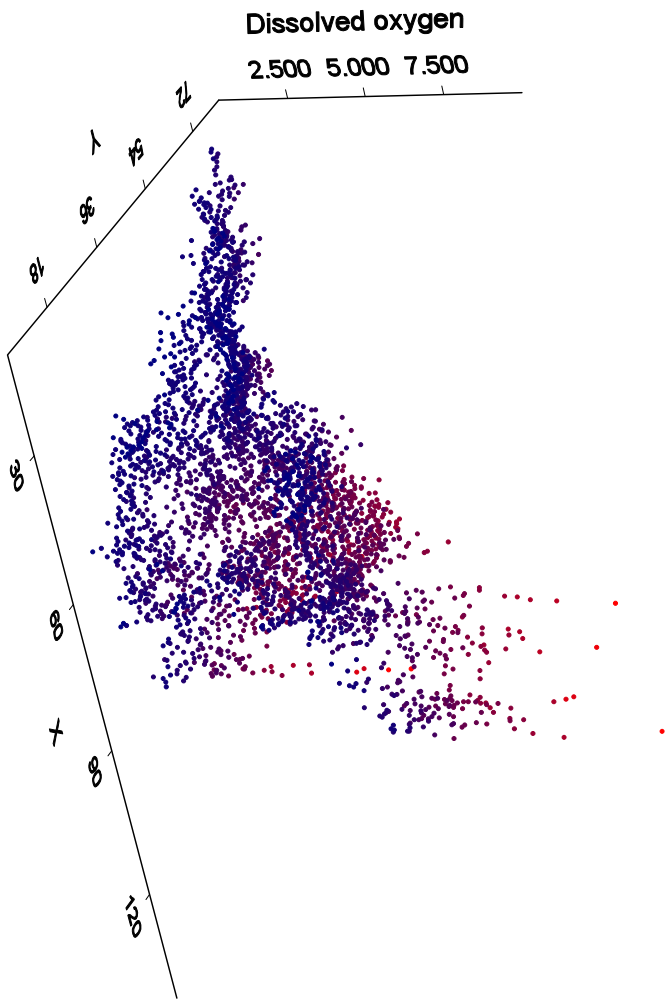
Dissolved oxygen
2.500 5.000 7.500
Z
Y
34
36
18
38
X
8
12

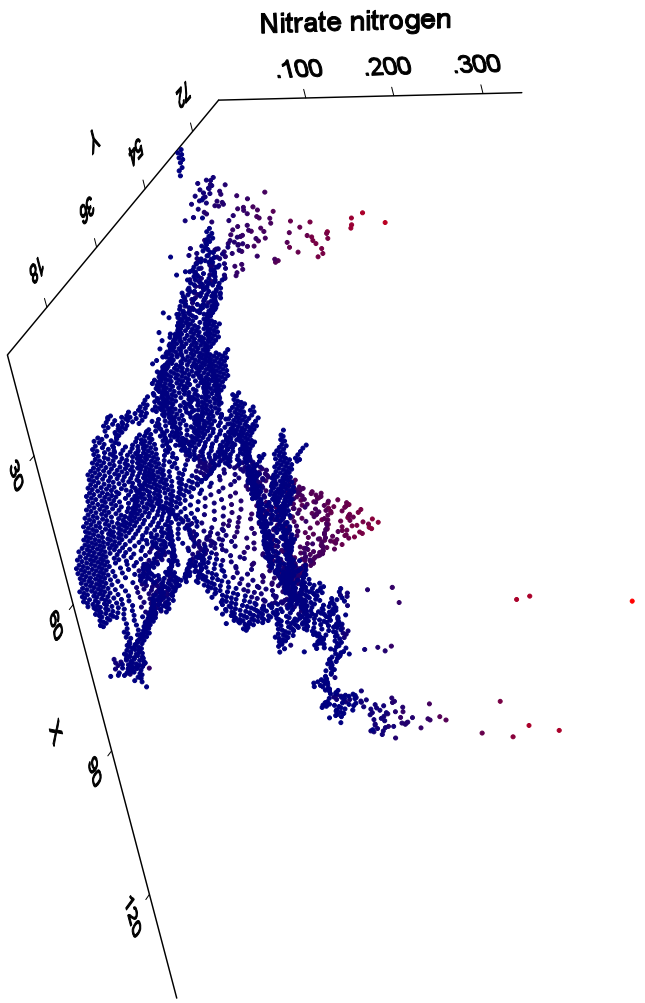
Nitrate nitrogen
.100 .200 .300
Z
Y
34
36
18
38
X
8
12

Unsaturated Hydraulic Properties of Anisotropic Soils

Basic Information

Title:	Unsaturated Hydraulic Properties of Anisotropic Soils
Project Number:	2010NV167B
Start Date:	3/1/2010
End Date:	2/28/2011
Funding Source:	104B
Congressional District:	NV01
Research Category:	Climate and Hydrologic Processes
Focus Category:	Hydrology, Water Supply, Methods
Descriptors:	None
Principal Investigators:	Jianting Julian Zhu

Publications

1. Zhu, J., and D. Sun. 2010. Capillary pressure-dependent anisotropy of unsaturated soils, Canadian Journal of Soil Science. 90(2):319-329.
2. Zhu, J., and D. Sun. 2010. Saturation-dependent anisotropy of unsaturated soils. 19th World Congress of Soil Science – Soil Solution for a Changing World, August 1 – 6, 2010, Brisbane, Australia, pp.40-43.
3. Zhu, J. 2010. Effective hydraulic functions in layered porous media. American Soil of Agronomy, Crop Science Society of America, Soil Science Society of America 2010 International Annual Meetings, October 31 – November 4, 2010, Long Beach, California, U. S. A.
4. Zhang, Y., J. Zhu, and D. Sun.2010. Non-Fickian mechanism of contaminant transport in unsaturated heterogeneous soils. American Soil of Agronomy, Crop Science Society of America, Soil Science Society of America 2010 International Annual Meetings, October 31 – November 4, 2010, Long Beach, California, U. S. A.
5. Zhu, J. 2010. Saturation-dependent anisotropy of structured and random layered soils. 2010 European Geoscience Union Annual General Assembly, May 2 – 7, 2010, Vienna, Austria.

Unsaturated Hydraulic Properties of Anisotropic Soils

Final Report

Problem and Research Objectives

Large scale soils usually demonstrate different moisture spreading behavior at different water saturation (or tension) levels, due to anisotropy (typically manifested as thin layering and irregularly shaped particles) associated with soil formation processes such as alluviation, sedimentation and particle orientation etc. This anisotropic behavior has important implications for recharge of groundwater, especially in arid and semi-arid areas where groundwater tables are typically very deep and saturation levels vary greatly from ground surface to groundwater tables since it might either facilitate or retard downward water movement of water at different saturation levels. Therefore, the conceptualization and quantification of unsaturated zone hydraulic conductivity anisotropy are important part of unsaturated zone characterizations which are necessary to more accurately estimate water flow behavior in the unsaturated zone. While the effects of saturation on soil anisotropy in unsaturated media have been recognized for long time, they have not been fully described conceptually. Previous studies proposed conceptual models to quantify saturation-dependent soil anisotropy assuming soil formations consisting of many thin layers each with its own hydraulic properties. The model results indicated that, as saturation decreases the anisotropy factor first decreases to a minimum, and then increases rapidly as the soil dries. Some other approaches have also been developed to study the soil anisotropy behavior in dealing with flow and transport problems in saturated and unsaturated soils, such as tensorial connectivity-tortuosity concept to describe the unsaturated soil hydraulic conductivity which assumed that only soil pore connectivity and/or tortuosity and the saturated hydraulic conductivity are anisotropic. In this project, we are interested in the anisotropy that mainly arises from a combination of both wide range of soil texture variations and within narrow range of texture units due to particle segregation and compaction that typically affect porosity or bulk density. Pedotransfer functions (PTFs) are often used to estimate soil hydraulic properties when direct measurements are too expensive. PTFs transform basic soil properties such as texture, bulk density into water retention and saturated or unsaturated hydraulic conductivity. Artificial neural network based PTFs have become increasingly more popular in the last decade or so. Compared to traditional PTFs, an advantage of neural networks is that it requires no a priori conceptual model.

The main objective of this project is to develop hydraulic conductivity models that quantify anisotropy of saturated and unsaturated soils composed of many thin layers distinguished by both the texture and the bulk density of soil. We propose a new approach to combine the neural network analysis results with the thin layer approach to explore saturation-dependent anisotropy behavior for a wide range of texture and bulk density conditions.

Methodology

Based on the results of the van Genuchten hydraulic parameters in relation to texture (using mean grain diameter as a surrogate) and the bulk density as established by the neural network

approach, we perform a regression (or least-square) analysis to establish the relationships between the van Genuchten hydraulic parameters and mean grain diameter and between the van Genuchten parameters and the bulk density. In other words, these relationships will relate hydraulic properties to the two main indicators, the mean grain diameter and the bulk density. That is, for each van Genuchten parameter, p, we will establish a functional relationship $p = f_p(d_m, \rho)$, where d_m is the mean grain diameter and ρ the soil bulk density.

We consider a soil consisting of a large number of thin, but distinguishable layers of different texture (as indicated by mean grain diameter) and the bulk density. Each layer is characterized by its own van Genuchten type hydraulic conductivity function, $K(\psi, p)$, where ψ represents the tension head. Because the van Genuchten parameter p has been related to d_m, ρ, the hydraulic conductivity can be written in a general form of $K(\psi, d_m, \rho)$. Then, the layered formation is expressed in terms of a joint probability density function, $f(d_m, \rho)$, of the mean grain diameter d_m and the bulk density ρ. Parallel to the layering, the hydraulic conductivity $K_h(\psi)$, is defined by the arithmetic mean of $K(\psi, d_m, \rho)$ for the layers,

$$K_h(\psi) = \iint K(\psi, d_m, \rho) f(d_m, \rho) dd_m d\rho \tag{1}$$

The hydraulic conductivity perpendicular to the layers, $K_v(\psi)$, is defined by the harmonic mean of $K(\psi, d_m, \rho)$ for the layers, which is expressed as follows,

$$K_v(\psi) = \left[\iint \frac{f(d_m, \rho)}{K(\psi, d_m, \rho)} dd_m d\rho \right]^{-1} \tag{2}$$

The anisotropy factor as function of ψ is then expressed as the ratio of the hydraulic conductivities in the horizontal and vertical directions,

$$A(\psi) = \frac{K_h(\psi)}{K_v(\psi)} \tag{3}$$

Principal Findings and Significance

The key findings from this project are summarized as follows.

- The coupled dependence of the hydraulic parameters on the texture and bulk density is important to determine the anisotropic behaviour of unsaturated soils. The minimum anisotropy at a certain capillary pressure head (or tension head) is only observed when both the saturated hydraulic conductivity K_S and van Genuchten parameter α are related to the mean grain diameter.
- When only one hydraulic parameter is related to the grain diameter or when both are not related to the same attribute simultaneously, the unsaturated soil anisotropy increases monotonically with the increasing capillary pressure head.
- The inter-relationships of soil texture, bulk density, and hydraulic properties may cause vastly different anisotropy behaviors of unsaturated soils.
- The correlation between the soil grain diameter and bulk density decreases the anisotropy effects of the unsaturated layered soils.

Information Transfer Activities

Journal Papers:

Zhu, J. 2011. Effect of layered structure on anisotropy of unsaturated soils. Soil Science, submitted.

Zhu, J., and A. W. Warrick. 2010. Effective unsaturated hydraulic conductivity for layered soils of structured heterogeneity. Soil Science Society of America Journal, submitted.

Zhu, J., and D. Sun. 2010. Capillary pressure-dependent anisotropy of unsaturated soils. Canadian Journal of Soil Science. 90(2):319-329.

Full Conference Proceeding Paper:

Zhu, J., and D. Sun. 2010. Saturation-dependent anisotropy of unsaturated soils, 19th World Congress of Soil Science – Soil solution for a changing world, August 1 – 6, 2010, Brisbane, Australia, pp.40-43.

Abstracts and Presentations:

Zhu, J. 2010. Effective hydraulic functions in layered porous media, ASA-CSSA-SSSA 2010 International Annual Meetings, October 31 – November 4, 2010, Long Beach, California, U. S. A.

Zhang, Y., J. Zhu, and D. Sun.2010. Non-Fickian mechanism of contaminant transport in unsaturated heterogeneous soils, ASA-CSSA-SSSA 2010 International Annual Meetings, October 31 – November 4, 2010, Long Beach, California, U. S. A.

Zhu, J. 2010. Saturation-dependent anisotropy of structured and random layered soils, 2010 EGU General Assembly, May 2 – 7, 2010, Vienna, Austria.

Student Support

This grant was partly used to fund student training. Rongrong Zhang (a Ph.D. student from Hohai University, Nanjing, China) was funded partially from this grant to help with data analysis.

USGS Award No. G10AP00081 Yerington/Anaconda Mine Site Technical Support

Basic Information

Title:	USGS Award No. G10AP00081 Yerington/Anaconda Mine Site Technical Support
Project Number:	2010NV177S
Start Date:	3/15/2010
End Date:	3/14/2011
Funding Source:	Supplemental
Congressional District:	2
Research Category:	Engineering
Focus Category:	Acid Deposition, Toxic Substances, Groundwater
Descriptors:	
Principal Investigators:	William H Albright

Publications

There are no publications.

USGS Award No. G10AP00081 Yerington/Anaconda Mine Site Technical Support

Problem and research objectives:
Processing of copper ore at the Yerington NV mine site was accomplished by leaching with sulfuric acid. Residual materials, both solid residual ore and process fluids, pose considerable hazard to the local environment. The most likely method for spread of contaminants is through movement of meteoric water through heap leach and drain-down pond facilities and, thus, to groundwater. Hydraulic control at the surface via a final cover is likely a viable option for closure of several of the site features. The purpose of this effort is exploration of the feasibility of a particular solution – a water balance cover - not only at the Yerington site, but throughout the Great Basin.

Methodology:
In this study, we conducted initial evaluation of the available soil resources for use in a water balance cover. Soil resources at the mine are very complex and range from undisturbed sources to mine spoils placed over years of activity. Index properties, primarily particle size distribution, allowed estimates of unsaturated soil properties including soil water storage. The climate of the site was evaluated with a new method described by Albright et al (2010) which compares precipitation to potential evaporation on a monthly basis to determine the required soil water storage for a cover. Required storage was computed for the wettest year on record. A survey of available soils was conducted by the site owner to give a more comprehensive view but, unfortunately, those results were only recently made available and no further analysis has been done.

Principal Findings:
Analyses to date suggest a cover of moderate thickness (~1-1.2 m) and vegetated with local species will likely provide sufficient control of percolation. That thickness allows for plant viability and is economically feasible. Further work will be required to evaluate the effect of the considerable variability in the available soils on expectations of performance.

Information Transfer Activities:
There are no papers to date on this effort.

Information Transfer Program Introduction

None.

USGS Summer Intern Program

None.

Student Support					
Category	**Section 104 Base Grant**	**Section 104 NCGP Award**	**NIWR-USGS Internship**	**Supplemental Awards**	**Total**
Undergraduate	2	0	0	0	2
Masters	5	0	0	0	5
Ph.D.	2	0	0	0	2
Post-Doc.	0	0	0	0	0
Total	9	0	0	0	9

Notable Awards and Achievements

The Lake Mead Quagga Mussel project allowed the PI (Acharya) to collect preliminary data. The preliminary data led to additional funding through two new projects by National Park Service and NSF-SBIR through the Marrone Bio-innovations, a California based bio-control company. The project has allowed the PI to establish Quagga mussel research infrastructure in DRI. This has increased institute's competitiveness in the field of Quagga mussel research and provided additional local research capability for Southern Nevada and Lake Mead.